P-01

Enhanced electrical properties and air stability in high-density amorphous organic films

Yu Esaki,[1] Takeshi Komino,[1,2] Toshinori Matsushima,[1,2,3] and Chihaya Adachi[1,2,3]

1. OPERA, Kyushu University, 2. JST ERATO, 3. WPI-I^{2}CNER
744 Motooka, Nishi, Fukuoka, Fukuoka, 819-0395, Japan
Tel: +81-92-802-6920, Fax: +81-92-802-6921
E-mail: esaki@opera.kyushu-u.ac.jp, adachi@cstf.kyushu-u.ac.jp

1. Introduction

Organic light-emitting diodes (OLEDs) are commonly composed of several amorphous organic thin films. There are many microscopic voids formed by disorder of molecular arrangement in amorphous films. These voids impede carrier hopping because they work as carrier traps and energy barriers, and reduce air stability by water and oxygen molecules migrating through the gaps. Ediger's group has established that controlling substrate temperature during vacuum deposition (T_{sub}) can produce thermally stable amorphous films with high film density and molecular anisotropy [1–3]. This is because T_{sub} governs kinetic mobility of molecules migrating on a film surface during deposition, which strongly affects resulting film morphologies [1–3]. Therefore, it is expected that if highly densified amorphous films can be obtained by controlling T_{sub}, these films should display enhanced electrical properties and air stability. In this study, we comprehensively investigate the influence of T_{sub} on the film density, molecular orientation, electrical properties, and air stability of amorphous films of a typical hole-transporting material, α-NPD [4].

2. Experimental

Film fabrication and structure analysis

For an estimation of density and molecular orientation, α-NPD films having a thickness of approximately 100 nm were vacuum-deposited on bare Si substrates kept at various T_{sub} ranging from 212 to 342 K. Variable angle spectroscopic ellipsometry (VASE) was performed on the α-NPD films and the results were fitted with an optical model considering anisotropy to evaluate their orientational order parameter *S*, refractive index *n*, extinction coefficient *k*, and film thickness *d*. The relative density (ρ_{rel}) of each α-NPD film was estimated from the ratio of *d* values before and after annealing at a temperature higher than the glass transition temperature ($T_{g,bulk}$) [3].

Fabrication of HODs and measurement of electrical properties

For an investigation of T_{sub} affecting the electrical properties and air stability of α-NPD films, hole-only devices (HODs) containing an α-NPD layer were fabricated. The structure of the HODs was a glass substrate/indium tin oxide (ITO) anode (100 nm)/α-NPD (about 350 nm)/MoO_3 (30 nm)/Au cathode (50 nm). The α-NPD layer was vacuum-deposited at different T_{sub} and the MoO_3 and Au layers were vacuum-deposited on room-temperature substrates. Current density (*J*) – voltage (*V*) properties of HODs were measured under nitrogen in the dark. Because the actual thicknesses of deposited α-NPD showed a slight variation between samples, we used electric field *E* instead of *V* to allow better comparison of the film parameters. After the *J*-*V* measurements, the air stability of HODs was evaluated from the temporal change of driving voltage under continuous current application at 0.1 mA/cm^2 in air (without encapsulation) under dark conditions.

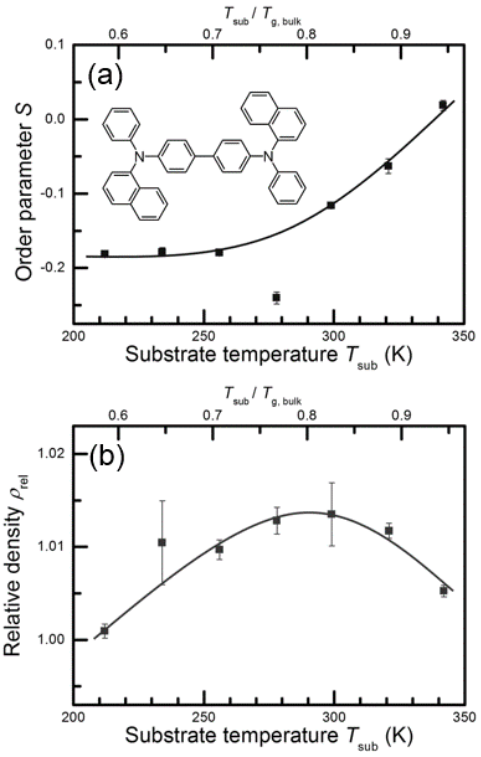

Fig. 1. Plots of (a) *S* and (b) ρ_{rel} as a function of T_{sub}. The chemical structure of α-NPD is shown in the inset of (a).

3. Results and discussion

Film structure analysis

Figure 1(a) and (b) shows *S* and ρ_{rel} of α-NPD films deposited at different T_{sub}. While molecular orientation changed from horizontal relative to a substrate to random as T_{sub} was increased, ρ_{rel} exhibited a convex trend with a maximum value between 270 and 300 K (0.75−0.83 $T_{g,bulk}$). These *S* and ρ_{rel} changes can be explained by kinetic mobility of molecules on a film surface during vacuum-deposition. If the kinetic mobility is too small in the low T_{sub} region or too large in the high T_{sub} region, the density becomes lower because molecules are less likely to reach or stop at an energetically stable position, respectively. However, when the kinetic mobility is suitable (0.75–0.83$T_{g,bulk}$), molecules can move a large distance on a film surface to find a stable position. For this reason, films fabricated at 0.75–0.83$T_{g,bulk}$ have higher density than

those formed at other T_{sub}. When the kinetic mobility is small at low T_{sub}, molecules cannot move much and therefore keep their horizontal orientation. As the kinetic mobility of molecules increases at higher T_{sub}, molecules move intensely, which causes the orientational order to gradually become random.

Electrical properties

Figure 2(a) shows *J*-*E* properties of the HODs. It is clear that the *J*-*E* properties are strongly affected by T_{sub}. The *J* values at an *E* of 1.0×10^5 V/cm are plotted as a function of T_{sub} in Fig. 2(b). *J* changes in a similar manner to that of ρ_{rel} in Fig. 1(b). A higher ρ_{rel} indicates decreased intermolecular distance because the α-NPD molecules are packed more closely, which might be expected to enhance carrier transport in a film. Moreover, in films with higher density, the width of their density of states (DOS) might be expected to be narrower because of the location of molecules at stable positions. This DOS narrowing can result in a lower barrier between neighboring states near the center of the DOS distribution. The changes of tail state and state-to-state barrier caused by the DOS narrowing could lead to a decrease in activation energy and enhanced rate of carrier hopping. In contrast, there was no clear relationship between *J* and *S*, even though it has been reported that the horizontal orientation on a substrate leads to enhanced carrier transport because of the better overlap of π orbitals between neighboring molecules in a substrate normal.

Air stability

The temporal changes of driving voltage *V* offset to the initial voltage $V_{initial}$ are shown in Fig. 3(a). For most of the devices, $V - V_{initial}$ values increased monotonically over time. To quantitatively evaluate the air stability of the HODs, $V - V_{initial}$ curves were divided by the elapsed time of 300 h; the slopes are displayed in Fig. 3(b). In this figure, a smaller slope means higher air stability. The air-stability data well-matched with the ρ_{rel} curve in Fig. 1(b). These data reveal that α-NPD films with higher ρ_{rel} have higher air stability, while *S* has no relation to not only the electrical properties but also the air stability of the films. Although the detailed mechanism is now under investigation, suppressed absorption of water and oxygen molecules and crystallization and reorientation of α-NPD molecules are possible reasons of the enhanced air stability.

4. Conclusion

The relationship between molecular orientation, film density, electrical properties, and air stability were investigated. For α-NPD, the film density has more influence on carrier transport than the molecular orientation does. An increase in driving voltage during continuous driving was suppressed in higher-density film, implying enhanced air stability. Even though the ρ_{rel} variation observed here is very small, just 1%–2%, the effect of ρ_{rel} on electrical properties and air stability is considerable.

References

[1] S. F. Swallen, K. L. Kearns, M. K. Mapes, Y. S. Kim, R. J. McMahon, M. D. Ediger, T. Wu, L. Yu, and S. Satija, *Science* **315**, 353–356 (2007).

[2] Y. Z. Chua, M. Ahrenberg, M. Tylinski, M. D. Ediger, C. Schick, *J. Chem. Phys.* **142**, 054506 (2015).

[3] S. S. Dalal, D. M. Walters, I. Lyubimov, J. J. de Pablo, M. D. Ediger, *Proc. Natl. Acad. Sci.* **112**, 4227–4232 (2015).

[4] Y. Esaki, T. Komino, T. Matsushima, and C. Adachi, *J. Phys. Chem. Lett.* **8**, 5891–5897 (2017).

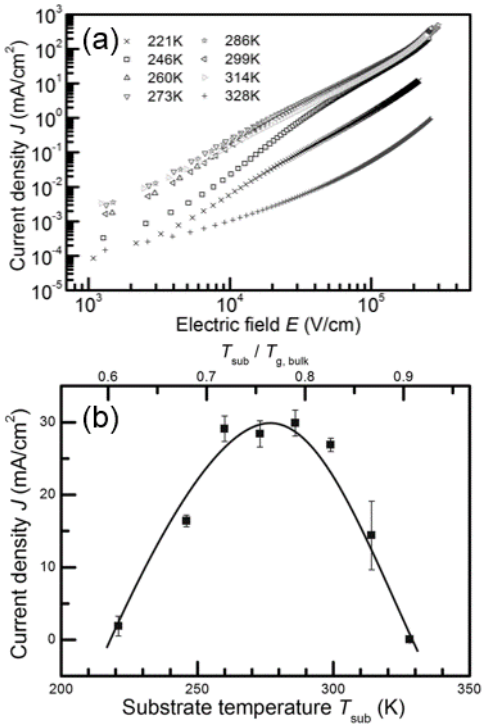

Fig. 2. (a) Representative *J*-*E* properties of hole-only devices with α-NPD layers vacuum-deposited at different T_{sub} and (b) a plot of *J* at $E = 1.0 \times 10^5$ V/cm versus T_{sub}.

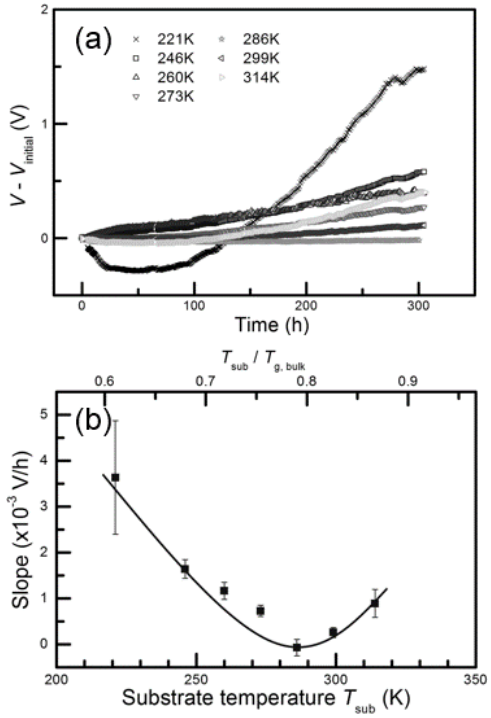

Fig. 3. (a) Temporal changes of *V* for HODs with α-NPD layers vacuum-deposited at different T_{sub}. The initial *V* at 0 h ($V_{initial}$) was offset to 0 V. (b) Slopes calculated by dividing $V - V_{initial}$ by the elapsed time (300 h).

P-02

Isoindigo benzodifuran based Ambipolar Organic Field-effect Transistors

Tomotsugu Takaya[1], Melaku Dereje Mamo[2], Makoto Karakawa[1] and Yong-Young Noh[2]

[1] *Kanazawa University, Kakuma-machi, Kanazawa, Ishikawa, 920-1192, Japan*
[2] *Dongguk University, 30 pildong-ro, 1-gil, Jung-gu, Seoul, 04620, Republic of Korea*
E-mail: karakawa@staff.kanazawa-u.ac.jp, yynoh@dongguk.edu

A combination of electron-donor unit and electron-acceptor unit is one of the most effective strategies to achieve high carrier mobilities in semiconducting polymers. It is also effective way to construct ambipolar semiconducting polymers because the bandgap can be fine-tuned by selecting donor and acceptor units. Isoindigo (**IID**) has been used as acceptor unit leading to significant developments of polymer field-effect transistors(FETs)[1]. Recently, the powerful acceptor unit, (3E,7E)-3,7-bis(2-oxoindolin-3-ylidene)benzo[1,2-b:4,5-b′]difuran-2,6(3H,7H)-dione (**IBDF**) was reported[2]. **IBDF** is recognized as a derivatives of **IID**, introduced 3,7-dihydrobenzo[1,2-b:4,5-b']difuran-2,6-dione (**BDF)** unit at the center of **IID** with double bonds. **IBDF** has large conjugated 2D-plane, therefore it facilitates interchain π-π stacking enhancing the carrier mobilities. The aim in this study is to investigate the effect of introducing **BDF** into the center of **IID** unit. Combining each acceptor units with 3,3'-bis(alkoxy)-2,2′-bithiophene (**BTO**) as donor unit, **PI-BTO** and **PIBDF-BTO** (Figure 1) were synthesized, and measured polymer properties and carrier mobilities in FETs.

PI-BTO and **PIBDF-BTO** were synthesized via the Stille coupling reaction of **IID** or **IBDF** with **BTO**. Polymer properties were measured by UV-Vis-NIR absorption, Thermo Gravimetric Analysis and Ultraviolet Photoelectron Spectroscopy. Top-gate bottom-contact type FETs were fabricated to evaluate the carrier mobilities. AFM and XRD measurement were conducted to analyze the film state of polymers.

Transfer curves of FETs are shown in Figure 2. **PI-BTO** showed only p-type property, and **PIBDF-BTO** showed ambipolar property. The maximum mobilities were 8.1×10^{-4} cm^2 V^{-1} s^{-1} (p-type) for **PI-BTO**, 2.7×10^{-1} cm^2 V^{-1} s^{-1} (p-type), 2.2×10^{-1} cm^2 V^{-1} s^{-1} (n-type) for **PIBDF-BTO**. The detailed analysis and discussion will be summarized in the poster.

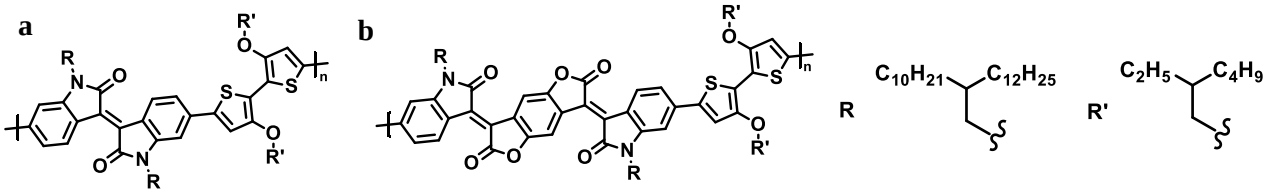

Figure 1 a) **PI-BTO** b) **PIBDF-BTO**

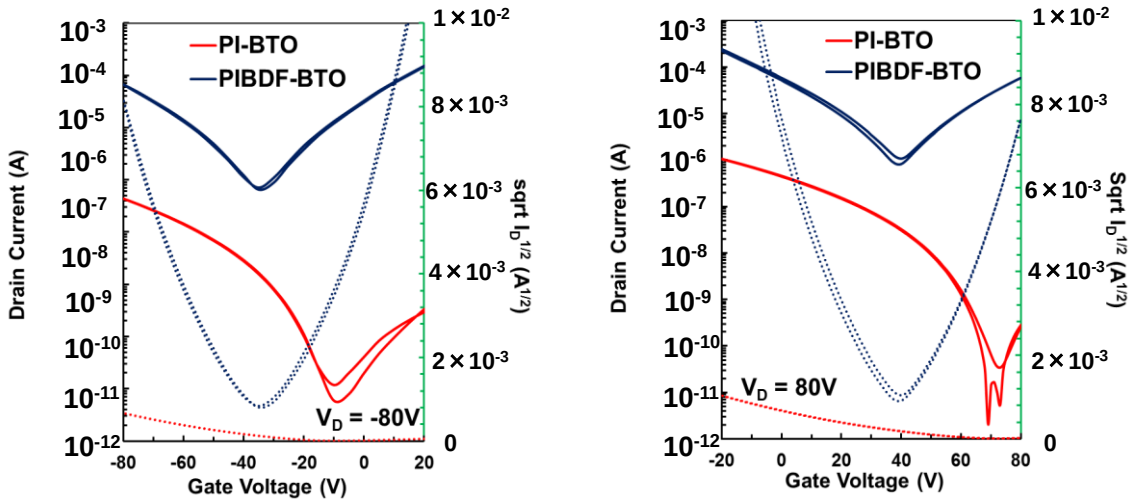

Figure 2 a) p-type transfer and b) n-type transfer curves

References

[1] R. Stalder, J. Mei, K. R. Graham, L. A. Estrada, and J. R. Reynolds, "Isoindigo, a Versatile Electron-Deficient Unit For High-Performance Organic Electronics," Chem. Mater., 26, 664−678, 2014.

[2] T. Lei, J.-H. Dou, X.-Y. Cao, J.-Y. Wang, and J. Pei, "Electron-Deficient Poly(*p*-phenylene vinylene) Provides Electron Mobility over 1 cm^2 V^{-1} s^{-1} under Ambient Conditions," J. Am. Chem. Soc., 135, 12168−12171, 2013.

P-03

TiO_2 micropattern formation on COP substrate by vacuum ultraviolet irradiation in dried air atmosphere

Cheng-Tse Wu, Ahmed I. A. Soliman, Toru Utsunomiya, Takashi Ichii and Hiroyuki Sugimura

Department of Materials Science and Engineering, Kyoto University, Yoshida-Hommachi, Sakyo, Kyoto, 606-8501, Japan
Tel: + 81 - 75 - 753 - 5990, Fax: +81 - 75 - 753 - 5484
E-mail: wu.chengtse.26e@st.kyoto-u.ac.jp

(1) Introduction

In recent years, TiO_2 thin film material has received a great interest since it possesses good chemical stability, photocatalytic properties, and transparency in visible light region. It has been studied in various application ranging from anti-fog coating, self-cleaning coating, solar cell, to thin film FET. To fabricate TiO_2 thin film, several methods have been developed such as reactive magnetron sputter, molecular beam epitaxy, pulsed laser deposition, sol-gel synthesis, however, most of those require the heat process which is not favorable for thermal sensitive substrates. Patrick and coworkers developed a photochemical method involving the conversion from thin film of titanium alkoxide compound into titanium oxide by VUV (main peak 172 nm) exposure in oxygen-enriched nitrogen atmosphere[1]. As VUV light propagates in air, it is absorbed by oxygen, leading to the generation of active oxygen species such as atomic oxygen species and ozone. The existence of these reactive oxygen species accelerates dissociation of organic moieties in the precursor. Inspired by the idea of light-induced chemical conversion of titanium metal organic compounds, we expect that TiO_2 micropatterning can be achieved by the VUV lithographic process. In this study, we propose a method to fabricate TiO_2 thin film and micropattern on polymeric substrate, since the heat process can be avoided. The micro-patterning was obtained in ambient environment.

(2) Experimental Method

Cycloolefin Polymer (COP) substrate was irradiated by VUV to increase hydrophilicity of the surface. We chose titanium acetylacetonate (TAA) as precursor instead of titanium alkoxide compounds since TAA is more chemically stable in ambient environment[2]. The TAA solution was spin-coated on VUV-modified COP substrate. After VUV exposure through photomask, the substrate was further cleaned by rinsing in isopropanol.

XPS, FTIR were conducted to characterize the conversion of precursor. SEM-EDX, AFM, TEM were exploited to characterize the morphology and element distribution of TiO_2 micropattern.

(3) Results and Discussions

In Fig. 1. FTIR spectra show that during the irradiation time, absorption bands from the organic moieties decreased, and after 120 min irradiation, the photochemical reaction was completed. In Fig. 2. SEM-EDX illustrates that micropattern was clearly obtained. VUV irradiation through photomask converted TAA to TiO_2. The unprocessed TAA in the masked area was removed by isopropanol rinsing. The results of HR-TEM and SAED showed that the photochemically obtained TiO_2 was amorphous.

In the present stage, we are working on photoreduction of cupric ion induced by the photocatalytic properties of TiO_2 micropattern.

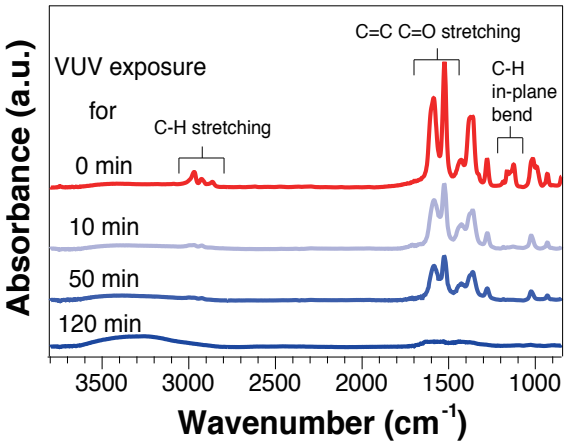

Fig.1. FTIR absorption spectra in different VUV irradiation time

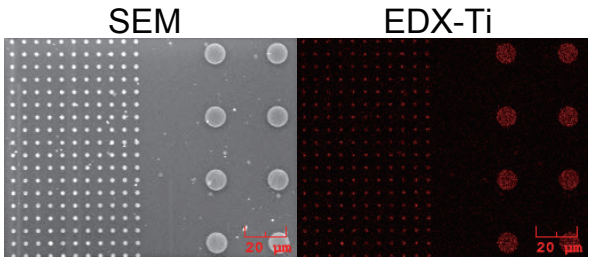

Fig.2. SEM image and Ti mapping images after micropatterning

References

[1] P. C. With, U. Helmstedt, S. Naumov, A. Sobottka, A. Prager, U. Decker, and L. Prager, Chem. Mater. **28(21)** 7715 (2016).
[2] D. M. Antonelli, and J. Y. Ying, Angew. Chemie - Int. Ed. **34(18)**, 2014 (1995).

P-04

Direct bonding of ultra-flat titanium thin film and polymer at ambient temperature

Lihting LIN, Toru UTSUNOMIYA, Takashi ICHII and Hiroyuki SUGIMURA

Department of Materials Science and Engineering, Kyoto University, Yoshida-honmachi, Sakyo-ku Kyoto 606-8501, Japan
Tel: + 81 - 75 - 753 - 5990, Fax: +81- 75 -753 - 5484
E-mail: lin.lihting.58e@st.kyoto-u.ac.jp

(1) Introduction

Vacuum ultraviolet (VUV; $100 < \lambda < 200$ nm) light irradiation is famous for improving the adhesivity of in nonpolar polymers [1]. In our previous studies, photo-activated bonding of cyclo-olefin polymer (COP)-to-aluminum and COP-to-silicon without using any extra adhesive have been successfully achieved under low temperature [2,3]. However, the effects of surface conditions on bonding between these kinds of organic-inorganic composite materials is still not well understood. Thus in this study, by creating different kinds of surface conditions, we explored the possibilities of direct bonding between COP and titanium at ambient temperature. In addition, the effects of surface conditions on bonding strength were studied as well.

(2) Experimental

Self-assembled monolayer (SAM) using hexadecane as a precursor was formed on a monocrystalline silicon (111) wafer as a template. The ultra-flat titanium thin film was made by template-stripping (TS) method using this template. In addition, the Octadecylphosphonic acid (ODP) modified Ti surface was made by immersing a physical vapor deposited titanium (PVD-Ti) sample into ODP/ethanol solution for 48 h. The samples were exanimated by X-ray photoelectron spectroscopy (XPS), atomic force microscopy, and water contact angle (WCA) goniometer. COP films and titanium samples were photo-activated using VUV light at a wavelength of 172 nm in dry air. The modified surfaces were pressed face-to-face at ambient temperature. After pressing, the 90-degree bonding strength test was performed.

(3) Results and discussion

Figure 1 shows the XPS C1s spectra for each samples. It can be found that only one peak appears in the spectrum of ODP-SAM modified PVD-Ti (ODP-Ti) samples. After VUV modification, peak appeared from 287.5 to 289.5 eV, which is related to oxygen functional groups. The hydrophilization of VUV modified ODP-Ti was confirmed by water contact angle, which is 8° . The XPS and WCA results were the clear evidences that oxygen functional groups were formed on the surface, and surface energy increased at the same time. Unfortunately, The VUV modified ODP-Ti, with a surface roughness of 5.7 nm (R_{RMS}), did not succeed in bonding with COP at ambient temperature. In contrast, bonding between COP and ultra-flat TS made-Ti (TS-Ti), with a surface roughness of 0.08 nm (R_{RMS}), was succeeded. Both TS-Ti and COP are extremely flat. Therefore, the effective contact area between them is enough for ambient temperature bonding. The maximum bonding strength was measured to be 8.8 N cm^{-1}. In conclusion, for direct bonding between different materials at ambient temperature, the flatness of the material surfaces are more effective than the amount of oxygen functional groups on the surface.

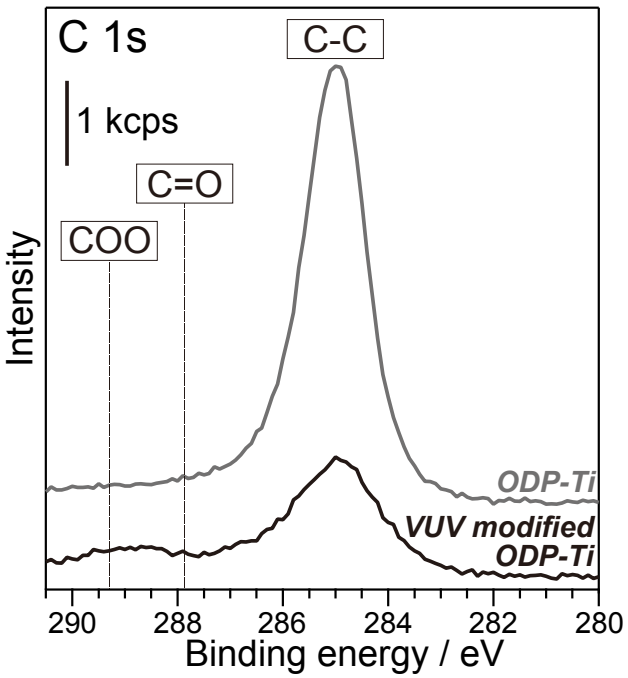

Fig. 1. C1s XPS spectra obtained from ODP modified titanium surfaces before and after VUV irradiation.

References

[1] Y. Kim, Y. Taniguchi, K. Murase, Y. Taguchi, H. Sugimura, Appl. Surf. Sci. **255**, 3648-3654 (2009).
[2] Y. Fujiwara, T. Utsunomiya, T. Ichii and H. Sugimura, " Room temperature bonding of polymer and silicon wafer using vacuum ultraviolet surface activation," AVS 63rd in Nashville., Tennessee, USA, no.SE-TuP1, pp.1, Nov. 2016.
[3]Z. Luo, T. Utsunomiya, T. Ichii and H. Sugimura, " Photo-activation bonding between highly smooth aluminum and polymer," 66th Symposium on Macromolecules., Ehime, Japan. no.2Pa045, Sep. 2017

P-05

Highly efficient photoreduction of graphene oxide using alcohol solutions

Kunhua Yu，Yudi Tu，Toru Utsunomiya，
Takashi Ichii，Hiroyuki Sugimura

Department of Materials Science and Engineering, Kyoto University,
Yoshidahonmachi, Sakyo Ward, Kyoto 606-8501, Japan
Tel: + 81 - 080 - 4824 - 3489, Fax: +81- 075 -753 - 5484
E-mail: yu.kunhua.83m@st.kyoto-u.ac.jp

Recently, alcohol-assisted reduction of graphene oxide (GO) has attracted much attention as the alcohol can be used as carbon feedstock to restore the structural defects on GO surface [1,2]. However, these methods need to heat GO over 900℃ and supply alcohol vapor continuously, which would consume large amount of energy and make experiment much complex. Compared with thermal reduction, photoreduction process has their special advantage *e.g.*, higher efficiency, less energy consumption and non-release of toxic pollutants [3]. In this study, GO on hydrogen terminated silicon substrate (H-Si) was photoreduced by vacuum-ultraviolet (VUV) light irradiation. Before photoreduction process, around 100 nm alcohol solution layer (10 mmol·L^{-1} ethanol or 10 mmol·L^{-1} methanol in decane solution) was deposited on GO surface and the alcohol solution was sealed within a O-shape photomask.

The surface chemical state and tribological properties of GO and reduced-GO (rGO) were measured by X-ray photoelectron spectroscopy (XPS) and lateral force microscopy (LFM), respectively. From the LFM analyzation, the friction force of GO sheets decreased obviously after alcohol-assisted photoreduction, even lower than that reduced in high vacuum condition (<10^{-3} Pa). Fig .1 showed the plots of friction force versus load force of ①GO, rGO photoreduced in ②high vacuum vacuum-ultraviolet (HV-VUV), ③ethanol decane solution (10 mmol·L^{-1}) and ④methanol decane solution (10 mmol·L^{-1}). The GO exhibited the highest friction force while the alcohol-assisted photoreduced rGO exhibited extremely low friction force at the same load force. These results can be explained by removing large amount of oxygen functional groups (OFGs) on GO surface during the photoreduction process and also can be confirmed in X-ray photoelectron spectroscopy (XPS, Figure 2). Figure 2 showed the XPS C1s spectra of GO and rGO (photoreduced in various condition). After photoreduction in high vacuum condition, the O/C ratio of GO decrease from 0.36 to 0.21. The O/C ratio can decrease further to 0.17 or 0.15 as ethanol or methanol solution were utilized during the reduction process, which indicated that the alcohol molecule can contribute to remove the OFGs on GO surface and improved the efficiency of GO photoreduction.

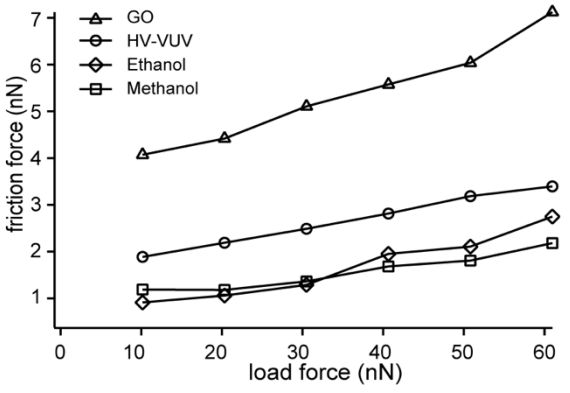

Fig.1 Friction force versus various load force plots of GO, rGO photoreduced in HV-VUV, 10 mmol·L^{-1}ethanol decane solution and 10 mmol·L^{-1} methanol decane solution.

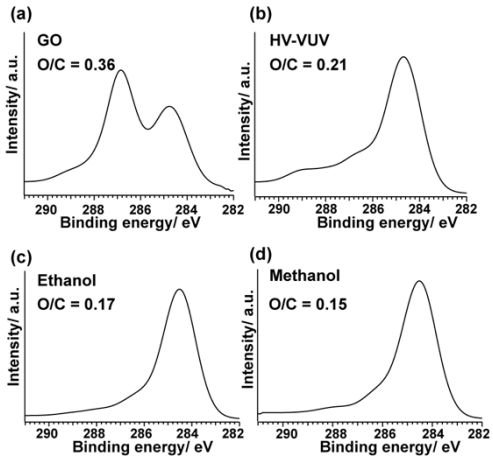

Fig.2 XPS C1s spectra of GO, rGO photoreduced in HV-VUV, 10 mmol·L^{-1}ethanol decane solution and 10 mmol·L^{-1} methanol decane solution.

References

[1] Su. C. Y, Xu. Y, Zhang. W, Zhao. J et al. “Highly efficient restoration of graphitic structure in graphene oxide using alcohol vapors.” Acs Nano, 4(9), 5285-5292, 2010.
[2] Negishi. R, and Kobayashi. Y, “Extraordinary suppression of carrier scattering in large area graphene oxide films,” Applied Physics Letters, 105(25), 253502, 2014.
[3] Zhang. Y. L, Guo. L, Xia. H, Chen. Q. D et al, “Photoreduction of graphene oxides: methods, properties, and applications,” Advanced Optical Materials, 2(1), 10-28, 2014.

P-06

Preparation of TIPS pentacene/PS blend films by electrostatic spray deposition for organic field-effect transistors

Norio Onojima, Takumi Ozawa, Takuya Sugai, and Shunsuke Obata

Department of Electrical and Electronic Engineering, University of Yamanashi,
4-3-11 Kofu, Yamanashi, 400-8511 Japan
Tel: + 81 - 55 - 220 – 8503
E-mail:nonojima@yamanashi.ac.jp

Printed electronics based on organic materials have attracted significant attention because printing techniques, such as spraying, are expected to enable low-cost, large-area, and flexible device fabrication. Semiconducting small molecule/insulating polymer blends have been proposed to be ideal materials for organic field-effect transistors (OFETs), because the conjugated small molecules are ordered for π-electrons to sufficiently overlap each other resulting in excellent electrical properties and the polymers typically exhibit superior solution processability which can improve film connectivity and areal coverage. Previously, we reported device characteristics of top-contact OFETs based on blend films composed of 6,13-bis(triisopropylsilylethynyl) pentacene (TIPS pentacene) and poly(methyl methacrylate) (PMMA) prepared by electrostatic spray deposition (ESD) [1]. TIPS pentacene with lower surface energy and smaller molecular weight than PMMA is preferentially segregated at the air-film interface, and therefore vertically phase-separated structure can be spontaneously formed. However, the vertical phase separation between TIPS pentacene and PMMA was not sufficient during the ESD process due to partial evaporation of solvent in atomized submicron droplets before arriving at the substrate. The phase-separation phenomenon is initiated by solvent evaporation [2]. The phase-separated morphology was investigated by selective etching of TIPS pentacene with an orthogonal solvent, cyclohexane that avoids dissolution of the underlying PMMA and using atomic force microscopy (AFM). A relatively rough surface with some pinholes was observed in the cyclohexane-etched blend film (i.e., the phase-separated interface of the as-deposited blend film), which resulted in relatively low mobilities [3]. Because charge-carrier transport takes place at the semiconducting small molecule/insulating polymer interface laterally, the conducting pathway between the source/drain electrodes should be well-defined [4]. In this study polystyrene (PS) was used in place of PMMA as a blended insulating polymer, and blend films comprising TIPS pentacene and PS were prepared by ESD. Top-contact OFETs based on the TIPS pentacene/PS blend films exhibited higher mobilities than those of TIPS pentacene/PMMA blend ones, which is probably attributed to a well-defined phase-separated structure of TIPS pentacene and PS.

A schematic of our ESD system and device architecture fabricated in this study are illustrated in Figs. 1(a) and 1(b), respectively. ESD is a printing technique that enables us to deposit organic films selectively using a shadow mask. Heavily-doped n-type Si (100) substrates with 300-nm thick SiO_2 were used as bottom-gate electrodes. The substrates were cleaned by ultrasonication with conventional organic solvents followed by UV/ozone treatment. TIPS pentacene and PS (0.1 and 0.3 wt%, respectively) were dissolved in a mixed solvent of 1,2-dichlorobenzene (o-DCB) and acetone (1.5 and 8.5 ml, respectively). The solution feed rate of 2.0 ml/min was precisely controlled by a syringe pump. The substrate temperature was maintained at 50 °C during organic film deposition. The ESD process conditions were as follows: the spray-nozzle inner diameter was 250 μm, the distance from the nozzle to the substrate was 5 cm, and the voltage applied to the nozzle was 10 kV, which was controlled by a high-voltage DC power source. Finally, Au source/drain electrodes (ca. 30 nm in thickness) were thermally evaporated onto the blend film.

The electrical characteristics of the OFETs were evaluated by using drain current–drain voltage (I_d–V_d) and drain current–gate voltage (I_d–V_g) measurements. Figs. 2(a) and 2(b) show the output (I_d–V_d) and transfer (I_d–V_g) characteristics of the blend device with a channel length and width of 0.2 and 1.0 mm, respectively. Good p-channel behaviors (pinch-off and saturation characteristics) could be confirmed in the output characteristics, indicating that vertical phase separation between TIPS pentacene (top active layer) and PS (bottom insulator) can be induced during the ESD process as well as the case of TIPS pentacene/PMMA blend films. A field-effect mobility of 0.24 $cm^2/V{\cdot}s$ was derived from the transfer characteristics, which is one order of magnitude higher than that of the TIPS pentacene/PMMA blend OFETs. This result indicates that sufficient vertical phase separation of the TIPS pentacene/PS blend films was induced during the ESD process, which is different from PMMA blends, and the superior charge transport properties might be due to the well-defined phase-separated interface.

References

[1] N. Onojima, K. Hara, and A. Nakamura, “Vertical phase separation of 6,13-bis(triisopropylsilylethynyl) pentacene/ poly(methyl methacrylate) blends prepared by electrostatic spray deposition for organic field-effect transistors”, Jap. J. Appl. Phys. vol. 56, pp. 05EB03 1-4, March 2017.

[2] F. Wu, F. Ye, Z. Chen, Y. Cui, D. Yang, Z. Li, X. Zhao, and X. Yang, “Morphology construction of vertical phase separation for large-area polymer solar cells”, Org. Electron. vol. 26, pp. 48-54, July 2015.

[3] N. Onojima, S. Obata, A. Nakamura, and K. Hara, “Influence of phase-separated morphology on small molecule/polymer blend organic field-effect transistors fabricated using electrostatic spray deposition”, Thin Sold Films vol. 640, pp. 99-103, September 2017.

[4] S. G. Lee, H. S. Lee, S. Lee, C. W. Kim, and W. H. Lee, “Thickness-dependent electrical properties of soluble acene–polymer blend semiconductors”, Org. Electron. vol. 24, pp. 113-119, May 2015.

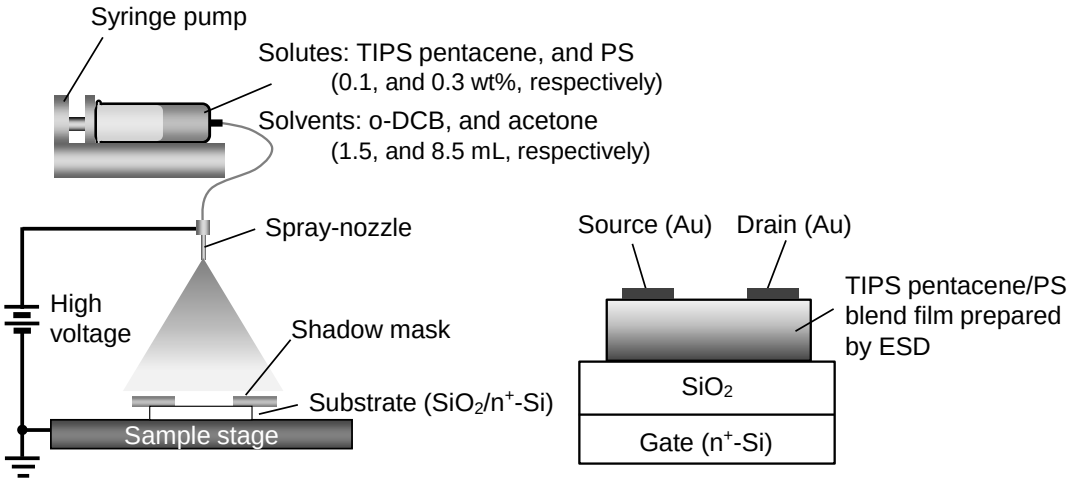

Fig. 1 Schematic of (a) our ESD system and (b) device architecture fabricated in this study.

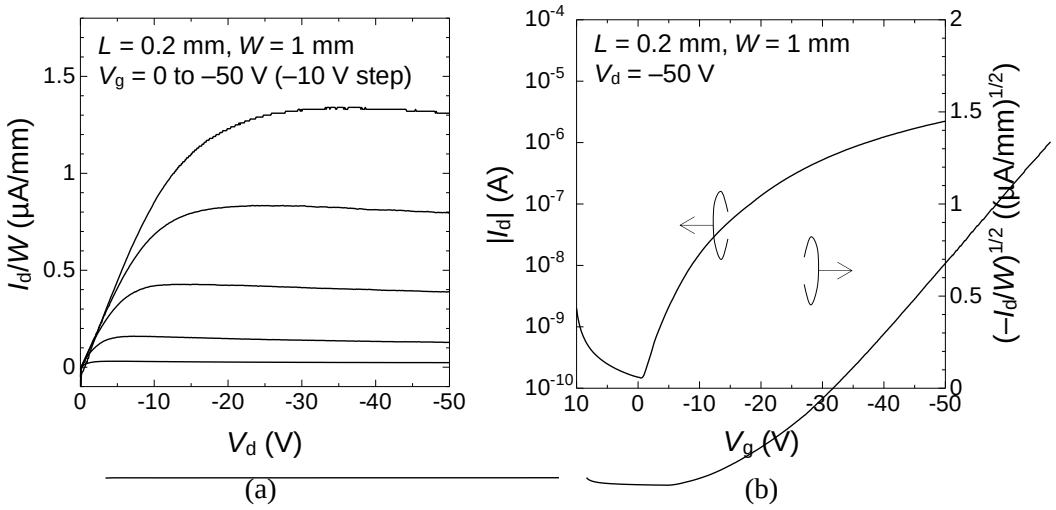

Fig. 2 (a) Output and (b) transfer characteristics of TIPS pentacene/PS blend OFET. Channel length and width are 0.2 and 1.0 mm, respectively.

P-07

Development of an Electrochromic Device Consisting of Ferrocene- and Viologen-Based Ionic Liquids

Kazuaki Uranaka, Hironobu Tahara, Takamasa Sagara, and Hiroto Murakami

Graduate School of Engineering, Nagasaki University,
1-14 Bunkyo, Nagasaki, 852-8521 Japan
Tel: + 81 - 95 - 819 - 2675, Fax: +81- 95 -819 - 2675
E-mail:hiroto@nagasaki-u.ac.jp

Introduction

A typical electrochromic (EC) device consists of a solvent, electrolyte, electrode, EC material, and sacrificial agent. However, volatilization of the solvent results in the degradation of EC performance. In order to overcome this problem, we have developed an EC device using redox-active ionic liquids (RAILs) as an EC material and sacrificial agent. In addition, RAILs have ionic conductivity and fluidity around room temperature. Therefore, we expected that RAILs play roles of solute and electrolyte. In this presentation, we describe the fabrication of the EC devices consisting of the RAILs and there EC performance.

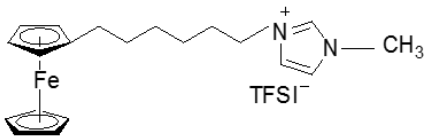

Fc

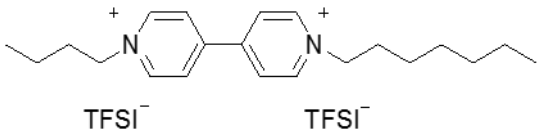

V

Methods

We designed a composite system consisting of a ferrocene- (Fc) and viologen-based (V) RAILs.[1,2] The composite RAILs molar ratios of **Fc** : **V** = 1 : 1 (**1**), 2 : 1 (**2**), 1 : 2 (**3**) mixed at were prepared with. The EC cell of each composite RAIL was fabricated with a symmetrical two-electrode configuration consisting of two indium thin oxide (ITO) glass substrate with the electrode area of 1.00 cm^2 defined using Himilan® thermal fusion bonding film (Dupont™). The separation of the two parallel ITO substrates was 25 μm. The EC performance of these EC cells were evaluated by electrochemical and electrospectroscopic measurements.

Results and Discussion

Figure 1a shows the cyclic voltammograms (CVs) of the composite RAILs at a scan rate of 20 mV s^{-1}. Four redox peaks were observed at ±0.878 and ±0.511 V for **1**, ±0.817 and ±0.531 V for **2**, and ±0.818 and ±0.557 V for **3**. These peak separations for both couples were 0.367 V for **1**, 0.286 V for **2**, and 0.261 V for **3**. The EC cell fabricated with **3** possesses the lowest resistance among them. However, the coloring efficiency (η) gave different results. Figure 1b shows the coloring efficiences of the composite RAILs at a voltage of 1.0 V and a wavelength of 540 nm. The Coloration efficiencies were calculated from the linear region of the Figure 1b. The η were 94 cm^2 C^{-1} for **1**, 84 cm^2 C^{-1} for **2**, and 77 cm^2 C^{-1} for **3**. In addition, high durability of composite RAILs without degradation was observed even when 13,000 cycles of potential step at a 30 second interval were applied between 0 and 1.0 V.

We will describe EC performance in detail in the presentation.

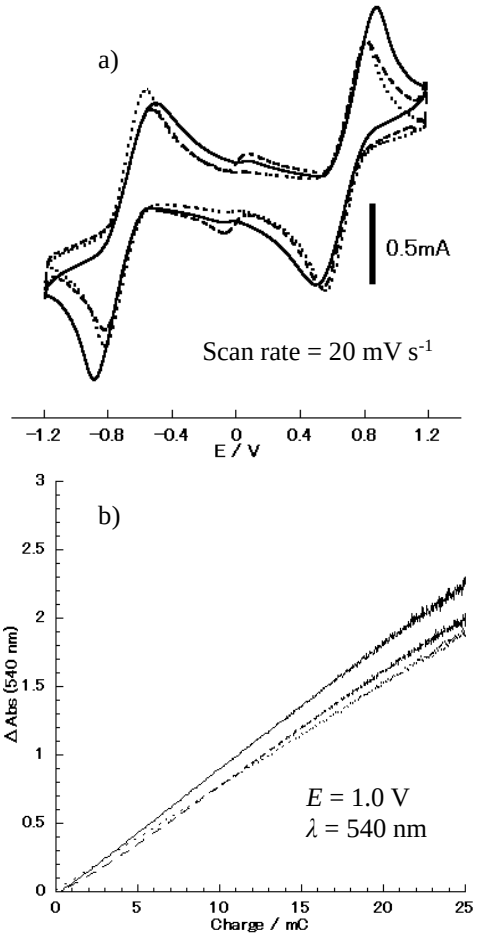

Fig. 1 CVs (a) and coloration efficences (b) of the composite RAILs : solid line, **1** ; dashed line, **2** ; dotted line, **3**.

References

[1] Gharib, B., Hirsch, A. *Eur. J. Org. Chem.* **2014**, 19, 4123-4136.
[2] Tahara, H., Furue, Y., Suenaga, C., Sagara, T. *Cryst. Growth. Des*. **2015**, 15, 4735-4740

P-08

Chemically modified apertures enhanced stability of free-standing bilayer lipid membranes

Daichi Yamaura 1, Daisuke Tadaki 1, Hideaki Yamamoto 2 and Ayumi Hirano-Iwata 1,3

1 Laboratory for Nanoelectronics and Spintronics, Research Institute of Electrical Communication, Tohoku University, 2-1-1 Katahira, Aoba-ku, Sendai, Miyagi, 980-8577, Japan.
2 Frontier Research Institute for Interdisciplinary Sciences, Tohoku University, 6-3 Aramaki-Aza-Aoba, Aoba-ku, Sendai, Miyagi, 980-8578, Japan.
3 Advanced Institute for Materials Research, Tohoku University, 2-1-1 Katahira, Aoba-ku, Sendai, Miyagi, 980-8577, Japan.
E-mail: daichi.yamaura.t5@dc.tohoku.ac.jp

[Introduction]

Ion channels are membrane proteins that play crucial roles as gated pores in the cell membranes. Incorporation of ion channels in artificial bilayer lipid membranes (BLMs) provides a well-defined system for studying the functions of ion channels and screening drug effects acting on them. However, the instability of BLMs hindered the widespread application of the BLM systems. For improving the stability of BLMs, we proposed combination of BLM formation and microfabrication.[1] Micro-apertures having nano-tapered edges were fabricated in silicon dioxide (SiO_2)/silicon nitride (SiN) septa and BLMs formed in the aperture showed high mechanical stability. In this study, we tried to further stabilize the BLMs by surface modification of the SiO_2/SiN septa. BLMs were formed in SiO_2/SiN septa which had been treated with various modifiers and the relationships between the properties of the modified surfaces and the stability of BLMs were investigated.

[Exeperimental]

SiO_2/SiN/Si substrates were immersed into solutions containing respective silane coupling agents (Table 1) in order to modify the surface of the substrates. Water and hexadecane contact angles, and diffusion coefficient of lipid monolayers formed on the silanized SiO_2/SiN/Si substrates were evaluated. Microapertures were fabricated in SiO_2/SiN/Si chips according to the procedure described in ref [2]. The fabricated chips were silanized in the same manner as the SiO_2/SiN/Si substrates. BLMs were formed in the SiO_2/SiN/Si chips by the folding method and the stability of the BLMs were evaluated in terms of tolerance to an applied fcentrifugal force (40 x *g*) with and without proteoliposomes and tolerance to movements of buffer solutions surrounding BLMs.

[Results and Disucssion]

SiO_2/SiN/Si substrates modified with long perfluorocarbons (PFDS, PFDDS) showed high lipophobicity, while those modified with a short perfluorocarbon (FPDS) or a short hydrocarbon (CPDS), showed low lipophobicity. Lipid monolayers formed on the high lipophobic surface showed high diffusion coefficient. Then we prepared BLMs in SiO_2/SiN/Si chips treated with (PFDS) and (CPDS), and compared their mechanical stabilities. It was found that the stability of the BLMs formed in PFDS-modified chips was superior to those formed in CPDS-modified ones in terms of tolerance to an applied cenrifugal force with and without proteoliposomes and tolerance to movement of buffer solutions induced by repetitive water aspiration. These results demonstrate that the stability of free-standing BLMs is dependent on the surface property of the substrate that suspends the BLMs and that BLMs on highly lipophobic surfaces are mechanically stable. Therefore, this appoarch for the formation of highly stable BLMs should contribute to development of high-throughput drug screening devices for ion channel proteins.

[References]

[1] A. Hirano-Iwata, et al. *Langmuir* **26** (2010) 1949–1952.
[2] D. Tadaki, et al. *Sci. Rep.* **7** (2017) 17736.

This work was supported by CREST program of the Japan Science and Technology Agency.

Table 1 Silane coupling agents

OTS	octadecyltrichlorosilane
PFDS	(tridecafluoro-1,1,2,2-tetrahydrooctyl)dimethylchlorosilane
PFDDS	(heptadecafluoro-1,1,2,2-tetrahydrodecyl)dimethylchlorosilane
PFTS	(tridecafluoro-1,1,2,2-tetrahydroocty)ltrichlorosilane
CPDS	3-cyanopropyldimethylchlorosilane
FPDS	3,3,3-trifluoropropyldimethylchlorosilane

P-09

Ion channel array based on silicon (Si) microfabrication

Ryusuke Miyata, Daichi Yamaura, Daisuke Tadaki, and Ayumi Hirano-Iwata

Tohoku University, 1-1 Katahira, Aoba-ku, Sendai 980-8577, Japan
Tel: +81-22-217-6344, Fax: +81-22-217-5967
*e-mail: ryusuke.miyata.s2@dc.tohoku.ac.jp

1. Introduction

Ion channel proteins are one of the primary targets in drug discovery. Recording ion-channel currents represents an efficient method for investigating the functions of ion channels and screening the drug effects acting on them. Development of high-throughput recording systems for ion-channel currents is of great importance to improve the screening efficiency. Several platforms for simultaneous recordings of ion-channel currents have been proposed, including patch-clamp arrays and bilayer lipid membrane (BLM) arrays.[1] Although the patch clamp method is considered to be the gold standard for evaluating channel activities, the method also has limitations in that the observed currents are dependent on the condition of the target cells.[2] Therefore, the development of an alternate method for recording ion channel activities would be highly desirable. Reconstitution of ion channels in artificial free-standing BLMs is another approach for recording ion channel activities under chemically controlled conditions. However, instability of BLMs reduces experimental efficiency and prevent them from being widely used. Recently, we succeeded in formation of mechanically stable BLMs which were formed in microfabricated silicon (Si) chips.[3,4] In the present study, we have extended this stable BLM system to a 16-well array format. Simultaneous recordings of channel activities from the multiple BLMs were investigated by using a human *ether-a-go-go*-related gene (hERG) channel as a representative example.

2. Experimental

Microapertures were fabricated in a Si substrate, one side of which was covered with a ~220 nm thick Si_3N_4, based on photolithography and isotropic wet etching, according to the procedures in ref. 5. The fabricated Si chips was silanized with (tridecafluoro-1,1,2,2- tetrahydrooctyl) dimethylchlorosilane. 16 chips thus treated were arrayed in a 4x4 format in the middle of a recording chamber (Fig. 1). 16 BLMs were then formed by the monolayer folding method. The hERG channels were incorporated into the BLMs and their channel currents was measured using an Axopatch 200B patch-clamp amplifier (Molecular Devices).

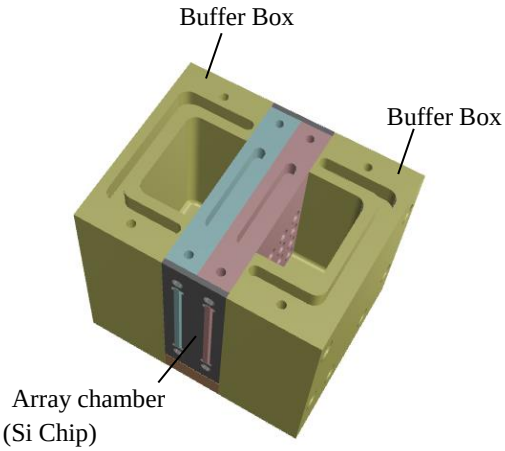

Fig.1. Schematic drawing of an array chamber system.

3. Result and Discussion

We first investigated the simultaneous formation of multiple BLMs in the present array system. BLMs were automatically formed by folding up two lipid monolayers in the apertures using a syringe pump. BLMs having the resistance higher than 100 GΩ were successfully formed in the array system. We then extended this system to recording activities of hERG channel proteins. This channel has attracted attention because many kinds of drugs have been found to adversely block the hERG channels, inducing potentially life-threatening arrhythmias. The hERG channel was extracted from HEK 293 cell lines expressing the channel and incorporated into the BLM array via vesicle fusion. Stepwise currents with a single channel conductance of 12 pS were recorded. This conductance level was similar to those (11-13 pS) reported for hERG channels in a BLM reconstitution system.[4] In addition, multiple channel currents were simultaneously recorded from different wells. These channel activities were blocked after addition of E-4031, a specific inhibitor for the hERG channel. These results demonstrate that hERG channel activities in different BLMs were parallelly recorded in the array system. Such BLM-based hERG-channel array system will have a potential to serve as a new high-throughput platform that would be an alternative to the conventional patch-clamp method

This work was supported by the JST-CREST program (JPMJCR14F3).

4. References

[1] A. Hirano-Iwata, et al., Chem. *Asian J.* **10**, 1266–1274 (2015).
[2] J. Dunlop, et al., *Nat. Rev. Drug Discov.* **7**, 358–368 (2008).
[3] A. Hirano-Iwata, et al., *Langmuir*, **26**, 1949 (2010).
[4] A. Oshima, et al., *Anal. Chem*., **85**, 4363−4369 (2013).
[5] D. Tadaki, et al, *Sci. Rep.*, **7**, 17736 (2017).

P-10

Ferrocenyl-Alkyl Mixed Self-Assembled Monolayer Formed on Hydrogen-Terminated Silicon

Toru Utsunomiya, Yuki Takatani, Takashi Ichii, and Hiroyuki Sugimura

Department of Materials Science and Engineering, Graduate School of Engineering, Kyoto University,
Yoshida-hommachi, Sakyo-ku, Kyoto, 606-8501 Japan
Tel: + 81 - 75 - 753 - 5990, Fax: +81- 75 -753 - 5484
E-mail:utsunomiya.toru.5v@kyoto-u.ac.jp

Self-assembled monolayers (SAMs) formed on solid surfaces have been intensively studied as a key component for controlling the surface properties[1]. In particular, the functionality of the terminal group can be used to engineer surface properties for specific applications. Mixed SAMs increase the flexibility of the surface design. These layers are formed from mixtures of precursors with different terminal groups. However, in mixed SAMs, the mole fraction on the surface is not necessarily the same as the mole fraction in the solution, and homogeneity can become an issue[2,3]. Several factors influence the character and composition of SAMs including the relative concentrations, the solvent, the terminal functionality and the chain length. In this study, we report a self-assembly of a mixture of 11-Ferrocenyl-1-undecanethiol (FUT) and octanethiol (OT) on the hydrogen-terminated Si(111) (H-Si).

We performed the photochemical grafting of these precursors on H-Si substrates (n-type, Resistivity: 1-10 Ω•cm). The prepared H-Si substrate was transferred to a quartz photocell containing deoxygenated decane solution with 5 mM FUT and OT, and irradiated with visible light (400 mW cm^{-2}) for 4 h under nitrogen purging. The prepared samples were characterized by using atomic force microscopy (AFM), X-ray photoelectron spectroscopy (XPS), and cyclic voltammetry (CV).

Fig. 1 shows an AFM topographic image of the Si substrate treated with the FUT and OT mixed solution. The step-terrace structure similar with the H-Si(111) substrate was confirmed, showing the homogeneous SAM formation on H-Si(111). A CV measurement result of the prepared sample under the visible light irradiation is shown in Fig. 2. Since the peak potential was obtained in the vicinity of -40 mV, it was shown that the Si substrate surface covered with mixed SAM also has redox activity similar to that of FUT-SAM. Integration of the oxidation and reduction currents resulted in an effective charge of the surface-confined redox process, which can show the coverage of the Ferrocene moieties. The estimated coverage derived from Fig. 2 is 1.3×10^{-10} mol cm^{-2}, which is around 40% coverage of un-mixed FUT-SAM case (3.3×10^{-10} mol cm^{-2}). The one distinct current peak at CV also indicates that the environment of the surface-confined Fc-moieties is rather homogeneous on the H-Si(111) surface.

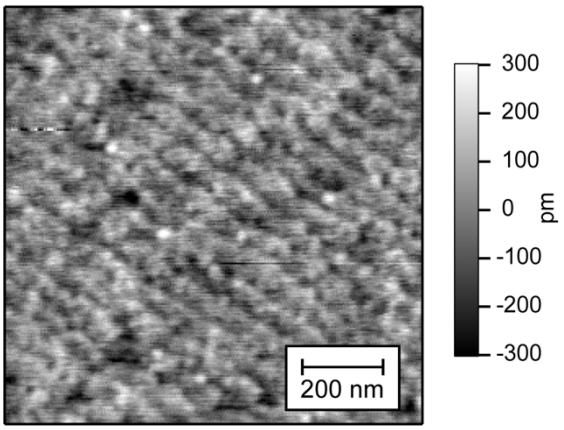

Fig. 1 AFM image of FUT-OT mixed SAM

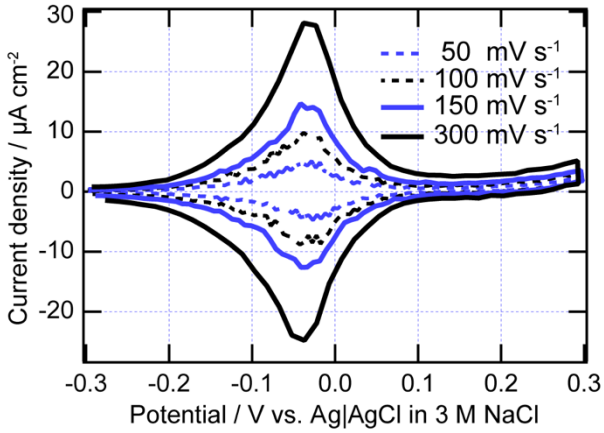

Fig. 2 Cyclic Voltammogram of FUT-OT mixed SAM

References

[1] J. C. Love, L. A. Estroff, J. K. Kriebel, R. G. Nuzzo, and G. M. Whitesides, "Self-assembled monolayers of thiolates on metals as a form of nanotechnology" Chem. Rev., vol.105, no.4, pp.1103-1169, 2005.

[2] L. Y. S. Lee, T. C. Sutherland, S. Rucareanu, and R. B. Lennox, "Ferrocenylalkylthiolates as a probe of heterogeneity in binary self-assembled onolayers on gold" Langmuir, vol.22, no.9, pp.4438-4444, 2006.

[3] S. Fujii, S. Kurokawa, K. Murase, K. Lee, A. Sakai, and H. Sugimura, "Self-assembed mixed monolayer containing ferrocenylthiol molecules: STM observations and electrochemical investigations" Electrochim. Acta, vol.52, no.13, pp.4436-4442, 2007.

P-11

Probing internal electric field in organic photoconductors by using electric-field-induced optical second-harmonic generation

Dai Taguchi[1], Takaaki Manaka[1], Mitsumasa Iwamoto[1],
Kazuko Sakuma[2], Kaname Watariguchi[2], and Masataka Kawahara[2]

[1] *School of Engineering, Tokyo Institute of Technology*
2-12-1 O-okayama, Meguro-ku, Tokyo, 152-8552 Japan
Tel: + 81 - 3 - 3433 - 2191, Fax: +81- 3 -3433 - 2191
E-mail: iwamoto@pe.titech.ac.jp

[2] *Specialty Chemicals Development Center, Canon Inc.*
4202 Fukara, Susono, Shizuoka, 410-1196 Japan

Organic photoconductors (OPC) have been an important research and development topics for production of high quality electrophotographic images. Among them are single-layer organic photoconductors, double-layer photoconductors, and so on. Electrical measurements such as Time-of-flight (TOF) measurement and Thermally stimulated current (TSC) measurement are conventional for characterizing these photoconductors. However, it is of hard task to selectively probe carriers in one layer of the multiple layers such as double-layer OPC. We have been developing an electric-field-induced optical second-harmonic generation (EFISHG) measurement, which is available for selectively probing carrier behaviors in organic semiconductor devices. Using the EFISHG, the specific operation of organic field-effect transistors (OFETs), organic light-emitting diodes (OLED), and others, having multilayer structure, has been investigated [1,2]. In this presentation, we show the EFISHG results of multilayer type organic photoconductor, where excess charge accumulation due to photo-conducting effect is directly probed.

OPCs used here have a double-layer structure with charge generation (CG) layer (thickness, d_1=0.3 μm) and transport (CT) layer (d_2=10 μm) coated on an Al electrode grounded electrically. Indium-tin-oxide electrode was deposited as a top electrode to apply external voltage in reference to the Al electrode. In the EFISHG measurement, probing laser wavelength was set at 1140 nm and optical second-harmonic generation signals at the wavelength of 570 nm was detected. Note that EFISHG utilizes near-infrared laser beam as a probe light which do not lead to photoconduction processes. In this set-up, we can selectively probe electrostatic field formed in the CG layer in the double-layer OPC. The EFISHG signal is a nonlinear optical process and its signal intensity $I_{2\omega}$ change in proportion to second harmonic nonlinear polarization $P_{2\omega}$ as $I_{2\omega} \propto \left|\vec{P}_{2\omega}\right|^2 = \left|\varepsilon_0 \vec{\chi}^{(3)} : \vec{E}_0 \vec{E}_\omega \vec{E}_\omega\right|^2$ (ε_0: dielectric constant of vacuum, $\vec{\chi}^{(3)}$: the third order susceptibility tensor, $\vec{E}_0$: electrostatic field, $\vec{E}_\omega$: electric field of the probing laser beam). The electrostatic field $\vec{E}_0$ is formed in the CG layer as $E_0 = \left|\vec{E}_0\right| = 1/d_1 \cdot Q_s/(C_1 + C_2)$ where C_1 and C_2 are parallel electrode capacitance of CG and CT layer, respectively, and Q_s is charge density accumulated at CG/CT interface. EFISHG results in dark and under illumination showed that holes excessively accumulate at the CG/CT interface (Q_s = 5.2 nC/cm^2) under red light illumination (635 nm, 26 μW/cm^2) and its density increased by increasing illumination intensity from 26 – 43 μW/cm^2. This result evidently shows that CG layer under red light illumination behaves like an electrical conductor due to photo-carrier generation, and holes excessively accumulate at the CG/CT interface, followed by a hole transportation across the CT layer. EFISHG measurement under ultra-violet light illumination clarifies that photovoltaic effect is also responsible for electric field formation in CG layer at short wavelength of 405 nm.

In summary, EFISHG is available for directly probing charge accumulation and transportation in multilayer OPC.

References

[1] M. Iwamoto, T. Manaka, D. Taguchi, (Invited Review Paper), Jpn. J. Appl. Phys., Vol. 53, pp. 100101/1-11, 2014.
[2] M. Iwamoto, T. Manaka, D. Taguchi, (Invited Review Paper), IEEJ Trans. Fundamentals and Materials, Vol. 136, pp. 678-684, 2016. [in Japanese]

P-12

Visualizing distribution of triboelectric charge on PMDA-ODA polyimide film by using optical second-harmonic generation imaging technique

Dai Taguchi, Takaaki Manaka, Mitsumasa Iwamoto,

School of Engineering, Tokyo Institute of Technology
2-12-1 O-okayama, Meguro-ku, Tokyo, 152-8552 Japan
Tel: + 81 - 3 - 5734 - 2191, Fax: +81- 3 -5734 - 2191
E-mail: iwamoto@pe.titech.ac.jp

Triboelectric generators are attracting much attention as the next-generation eco-friendly electrical power source. Recently, material processing technology has greatly advanced and triboelectric generator with high power density over 30 mW/cm^2 has been reported. Many new applications such as interactive books and power management circuit will be realized in our daily life by utilizing triboelectricity as a power source. Since the discovery of electrification of materials, control of triboelectricity has been a very important research topic which should be explored in industries in the fields of electrophotography, plastic films, pharmacy and others. Accordingly, concept of triboelectric series, idea of interface states and others have been proposed for deep understanding of electrification. Nevertheless, the complexity of the electric phenomena induced by triboelectrification has lead us to a puzzling situation. We need to develop a novel experimental technique that can explore triboelectric charges microscopically. The authors have been developing a novel optical method of optical second harmonic generation measurement system that can identify origins of triboelectric charges and visualize the spatial distribution of the charges in materials.

We here demonstrate that our developed optical second harmonic generation measurement system can probe the triboelectric charges and distinguish the charges due to electron displacement and charges due to dipole orientational ordering, by choosing appropriate optical wavelength of the probing laser beam. Kapton-type polyimide tape was used as a triboelectric generation layer. After rubbing this film surface by metal Ni foil, the film surface was negatively charged (V_S ~ -500 V). The SHG optically visualized the spatial triboelectric patterns of electron transfer and orientational dipole ordering of this charged polyimide surface. We choose laser wavelength 1140 nm (SHG wavelength: 570 nm) to selectively visualize electron transfer, and 570 nm (SHG wavelength: 285 nm) for visualizing orientational ordering of dipoles of polyimide. Figure 1 shows the optical arrangement of the SHG measurement for visualizing triboelectric generation process. Figure 2 is an example of visualized charge distribution generated after rubbing the Kapton-type polyimide tape, where the probe laser wavelength was set at 1140 nm to visualize the triboelectric pattern due to electron displacement.

In summary, SHG measurement is available to visualize triboelectric charge patterns, and is a powerful method for identification of origins of triboelectric charge carriers microscopically.

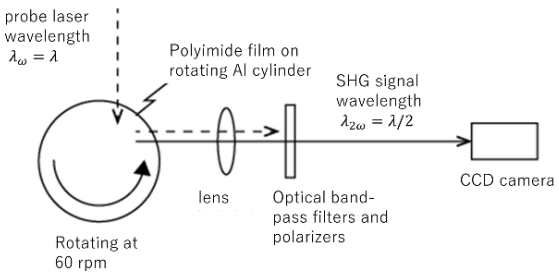

Figure 1. SHG measurement setup for visualizing triboelectric charges.

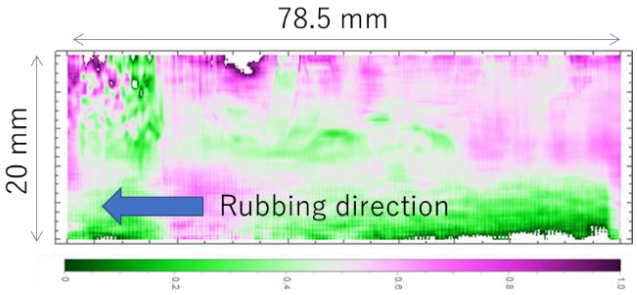

Figure 2. SHG image visualizing tirboelectric charge distribution. The image was taken by 1 s meanwhile polyimide film is rubbed in the direction of the arrow.

References

[1] M. Iwamoto, T. Manaka, D. Taguchi, (Invited Review Paper), Jpn. J. Appl. Phys., Vol. 53, pp. 100101/1-11, 2014.
[2] M. Iwamoto, T. Manaka, D. Taguchi, (Invited Review Paper), IEEJ Trans. Fundamentals and Materials, Vol. 136, pp. 678-684, 2016. [in Japanese]

P-13

Decomposition of Dipicolinic Acid Using RF Oxygen Plasma Sterilizer

S. Hori, N. Hayashi

Interdisciplinary Graduate School of Engineering Sciences, Kyushu University,
6-1 Kashugakouen, Kashuga-shi, Fukuoka, 816-0943 Japan
*Tel: + 81 - 92 - 583 - 7547, Fax: +81- 3 -3433 - ****
E-mail: 2ES17222T@s.kyushu-u.ac.jp

1. Introduction

Recently, plasma sterilization method at low-temperature suppressing harmful gas has attracted much attention. Detailed mechanism of spore forming bacteria inactivation owing to plasma irradiation has not been clarified. One of the inactivation mechanism of bacterial spore is speculated to be decomposition of dipicolinic acid (DPA) that is a major substance of the spore. DPA occupies 10-15% of the dry weight of spores. DPA forms Ca-DPA chelate during sporulation, and there is relationship between the dissociation of Ca-DPA and the loss of heat resistance of the spore [1]. If DPA is decomposed by active oxygen species, it indicates that decomposition of DPA may be one mechanism of spore inactivation. In this study, the decomposition characteristics of DPA is investigated to clarify the inactivation mechanism of spore.

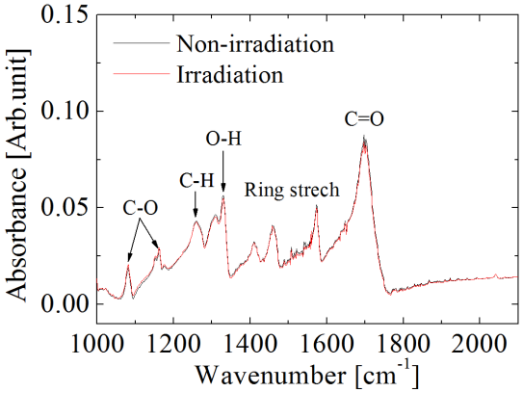

Fig.1. IR spectra of dipicolinic acid.

2. Experimental procedure

Dimension of the vacuum vessel is 200 mm in inner diameter, 500 mm in length and 17 L internal volume. Inside the vessel, the electrode is set parallel to object to be sterilized and distance between RF discharge electrode and object to be sterilized is 47 mm. After evacuation, oxygen gas is introduced and radio-frequency power (13.56 MHz) is supplied to the electrode to generate capacitively coupled plasma (CCP). Increase of the temperature of target to be sterilized due to heating of the electrode is suppressed by the water circulation system inside the electrode.

Dipicolinic acid aqueous solution with a concentration of 3.0×10^{-5} g/cm^2 is coated on a CaF_2 plate and dried. DPA sample is enclosed in a sterilized bag and irradiated by the oxygen plasma. Irradiation conditions are RF input power of 130 W, irradiation time of 50 minutes and pressure ranged from 50 to 400 Pa. The decomposition rate is estimated from the largest C═O bond peak of dipicolinic acid at around 1700 cm^{-1} in IR spectra those are measured by fourier transform infrared spectrometer (FTIR). A paper-type biological indicator (BI) which is an indicator for sterilization assurance is sterilized in same experimental condition and decomposition rate of DPA and sterilization result are compared.

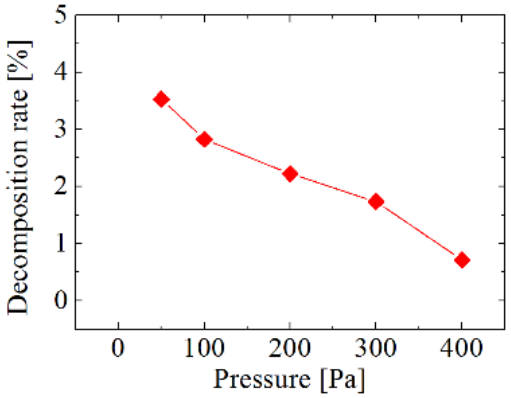

Fig.2. Decomposition rate of DPA.

3. Results and discussion

Figure 1 shows IR spectra of DPA after plasma irradiation according with non-treated DPA. No significant change in DPA composition is observed before and after plasma irradiation, and formation of by-products is not observed in IR spectra. Figure 2 shows decomposition rate of dipicolinic acid changing oxygen pressure. The C═O bond in dipicolinic acid is decomposed with pressure decrease. Maximum decomposition rate is 3.5 % that obtained at 50 Pa, lowest pressure in this experiment. However, the tendency of this result is different from the tendency of the result of sterilization result of BI. Decomposition of C=O is probably owing to dissociation of the C=O double bond by collision with high energy particles. Another inactivation mechanisms of spore have been also investigated as well as decomposition of dipicolinic acid. Possible factors of inactivation mechanism of spores include destruction of spore due to collision with high energy particles, denaturation of proteins constituting bacterial spore and DNA damage due to active oxygen species and UV light.

Reference

[1] G.W.Gould, G.J.Dring, Advance in Microbial Physiology, 11,137-164(1974)

P-14

Ozone Concentration Effect on Sterilization of Fruit Surface

K. Yamamoto, N. Hayashi

Interdisciplinary Graduate School of Engineering Sciences, Kyushu University,
6-1 Kasugakouen, Kasuga, Fukuoka 816-8580, Japan
Tel: + 81 - 92 - 583 - 7651
E-mail:2ES17208W@s.kyushu-u.ac.jp

Strawberry was irradiated by ozone produced in atmospheric air plasma to keep its freshness for several weeks. Sterilization effect depends on the ozone concentration when the CT value is fixed. In case of high concentration of ozone irradiation, colony count measurement of yeast and mold is less than 10% of control.

1. Introduction

Recently, plasma application technology has attracted attention as the method of sterilization of fruit surface without pesticide [1]. CT value of ozone, which is the product of ozone concentration and irradiation time, is used generally as the control parameter of ozone treatments [2]. However, the sterilization effect and the damage to agricultural products have not been investigated keeping the CT value constant, when the ozone concentration is changed. In this study, the dependence of the ozone concentration on the sterilization effect of strawberry is determined keeping the CT value constant. Also, sterilization effect by active oxygen species as well as is evaluated.

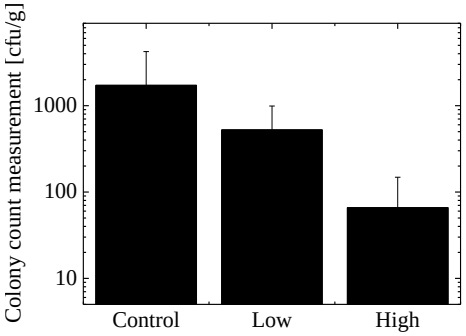

Fig. 1 Colony count measurement of each irradiation condition.

2. Experimental procedure

The surface discharge is a kind of DBD occurring along a metal electrode on surface of thin ceramics as a dielectric. Strawberry is used for model fruits. After the plasma irradiation, the colony of yeast and mold of strawberry surface are measured. In addition, decay ratio are measured after preserving at 15 °C for one week. In this study, ozone CT values were set at 1500 ppm*min. When the low concentration irradiation, the ozone concentration was about 50 ppm and the irradiation time was set to 35 min to keep the above CT values. For the ozone concentration was kept to 200 ppm that is the high concentration mode, the irradiation period was 9.8 min.

Table 1 Decay ratio of each irradiation condition.

	Control	**Low**	**High**
(Decayed sample) / (All sample)	11/16	11/16	7/16

3. Result and discussion

Figure 1 shows colony count measurement of each irradiation condition. In both high and low concentrations colony count measurement is less than control. Especially, in case of high concentration, it is less than 10% of control. Typically, it is effective as a sterilization method if 90% sterilization can be achieved. So, high concentration irradiation meet the sterilization criteria. Table 1 shows decay ratio of each irradiation condition. Control and low concentration of decay ratio were equal. High concentration was lowest and about 50% strawberry didn't decay. Yeast and mold have thick cell walls and are resistant to oxidation by ozone. [3] At high concentration, ozone collides with the cell wall of the microorganism intensively in the short time, so the sterilization effect is thought to be high.

4. Conclusion

It is found that there is ozone concentration dependency in agricultural product sterilization effect. And, from the result of decay ratio, it was confirmed that the whole fruit surface was irradiated with ozone.

References

[1] N. Hayashi, Y. Akiyosi, Y. Kobayashi, K. Kanda, K. Ohshima, M. Goto:, Vacuum. 88 , 173-176, (2013).
[2] H.Sugimitsu, IEEJ, 114, 637-639, (1994).
[3] S.Naitou: Jpn.J.Food Microbiol. **11**(1994), 11-17

P-15

Characteristics of narrow tubular medical devices sterilization by using active oxygen species with low-pressure plasma

Yu-shian Liao, Shogo Miura and Nobuya Hayashi

Interdisciplinary Graduate School of Engineering Sciences, Kyushu University,
6-1 Kasuga-kouen Kasuga, Fukuoka, 816-8580 Japan
Tel: + 81 - 92 - 583 - 7649
E-mail:2ES17218S@s.kyushu-u.ac.jp

Introduction

In the hospital, the sterilization of medical equipment is important to prevent infections. For reusing no heat-resistance devices at medical setting, sterilization treatment under low temperature circumstance is required. Low temperature sterilizer such as EOG and hydrogen peroxide sterilizers can treat no heat-resistance devices but narrow tubes such as catheters and endoscopes are difficult to be sterilized. Therefore, no sterilization method for interior of narrow tubes has been established yet. Recently, plasma sterilization methods for non-heat resistive narrow tubes have been studied [1, 2]. The plasma sterilization methods use no toxic gas such as EOG. In this study, we have investigated sterilization characteristics of narrow tubular medical devices by using the low pressure oxygen plasma to determine sterilization factors and period required for the sterilization.

Table 1. Sterilization results changing treatment period.

Catheter size	60 min	120 min	180 min
100 mm	3 / 3	3 / 3	-
200 mm	2 / 3	3 / 3	3 / 3
300 mm	0 / 3	2 / 3	3 / 3
500 mm	0 / 3	0 / 3	1 / 3

Successful sterilization / Total number of BI

Experimental apparatus

A cylindrical stainless chamber with 210 mm of inner diameter and 500 mm of length is used for the plasma production. The chamber is evacuated by a vacuum pump and oxygen gas is filled to designated pressure. RF power of 13.56 MHz and 80W is applied to the RF electrode in the chamber to generate a capacitively coupled plasma. The process challenge device (PCD) is placed on the 130 mm below the top of electrode to confirm sterilization. PCD consists of a silicon rubber tube and a capsule connected to the edge of the tube. The dimension of the tube used for experiment is 4mm inside diameter and 100 mm to 500 mm in length. Sterilization capability is confirmed by a biological indicator (BI), which is consists of thermophilic spore of G. *stearothermophilus* with population of 10^6. Amount of active oxygen species reaching the thermophilic spore in the capsule is measured by the color of chemical indicator (CI). Since ions in the plasma may damage medical devices, PCD is enclosed in a sterilization bag for preventing the ion impact during plasma treatment.

Results and discussion

The largest color change of the CI, which indicates the maximum production of active oxygen, is observed at the oxygen gas pressure of 20 Pa when pressure varies from 20 Pa to 140 Pa. Since the pressure dependence on the sterilization rate of the BI has similar tendency to the CI color variation, active oxygen species could be one of the sterilization factor for tubular devices sterilization. As shown in Table 1, sterilization of the BI is successful for 60 and 120 min, when BIs are placed at 100 and 200 mm in the tubes with diameter of 4 mm, respectively. It is necessary to be irradiated for 180 min to sterilize BI in the 500 mm length tube. Since color change of the CI is not significant in this case, high energy active oxygen species those change dyes of the CI cannot reach the PCD until 180 min treatment. Therefore, one of candidate for the sterilization factor in 4 mm catheter would be the active oxygen species which will oxidize with lower oxidizing energy. Effects of heat and ultraviolet radiation have also been investigated. BI test results indicate that the 85 ℃ heat treatment, which is higher temperature than that of the plasma sterilization, and the ultraviolet lamp irradiation cannot sterilize the tubular medical device.

Conclusion

Sterilization of the BIs is successful for 60 and 180 min using 100 and 500 cm tubes, respectively, using low-pressure oxygen plasma. According to the color change of the CI, the sterilization factors in the oxygen plasma are active oxygen species with lower oxidizing energy.

References

[1] A. Yonesu, K. Hara and N. Hayashi, Japanese Journal of Applied Physics 55, 07LG08 (2016)
[2] S. Kitazaki, A. Tanaka and N. Hayashi, Vacuum 110, 217- 220(2014)

P-16

Sterilization of Spore-forming bacteria in Small Vial Using Electron Cyclotron Resonance Plasma

Tatsuya NISHIKAWA[1], Nobuya HAYASHI[1] and Akira YONESU[2]

[1]*Interdisciplinary Graduate School of Engineering Science, Kyushu University, 6-1 Kasuga-Koen, Kasuga-shi, Fukuoka 816-8580, Japan*
[2] *Department of Electrical and electronics Engineering, University of the Ryukyus, 1 Senbaru, Nishihara-cho, Okinawa 903-0213, Japan*
Tel: + 81 -92 – 583 - 7649
E-mail: hayashin@aees.kyushu-u.ac.jp

Abstract

The surface sterilization of spore-forming bacteria using pulsed Electron Cyclotron Resonance (ECR) plasma was investigated. The pulsed ECR plasma is produced in small vials with a volume of 20 ml. A biological indicator, *G. stearothermophilus*, of 3.0 ×10^5 spores was sterilized for 13 min 53 sec maintaining a temperature of vial 65 ℃ by adjusting the microwave power pulsed conditions.

1. Introduction

Plasma sterilization techniques have excellent characteristics such as short treatment times, non-toxicity, and low thermal damages to the materials to be sterilized. In our previous study, we reported that the characteristics of surface sterilization using Electron Cyclotron Resonance (ECR) plasma. ECR plasma has high electron temperature and high plasma density compared with the other plasma. In the present study, we investigated the surface sterilization of vial interior using pulsed ECR plasma to confirm the influence of microwave power pulsed conditions (pulse width and pulse frequency) on plasma sterilization efficiency and the treatment temperature.

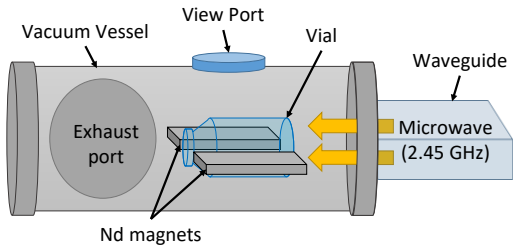

Fig.1 Schematic of experimental set up.

Table.1 Antibacterial effects of pulsed ECR plasma

Pulse Width [msec]	Pulse Frequency [Hz]	Average Power [W]	Temperature [℃]	Sterilization Result
5	6	15	85～90	–
2.5	12	15	85～90	–
2.5	6	7.5	60～65	+
1.5	10	7.5	60～65	– ++
1	15	7.5	65～70	–
1	12	6	～65	– – –
1	10	5	～60	+

(+: Failure –: Success)

2. Experimental Apparatus and Method

The experiment was performed in a stainless-steel cylindrical vacuum chamber which contains a pair of rectangular Nd magnets (54 × 5 × 15 mm^3) and a small vial (Φ 30 × 60 mm 20 ml), as shown in Fig. l. These magnets are aligned parallel to each other with a distance of 37mm and the vial is placed between two magnets. The magnetic field to realize ECR (875 G) is generated at a distance of 3 mm from the inner surface of the vial. The working gas is air. When microwave with frequency of 2.45 GHz is introduced into the vacuum chamber, the ECR plasma was produced around the ECR point. The sterilization test was conducted using the biological indicators (BI) with spore of *Geobacillus Stearothermophilus*, ATCC7953, of population of 3.0 ×10^5 CPU/carrier. The BI was placed on the inner surface of the vial. After incubation, the spore survival was determined by observing the color change of the tryptic soy broth. The temperature of the vial during the treatment was measured by the thermolabel.

3. Experimental Result

The ECR plasma is generated in a small vial by controlling the magnetic field distribution and the electric field. To confirm the influence of pulsed conditions of microwave on the sterilization efficiency and the treatment temperature, sterilization tests using a BI in the small vial are performed. The peak microwave power of 500W, total plasma exposure time of 10 sec and gas pressure of 0.05 Pa are kept at constant. The result is shown in Table 1. Minus signs indicate the success of sterilization. As shown in the table, the temperature of vial decreased with decreasing the average power. The sterilization result was deferent with pulse width and pulse frequency at the same average power. As a result, we succeeded sterilization of *G. Stearothermophilus*, placed in the small vial with a volume of 20 ml under the low temperature of 65°C by being exposed to pulsed ECR plasma with pulse width 1 msec and pulse frequency 12Hz.

P-17

Fabrication Using 2-step and Air-Flowing Process for Organic Perovskite Solar Cells

Yoshiki Kondo, Masaki Kawai, Vincent Obiozo Eze, Yoshiyuki Seike, Tatsuo Mori
Aichi Institute of Technology
Yachigusa, Yakusa-cho, Toyota, 470-0392 Japan.
Email: t2mori@aitech.ac.jp

Introduction

The power conversion efficiency (PCE) of the organic perovskite solar cells (OPSCs) sharply rises and it reaches till 22% in 2016. OPSCs are attracted attention as next generation solar cells because they can be easily fabricated by a coating process. Our group reported that the devices with high reproducibility and high PCE can be used by air flow during coating[1,2]. In a one-step method, a perovskite film on a substrate is directly formed the solution that dissolving all materials. In a two-step method, a perovskite film is formed after the formation of a PbI_2 film. Therefore, the residual PbI_2 layer was observed in OPSCs fabricated by the two-step method. In this report, we tried the optimization of PbI_2 layer using XRD measurement.

Results and discussion

The thickness of the PbI_2 layer was changed by changing the concentration of PbI_2 solution. The thickness of the perovskite layer fabricated from PbI_2 concentration of 0.6, 0.8 and 1 mol/L under the air flow was 148 nm, 269 nm, and 333 nm, respectively. Fig. 1 shows XRD patterns of perovskite specimens. The crystal size of PbI_2 and perovskite crystals in PbI_2 and perovskite layers was calculated by Scherrer's equation. In the perovskite layer of 148nm-thick PbI_2 layer, the intensities of residual PbI_2 and perovskite region decreased by 49% and 46%, respectively, as compared with the perovskite layer of 333nm-thick PbI_2 layer. On the other hand, the crystal sizes of residual PbI_2 and perovskite decreased by 47% and 33%, respectively, as compared with the perovskite layer of 333nm-thick PbI_2 layer.

As the initial PbI_2 layer became thin, the thickness of the residual PbI_2 layer became thin after the perovskite was transferred. Since the crystal size of residual PbI_2 of 12～23nm is smaller than the crystal size of the PbI_2 single layer of 19～26nm, it is possible that the perovskite will be sea-island structure in the residual PbI_2 layer and then the PbI_2 crystal will shrink.

Fig. 2 shows the J-V characteristics of the devices. The PCE decreased when the thickness of the initial PbI_2 layer was thin. However, the PCE of the perovskite layer of 269nm-thick PbI_2 layer was slightly higher than the 333nm-thick perovskite layer. The residual PbI_2 layer in the perovskite layer of 269nm-thick PbI_2 layer was the thinnest of the three specimens. However, the transfer from the PbI_2 layer to the perovskite layer has not been optimized yet.

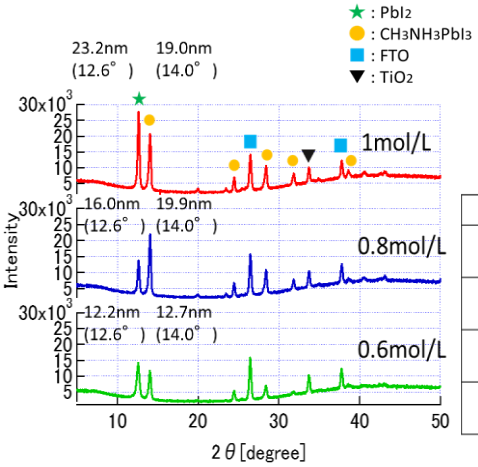

Fig. 1 Effect of PbI_2 thickness on the XRD patterns of perovskite layer with air flow. Crystal sizes of PbI_2 (12.6°) and perovskite (14.0°) are shown near peaks.

Table 1 XRD intensity and crystal size of PbI_2 and perovskite in perovskite layers.

Initial PbI_2 [nm]	229	175	86
XRD peak PbI_2 ($\times 10^3$)	27.7	13.4	14.2
Crystal size of PbI_2[nm]	23.2	16.0	12.2
XRD peak perovskite($\times 10^3$)	20.7	21.9	11.2
Crystal size of perovskite[nm]	19.0	19.9	12.7

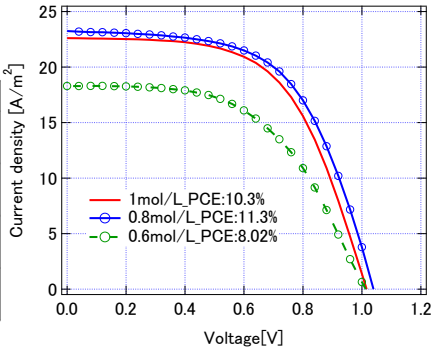

Fig. 2 Photo *J-V* curves of the OPSCs with air flow.

References

[1] B. Lei, V.O. Eze, T. Mori, High-performance $CH_3NH_3PbI_3$ perovskite solar cells fabricated under ambient conditions with high relative humidity, Jpn. J. Appl. Phys., 54, 100305 (2015).

[2] V. O. Eze, B. Lei, T.Mori, Air-assisted flow and two-step spin-coating for highly efficient $CH_3NH_3PbI_3$ perovskite solar cell, Jpn. J. Appl. Phys., 55 02BF01-08 (2016)

P-18

Vertical organic transistors using a hydrogen-bonded pigment

M. Okamoto[1], Cigdem Yumusak[2], Eric D. Głowacki[2], Niyazi S. Sariciftci[2], T. Suenobu[1], and K. Nakayama[1]

[1]Department of Material and Life Science, Osaka University, 2-1 Yamadaoka, Suita, Osaka 565-0871, Japan
Tel: +81-06-6879-7369, Fax: +81-06-6879-7370
[2]Linz Institute for Organic Solar Cells (LIOS), Johannes Kepler University Linz, Altenbergerstrasse 69, Linz 4040, Austria
E-mail: nakayama@mls.eng.osaka-u.ac.jp

Introduction: Most organic thin-film transistors (OTFTs) have field-effect transistors (FET) structure. In recent years, vertical organic transistors (VOTs) have been developed to conquer the weak points of organic FETs. In VOTs, current flow direction is perpendicular to the substrate, and the channel length corresponds to thin-film thickness of organic semiconductors. We developed a metal-base organic transistor (MBOT) which is one of VOTs [1]. The representative structure of MBOT is shown in Fig. 1. The MBOT is characterized by the current amplification similar to silicon bipolar junction transistors, and the high current modulation greater than 100 $mAcm^{-2}$. However, there are not so many choices of organic semiconductors to be adopted into MBOT. In this study, we employed quinacridone as an organic semiconductor used for the collector or emitter layer. Recently, it has been reported that hydrogen-bonded crystalline materials like quinacridone shows excellent air-stability in OFETs [2]. Quinacridone makes intermolecular hydrogen bond in thin film state, and hydrogen bond of quinacridone forms a high lattice energy and a thermal stability. We applied quinacridone to the collector or emitter layer of the MBOT and invesigated air-stability of MBOT in comparison with a conventional device using pentacene.

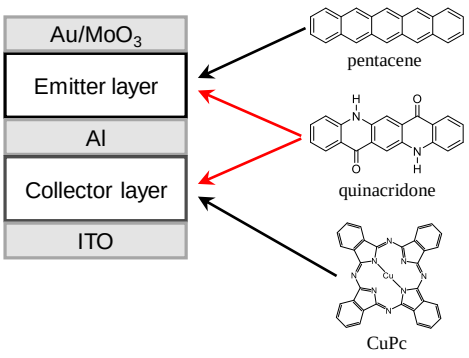

Fig. 1. Device structure of p-type MBOT and the molecular structure of organic semiconductors.

Experiment: Devices were fabricated by thermal vacuum deposition. The collector layer of CuPc or quinacridone, the base electrode of Al , the emitter layer of pentacene or quinacridone and the top emitter electrode of MoO_3/Au were deposited successively on an ITO glass. The final device structure was ITO/CuPc/Al/(quinacridone or pentacene)/MoO_3/Au and ITO/quinacridone/Al /pentacene/MoO_3/Au. The current modulation was measured under common emitter configuration. Air stability of the devices was evaluated in stored and operational conditions under controlled temperature and humidity.

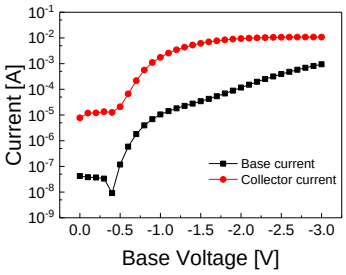

Fig. 2. Output and input characteristics of MBOTs using quinacridone for the collector layer.

Results and discussion: Fig. 2 shows the collector current and the base current of MBOT using a quinacridone for the collector layer. The output current was larger than the input current amplification. The initial output collector current (I_C) of quinacridone collector device was -271 mA/cm^2 for base voltage of -3 V and collector voltage of -5 V. This value of I_C was as much as that of conventional MBOT using a CuPc collector layer. Fig. 3 shows elapsed time dependence of I_C of MBOTs using quinacridone and pentacene for emitter layer, which were stored and measured under controlled air (25 °C, RH: 30%) for a long term. The initial I_C of quinacridone MBOT was lower than that of pentacene MBOT; however, the I_C of quinacridone MBOT did not decrease for a long period of time. These results show that quinacridone is suitable for the material of MBOT, and indicate that hydrogen-bonded quinacridone is effective to improve air-stability in the vertical organic transistors.

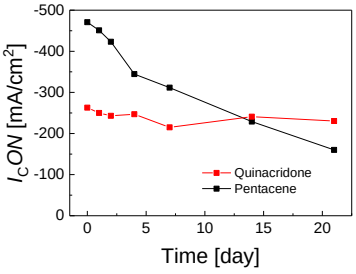

Fig. 3. Elapsed time dependence of output current density of pentacene and quinacridone MBOTs stored and measured under air.

Reference

[1] K. Nakayama, R. Akiba, and J. Kido, *Appl. Phys. Express* **5**, 094202 (2012).
[2] E. D. Głowacki, et al., *Adv. Mater*. **25**, 1563-1569 (2013).

P-19

Solution processable graphene template layer for the molecular orientation control of organic semiconductors

Keitaro Yamada [1], Chiho Katagiri [1,2], Kohta Kitagawa [1], Tomoyoshi Suenobu [1], and Ken-ichi Nakayama [1,2]

[1]*Department of Material and Life Science, Osaka University, 2-1 Yamadaoka, Suita, Osaka 565-0871, Japan*
[2]*Department of Organic Materials Engineering, Yamagata University, 4-3-16 Jonan, Yonezawa, Yamagata, 992-8510, Japan*
Tel: + 81 - 6 -6879 - 7369, Fax: +81- 6 -6879 - 7370
E-mail: nakayama@mls.eng.osaka-u.ac.jp

Introduction: Molecular orientation to the substrate surface is a fundamental problem in organic semiconductor devices due to the anisotropic nature of optoelectronic properties of organic semiconductors. A face-on molecular orientation with the molecular planes parallel to the substrate, is ideal for out-of-plane charge transport, light absorption for organic solar cells, and light emission for organic light-emitting diodes. It is usually difficult to induce a face-on molecular orientation on the substrate where intermolecular interactions are stronger than the molecule–substrate surface interactions. Template layer techniques have been proven to enhance the molecule–substrate surface interactions by inserting template materials between the substrate and organic layer. In recent years, it has been reported that monolayer graphene has strong templating effect allowing a face-on orientation of the organic molecules on the graphene surface due to the strong π-π interactions [1]. However, in order to fabricate the monolayer graphene sheets, complicated procedures including transferring processes from the growth substrate to the objective substrate are necessary. Polymer residue inhibiting the orientation control in the transferring processes is also problematic. In this study, we focused on water-soluble graphene oxide (GO) and reduced graphene oxide (rGO) to fabricate spin-coated graphene template layers, and demonstrated that the rGO layer has a strong templating effect as well as the monolayer graphene sheet.

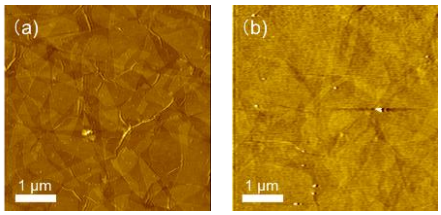

Fig. 1. AFM images of (a) graphene oxide (GO) and (b) reduced graphene oxide (rGO) films.

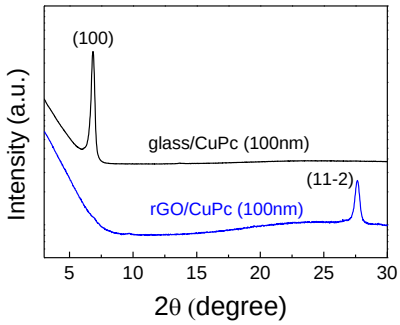

Fig. 2. Out-of-plane XRD patterns of CuPc films on (a) glass and (b) rGO.

Experiment: The rGO films were prepared by vapor reduction of spin-coated GO films on glass substrates. Copper phthalocyanine (CuPc) and pentacene were deposited on the rGO films. Molecular orientation of the molecules was investigated by XRD and UV-vis spectroscopy.

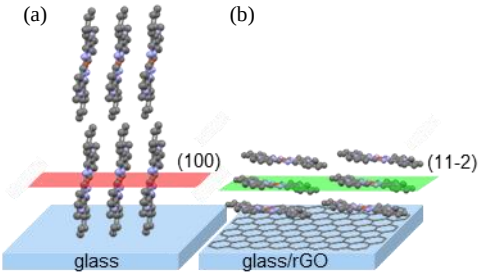

Fig. 3. Schematic representation of molecular orientation of CuPc on (a) glass and (b) rGO.

Result and discussion: The GO film composed of several layers of graphene flakes uniformly covered the substrate surface without large aggregations (Fig. 1a). The rGO film also showed uniform film structure (Fig. 1b). The CuPc film on the glass substrate exhibited a X-ray diffraction peak at 6.9° assigned to the (100) plane (Fig. 2a), indicating an edge-on orientation of the molecules (Fig 3a). In contrast, the (100) peak completely disappeared on the rGO film (Fig. 2b) and the (11-2) peak clearly appeared at 27.6° (d = 3.22 Å), suggesting the face-on orientation (Fig. 3b). In the same manner, pentacene films also showed a face-on alignment of the molecules where the long axis of pentacene is parallel to the substrate surface. These results indicates that the rGO films have strong templating effect to control the molecular orientation. The change of molecular orientation is consistent with UV-vis spectral data. Absorbance of the organic film on rGO increased due to the face-on orientation with the transition dipole moments parallel to the substrate surface. Order parameter S was calculated from the absorbance ratio of the films on the glass and rGO, and indicated the change of the molecular orientation predicted from the XRD results.

Reference:

[1] S. S. Roy, D. J. Bindl, and M. S. Arnold, *J. Phys. Chem. Lett.* **3**, 873–878 (2012).

P-20

Low Temperature Deposition Technique of Photovoltaic Cell by Electrospray

Daiki Tangiku, Nana Inagaki, Seiya Shiiba, Tatsuo Mori and Yoshiyuki Seike

Graduate School of Engineering Electrical and Electronics Engineering
Aichi Institute of Technology
Yachigusa, Yakusa-Cho, Toyota, Aichi, 470-0392, Japan
E-mail: y_seike@aitech.ac.jp

Introduction

In recent year, smart contact lens has been research and development [1][2]. We suggest the organic thin film solar cells as a means to supply 1 μW class electric power to this smart contact lens. However, the widely used the spin coating method is not suitable for coating a curved surface having a three-dimensional structure such as a contact lens. Therefore, the active layer of the organic thin film solar cells was fabricated using Electrospray(ES) technique because it has the possibility of deposition for flexible substrate [3]. In addition, low temperature film forming process is necessary, because the base material of the contact lens is a resin. However, although PEDOT: PSS used in the hole transport layer has good conductivity but it requires an annealing process at 120 to 200℃. Therefore, we used vacuum drying for PEDOT: PSS layer and fabricated the organic thin film solar cell at low temperature which does not use annealing process.

Experimental

In this study, the structure of our device is consist of ITO glass/ PEDOT:PSS layer (30nm)/ Active layer (100nm)/ Al(130nm). PEDOT: PSS layer is fabricated by spin coat method (3000rpm, 60second). Anneal temperature was 30 to 200℃. Vacuum dry process was -0.1MPa for 1 hour. The work function of the PEDOT: PSS film was measured by AC-2(Riken). The sprayed solvent is 1,2-dichlorobenzene. A concentration of solution is 0.5 mg/ml of PCDTBT and 1 mg/ml of phenyl-C61-butyric-acid methyl ester ($PC_{60}BM$). After dissolved, 10 vol% of acetonitrile is added. It is reported that acetonitrile of the high relative dielectric constant is solvent which can make ES [4]. The flow rate of the material, applied voltage to the nozzle, and the distance between the nozzle and substrate were 0.250ml/h, 9.1kV, and 100 mm. Also, the deposition time is 20 minutes, respectively.

Result and discussion

Fig.1 shows the measurement results of the work function of the PEDOT:PSS layer at an annealing temperature of 30 to 200℃. As the annealing temperature increased, the work function shifted 5.30 to 5.15eV. It was observed that the work function of PEDOT:PSS layer by vacuum drying was almost similar to an annealing temperature at 140 ℃. Fig.2 shows J-V characteristics, when the active layer is fabricated by electrospray method. It was observed that the device efficiency of the solar cell fabricated by ES method was almost similar to the performance of the device using spin coat method. Therefore, ES method and vacuum drying for PEDOT:PSS layer are can be used as low temperature deposition technique to curve surface.

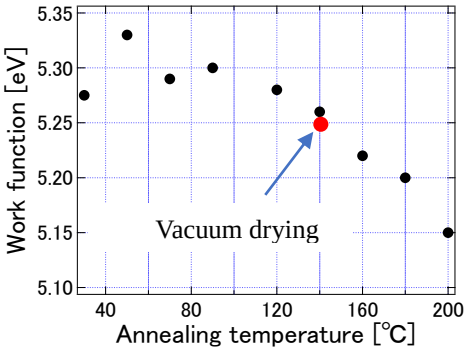

Fig.1 Work function of the PEDOT: PSS

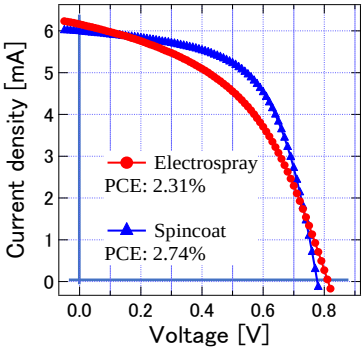

Fig.2 J-V characteristics of ES and spin coat method

Acknowledgment

This study was subsidized by “Special education and research support of Aichi Instituted of Technology”.

References

[1] A R Lingley , B A Parviz et al , J . Micromechanics and Microengineering,21,125014(2011)
[2] Mi-Sun Lee , Jang-Ung Park et al , Nano Lett , 13, No.6,p.p.2814-2821(2013)
[3] Y. Tajima et al. J. PHOTOPOLYM SCI TEC Volume 29 Number 2 (2016) 301-304.
[4] T. Fukuda et al. Thin Solid Films 520 (2011) 600.

P-21

Evaluation of exciton binding energy in organic thin films integrated into a planar device

Akinori Sejima[1], Tomoyoshi Suenobu[1] and Ken-ichi Nakayama[1]

[1]*Department of Material and Life Science, Osaka University, 2-1 Yamadaoka, Suita, Osaka 565-0871, Japan*
Tel: + 81 - 6 -6879 - 7369, Fax: +81- 6 -6879 - 7370
E-mail: nakayama@mls.eng.osaka-u.ac.jp

Introduction: Photocarrier generation in organic materials is fundamentally difficult due to strong Columbic attraction between hole and electron derived from low dielectric constant. The energy required for charge separation is called exciton binding energy (E_B) that is defined as energy difference between a free carrier state and an ion pair (or charge transfer) state. The bulk heterojunction system in organic photovoltaic (OPV) devices successfully avoids this problem in exchange for energy loss due to LUMO offset. However, for further improvement to reduce photovoltage loss, it is important to know the value of E_B in OPV materials. The photodissociation process in organic materials is described by the Onsager-Braun theory[1] (Fig. 1). Onsager-Braun analysis of *J-V* curves to estimate E_B can be performed using a sandwich-type device, but leakage current due to low film quality often becomes a problem. In this work, we employed a planar device for this analysis. The planar device can reduce the leakage current and realize uniform irradiation on the organic layer. We estimated the E_B for several kinds of OPV materials and discussed the validity of the value.

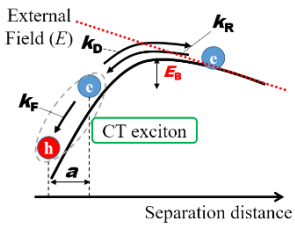

k_D: Dissociation rate
k_F: Recombination rate
k_R: Langevin recombination rate
E_B: Exciton binding energy
a: Initial distance of e^--h^+ pair

Probability $P(E) = \frac{k_D(E)}{k_D(E)+k_F}$

Dissociation rate $k_D(E) = k_R \frac{3}{4\pi a^3} \exp\left(-\frac{E_B}{kT}\right)\left(1+b+\frac{b^2}{3}+\frac{b^3}{18}+\frac{b^4}{180}+\Lambda\right)$

Exciton binding energy $E_B = \frac{e^2}{4\pi\varepsilon_0\varepsilon a}$ $b = \frac{e^3 E}{8\pi\varepsilon_0\varepsilon_r k^2 T^2}$

Fig. 1. Schematic chart and related equations representing Onsager-Braun model.

Experiment: PTB7 and P3HT:$PC_{61}BM$ films were spin-coated on a glass substrate with 5-μm-pitched comb-shaped gold electrodes (Fig. 2). The electric field dependences of dark current and photocurrent for monochromatic light (567 nm) from the upper side were measured by applying a bias voltage. The measurements were performed under vacuum (<1.0×10^{-2} Pa) at controlled temperature. The net photocurrent was estimated from difference between photocurrent and dark current. Charge separation probability (internal quantum efficiency) was calculated from a ratio of the number of electrons generated by photo irradiation to the number of absorbed photons from light intensity and UV-vis spectrum.

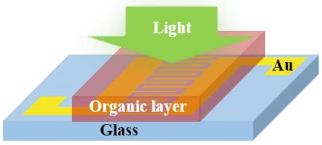

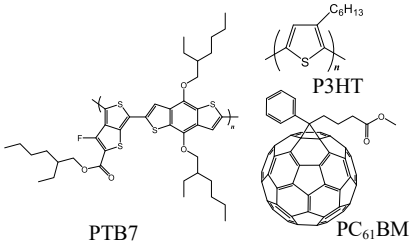

Fig. 2. Schematic representation of the device having comb-shaped electrodes with an organic layer composed of PTB7, P3HT, or $PC_{61}BM$.

Result and discussion: Figure 3 shows relationship between charge separation probability and an applied electric field. In the single component film of PTB7, the photocurrent generation efficiency was low and a downwardly convex curve was observed. This means that single component films require a high electric field for charge separation. In contrast, the bulk heterojunction film (P3HT:$PC_{61}BM$) showed much higher efficiency and clear saturation was observed in low electric field region. This behavior is expected in the Onsager-Braun model for high electric field region. In order to calculate E_B, the Onsager-Braun formula was fitted to the *J-V* curves (Fig. 1) using four variable parameters: initial distance of e-h pair (a), dielectric constant (ε), recombination probability (k_F), and mobility (μ). As a result, E_B for the single component device was found to be higher than that for the bulk heterojunction film.

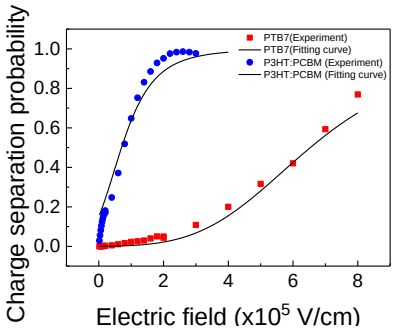

Fig. 3. Plots of charge separation probability vs. electric field (filled square: PTB7; filled circle: P3HT:$PC_{61}BM$), and fitted curves based on Onsager-Braun model for the P3HT:$PC_{61}BM$ and PTB7 devices.

Reference

[1] C. L. Braun, *J. Chem. Phys.*, **80**, 4157 (1984).

P-22

Properties of organic thin-film photovoltaic cells based on PTB7 and C_{60} using additive of PCBM

Naoki Hirohata, Kazumasa Uetani, Daiki Tangiku, Yoshiyuki Seike, Tatsuo Mori
Aichi Institute of Technology
Yachigusa, Yakusa-cho, Toyota, 470-392 Japan
Tel:0565-48-8121
E-mail:t2mori@aitech.ac.jp

Introduction

Although phenyl-C_{61}-butyric-acid-methyl ester (PCBM) is currently used for acceptor materials of many organic thin film photovoltaic cells (OPVs), PCBM is more expensive than original fullerene C_{60} in order to add substituents to fullerene. It is important to reduce the material cost of OPVs in order to be used instead of conventional sola cells. Tada have already reported OPVs fabricated using inexpensive C_{60} or C_{70} [1, 2]. In this study, we aimed to produce high performance OPVs at low cost by adding a small amount of PCBM based on C_{60}[3].

Result & Discussion

Poly({4,8-bis[(2-ethylhexyl)oxy]benzo[1,2-*b*:4,5-b′]dithiophene-2,6-diyl}{3-fluoro-2-[(2-ethylhexyl)carbonyl]thieno[3,4-*b*]thiophenediyl}) **(**PTB 7) and, C_{60} and PCBM were used as a donor and an acceptor materials, respectively. The devices structure consisted of ITO/PEDOT:PSS (30 nm)/active layer (~100 nm)/ Al. The weight ratio of donor and accepter materials was prepared at donor: accepter = 35: 65 [4]. Also the weight ratio of the acceptor material was C60: PCBM = 70: 30. Fig. 1 shows the AFM images of active layers. There are many blocks in the PTB7:C_{60} layer, while the PTB7:C_{60}:PCBM layer appears a uniform surface.

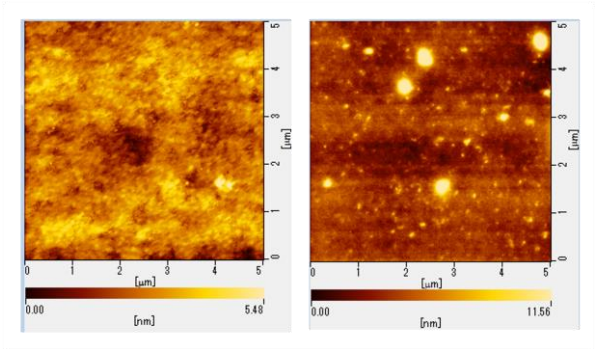

Fig. 1 AFM topographic images of active layers
PTB7:C_{60}:PCBM (left) PTB7:C_{60} (right)

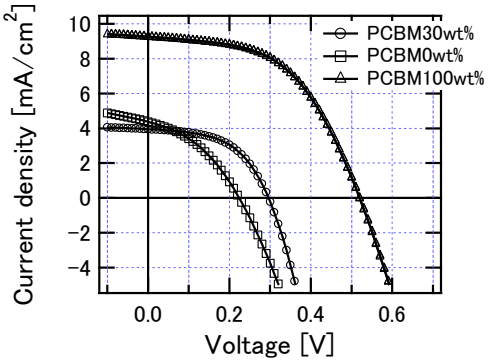

Fig. 2 The photo current – voltage curves of three OPVs

This shows that the solubility of the acceptor material is improved. However, since the PL intensity of 795 nm due to PTB7 is same in PTB7:C_{60} and PTB7:C_{60}:PCBM layers, the disperse of fullerene in PTB7 is thought to be similar between both two specimens. The blocks observed in Fig. 1 right may be the aggregation of C_{60}. Fig. 2 shows the photo current – voltage curves under the irradiation of 100 mW/cm^2, AM1.5G. PV parameters estimated from Fig. 2 is summarized in Table 1. Unfortunately the thickness of active layer, *d* differs because of no optimization of fabrication process. The short-circuit current density, J_{SC} of the PTB7: PCBM OPV is the highest of three specimens. This will be caused by twice thickness of active layer and the J_{SC} of the PTB7: PCBM OPV is almost twice higher than the other. If the disperse condition is same, the generation efficiency of free carrier at the donor/acceptor interface is thought to be same and the amount will depend on the thickness. But the open-voltage, V_{OC} of the other is lower than the V_{OC} of the PTB7: PCBM OPV. Low V_{OC} implies that an appropriate bulk-hetero junction is not formed but some pinholes exists between positive and negative electrodes.

Table 1 Summary of PV parameters in Fig. 2

specimens	d [nm]	J_{SC} [mA/cm^2]	V_{OC} [V]	FF	PCE [%]
PTB7:PCBM	108	9.26	0.520	0.521	2.51
PTB7:C_{60}	66	4.38	0.224	0.381	0.374
PTB7:PCBM:C_{60}	68	3.95	0.296	0.522	0.611

The fill factor, FF of the PTB7:C_{60} OPV is the poorest of three specimens. The addition of PCBM improves FF and the FF of the PTB7:C_{60}:PCBM OPV is same as the FF of PTB7: PCBM. Therefore, the addition of PCBM is effective for the improvement of C_{60}-based OPV. But the optimization of fabrication process is not enough and we must check the fabrication process such as dissolution, etc.

Refarences

[1] K. Tada, *Solar Energy Materials & Solar Cells*, **132** (2015) pp.15-20.
[2] K. Tada, *Polymer Bulletin*, 73, (2016) pp.2401-2408.
[3] T. Mori, D. Sato, T. Egami, and V. O. Eze, *J. Photopolym. Sci. Technol.*, **30** (2017) 581.
[4] Z. He, B. Xiaso, F. Liu, H. Wu, Y. Yang, S. Xiao, C. Wang, T. P. Russell and Y. Cao, *nature photonics*., (2015) pp.174-179.

P-23

Effect of active oxygen species in torch type DBD plasma on normal and cancer cells

Yukie Miyamaru, Nobuya Hayashi, Reona Aijima and Yoshio Yamashita

Graduate School of Engineering Sciences, Kyushu University,
6-1 Kasugakouen, Kasuga-shi, Fukuoka, 816-8580 Japan
Tel: + 81 - 92 - 583 - 7502, Fax: + 81- 92 - 583 - 7060
E-mail:2ES17216W@s.kyushu-u.ac.jp

Responses of normal and oral cancer cells to active oxygen species are found to be different, when the cells are irradiated by plasma. Cancer cells were selectively inactivated by plasma irradiation with lower applied voltage. The expression level of the protein phosphorylated in the cancer cell irradiated by the plasma revealed that phosphorylation of serine 46 of the tumor suppressor gene p53 occurs in the cancer cell HSC3.

(1) Introduction

In recent years, researches have been actively conducted to apply plasma to medical field [1]. Especially, cell inactivation technique using plasma is expected to be effective for treatment of cancer cells. However, effects of plasma irradiation on cancer and normal cells and their inactivation mechanisms remain unclear, and this is a barrier for practical use. Purpose of this study is to investigate inactivation effect of active oxygen species generated by torch-type DBD on oral cancer and normal cells.

(2) Experimental procedure

Figure 1 shows the schematic diagram of experimental apparatus. A cylindrical ceramic tube as a plasma torch is covered with a rectangular grounded electrode. A cylindrical stainless mesh electrode is set along the inner wall of the ceramic tube. The stainless mesh is connected to a high voltage and high frequency (10 kHz) power supply. DBD plasma generated in the ceramic tube is jet out by the gas flow in the tube. Material gas of plasmas is pure oxygen gas. HSC3, human oral cancer cell line, is used as a model of cancer cell. HaCaT is used as a model of normal cell. Cancer cells irradiated by plasma were lysed 24 hours after plasma treatment, and the extracted proteins were used for the western blotting.

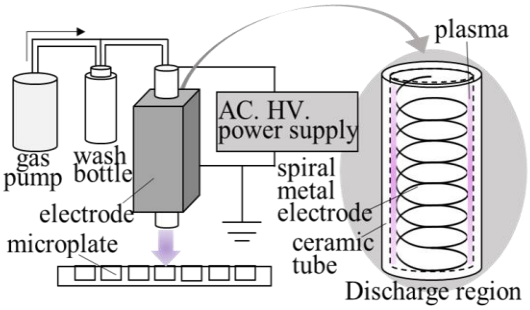

Fig.1 Schematic diagram of experimental apparatus.

(3) Results and discussion

When DNA suffers damage, the tumor suppressor gene p53 controls the cell proliferation cycle and prevents proliferation of cancerous cells. First, serine 15 and serine 20 of p53 are phosphorylated, and the cell cycle is stopped. When serious injury is received, serine 46 is phosphorylated, and apoptosis-inducing gene AIP1 is expressed and apoptosis is induced. p53 is a gene whose abnormality appears most frequently in malignant tumors. Also, there is a report that phosphorylation of serine 46 of p53 (p-p53-Ser46)) in HSC3 does not occur [2].

Therefore, the phosphorylation of serine 46 of p53 owing to plasma irradiation was confirmed by Western blotting. Figure 2 shows the results of the western blotting of serine 46. GAPDH was used as an endogenous control since its expression level is constant under various physiological conditions. The amount of p-p53-Ser46 increased in the cells irradiated by plasma depending on the irradiation period. It is considered that some effects of plasma irradiation would change characteristics of HSC3 lacking phosphorylation of serine 46. Then, phosphorylation of serine 46 occurs resulting in apoptotic cell death.

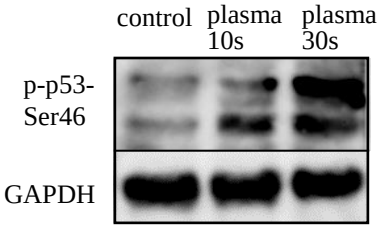

Fig.2 Phosphorylation of serine 46 of p53 in cancer cells irradiated by plasma.

References

[1] G. Fridman, A. Shereshevsky, M. M. Jost, A. D. Brooks, A. Fridman, A. Gutsol, V. Vasilets and G. Friedman," Floating electrode dielectric barrier discharge plasma in air promoting apoptotic behavior in melanoma skin cancer cell lines," Plasma Chem Plasma Process. vol.27, no.2, pp.163-176,April 2007.

[2] Ichwan SJ, Yamada S, Sumrejkanchanakij P, Ibrahim-Auerkari E, Eto K and Ikeda MA," Defect in serine 46 phosphorylation of p53 contributes to acquisition of p53 resistance in oral squamous cell carcinoma cells," Oncogene, vol.25, no.8, pp.1216-1224, February 2006.

P-24

SERS substrates applied with size-controlled silver nanoplates

Hirofumi Kawazumi[1)], Kazunori Sakakita[1)], Kengo Ito[2)], Naohiro Takeda[2)]

[1)] *Dept. of Biol. and Environ. Chemistry, Kindai University, Fukuoka, 820-8555 Japan*
[2)] *Ito Research Institute Co., Ltd., Kanagawa, 251-0002 Japan*
Tel: + 81-948-22-5655, Fax: +81-948-23-0536
E-mail: kawazumi@fuk.kindai.ac.jp

Nano-structures of noble metals can enhance Raman signal, so-called SERS (surface-enhanced Raman scattering). The extremely high enhancement factor allows an attractive technique for single molecule detection. Some SERS plates are commercially available for the convenient use and their SERS active substrates are mostly made by using top-down and/or dry techniques such as nanoimprint and vapor deposition.

We have succeeded in the manufacturing-scale preparation of silver nanoplates (AgPL) by a solution-processed bottom-up technique, where their size can be controlled automatically and systematically in the specific conditions [1]. This paper reports a prototype of SERS substrates applied with size-controlled AgPL. It is also found that hydrophobic clay intercalation compounds dispersively combine together AgPL and create a stable structure [2]. Therefore, we expect a clay-modified slide glass works a capable substrate for SERS with AgPL.

Experimental

Four kinds of AgPL solutions were used; AgPL-Y, M, N and I supplied by Ito Research Institute. This order corresponds the enlargement of AgPL size and their extinction spectra from localized surface plasmon resonance (LSPR) clearly show longer wavelength shift as shown in Figure 1. A slide glass was dipped in the toluene solution of clay (Kunimine Industries, SUMEKUTON-SAN) and then dried to make a clay undercoat layer. It was dipped again in the AgPL solution to make a SERS substrate. The glass plates colored semi-transparently due to the LSPR absorption.

Raman spectra were measured with DXR2 Smart Raman spectrometer (Thermo Fisher Scientific) after dropping the 4,4'-bipyridyl water solution of 10 µl on each SERS substrate. Two different excitation wavelengths were used at 532 nm (10mW) and 780 nm (100mW) as indicated by arrows in Figure 1.

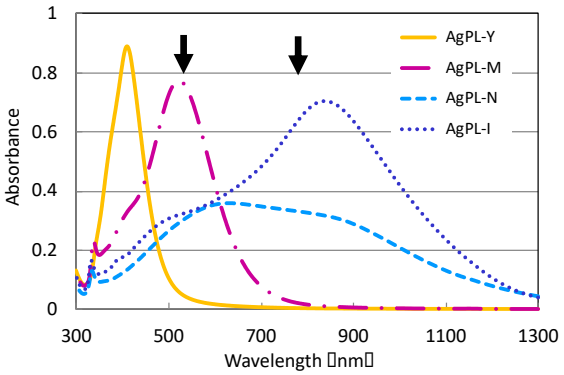

Figure 1 Extinction spectra of AgPLs.

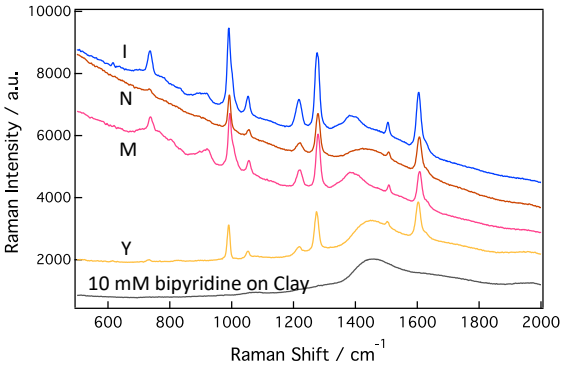

Figure 2 Raman spectra of 100µM-bipyridyl excited at 780nm on SERS substrates.

Results and Discussion

Simple drop-and-dry AgPL aggregations show SERS signal, but their enhancement factor is unstable and largely varied. On the other hand, our new SERS substrates present stable and remarkable enhancement as shown in Figure 2. The substrate with clay layer only shows faint peaks of bipyridyl even at 10 mM-concentration in the Raman spectrum. Every AgPL substrate shows intense peaks at the concentration of 100 µM both at 532 nm and 780 nm. It seems that the clay under-coating produces uniform dispersion of AgPLs and SERS active points increase.

The enhancement factor of each AgPL substrate is summarized in Figure 3. At 532 nm-excitation the smallest AgPL-Y substrate develops the largest SERS and at 780 nm AgPL-I the largest. A weak correlation between the excitation wavelength and the LSPR absorption is observed. It may be resulting from the counterbalance of the degree of the AgPL dispersion and the intrinsic SERS effect on the excitation wavelength.

To extend the application we prepare microtiter plates with AgPL SERS function and detect melamine as one of physio-logical molecules.

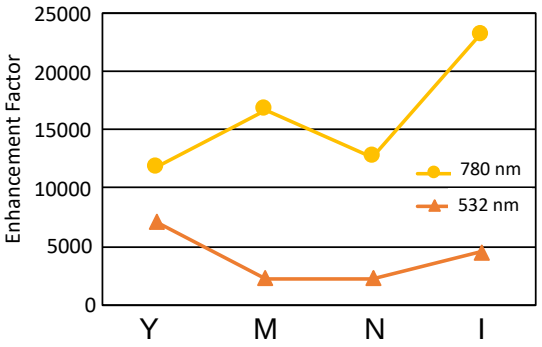

Figure 3 Enhancement factors of SERS on AgPLs.

[1] Japanese Patent No.5970638
[2] Japanese Patent No.6080233

P-25

Preparation of clay polymer nanocomposite film using glycol lignin as an organic binder.

Ryo Ishii, Asami Suzuki, Takeo Ebina, Thi Thi Nge, Tatsuhiko Yamada

National Institute of Advanced Industrial Science and Technology (AIST),
4-2-1, Nigatake, Miyagino-ku, Sendai, 983-0045, Japan
Forestry and Forest Products Research Institute (FFPRI),
1, Matsunosato, Tsukuba, Ibaragi 305-8687, Japan
Tel: + 81 - 22 - 237 - 3092, Fax: +81- 22 - 237 - 7027
E-mail:ryo-ishii@aist.go.jp

Clay polymer nanocomposite films with a high loading of clay show a high gas-barrier property and heat-resistant one compared with other clay polymer nanocomposite films having small additions of clay. The film consists of the platelet clay particles with a highly ordered layer-by-layer nanostructure. The structure brings about a long tortuous path in the film, resulting in the difficulty in the diffusion of dry gasses such as oxygen and hydrogen. The polymer plays a role in a binder for the clay particles, also inhibiting their diffusion. The dry-gas permeability suggests potential applications as a flexible substrate for sensors, keyboards, and printed circuits. However, the films have a poor moisture-barrier property because natural clays are hydrophilic. As a result, the industrial applications of the films are limited because the moisture barrier property is highly required for the electronic devices.

The aim of this work is to prepare clay lignin nanocomposite films with a high moisture-barrier property. Li+-exchanged bentonite as a water-resistant clay (Kunipia-M, Kunimine Industries Co. Ltd.) was used in this work. Lignin was also used as an organic binder. Lignin is a major cell-wall component in plans or wood. Its heat-resistant property is comparable to that of engineering plastics. In addition, the used lignin was obtained by acid-catalyzed solvolysis of the cedar with polyethylene glycol [1]. The PEG-modified lignin, which is denoted as glycol lignin (GL), has an advantage for the film preparation because the GL has miscibility in aqueous dispersions while the untreated lignin has difficulty in mixing in the dispersions. As a result, the GL is expected to be the suitable binder for Kunipia-M.

N-methyl-2-pyrrolidone (NMP) was added to the Kunipia-M aqueous dispersion. The dispersion was agitated using a planetary centrifugal mixer. A GL NMP solution was added to the dispersion and was passed through a strainer. The mixture was spread onto polyethylene terephthalate (PET) films using a film-casting knife. The films were dried at room temperature and removed from the PET film. The removed film was finally annealed for several hours at above 473 K. The moisture vapor transmission rates (MVTRs) of the obtained films were evaluated using metal cups (Tester Sangyo PA-201) at 313 K under a relative humidity of 90% (JIS Z 0208).

Brownish films were obtained by drying at room temperature and removed from the PET films. The films changed into dark-brown ones after the annealing. The resultant films were flexible and capable to treat with hands. The MVTRs were listed in Table. 1. The films annealed at 523 K showed higher MVTRs than that of a polyimide film (CAPTON® 100H/V, 84 $g \cdot m^{-2}day^{-1}$). Consequently, we have developed the clay and GL nanocomposite films with the high gas-barrier property. The details of the films will be presented in the conference.

Table 1. The components and the annealing temperatures, film thickness and MVTRs for the films.

	Kunipia M / wt%	GL / wt %	The annealing temperature / K	Film thickness / μm	MVTR / $g \cdot m^{-2}day^{-1}$
Film1	70	30	523	20	<3
Film2	70	30	493	20	<22
Film3	60	40	523	20	<3
Film4	60	40	493	20	<22

References

[1] T. T. Nge, E. Takata, S. Takahashi, T. Yamada, "Isolation and thermal characterization of softwood-derived lignin with thermal flow properties" ACS Sustain. Chem. Eng., pp 2861-2868, 2016.
etherlands, no.MoF4.6, pp.3-13, Sept. 1990.

P-26

Analyzing Carrier Behavior in Double-layer Organic Photovoltaic Cells with Different Organic Film Thickness Composition using Laser Beam Induced Current Measurement

Atsuo Sadakata

Faculty of Science and Engineering, Kyushu Sangyo University,
2-3-1, Matsukadai, Higashi-ku, Fukuoka city,
Fukuoka, 813-8503 Japan
Tel: + 81 - 092 - 673 - 5970, Fax: +81- 092 -673 - 5091
E-mail:sadakata@ip.kyusan-u.ac.jp

For analyzing carrier behavior in organic photovoltaic (OPV) cells, we have been developing an in-plane laser beam induced current (LBIC) measurement system. In order to understand a relationship between organic film thickness compositions and in-plane power generation characteristics in double-layer OPV cells, we measured photo-current distribution of the double-layer OPV by using the developed LBIC measurement system.

Figure 1 shows the device structure of double-layer OPV with a structure of indium tin oxide (ITO)/Pentacene/Fullerene (C60)/Al using different film thickness ratio of Pentacene and C60 layers. The film thickness of Pentacene layer d_p and C60 layer d_c were chosen as the total film thickness is 200 nm. We made 3 types of double-layer OPV. Group 1 is d_p = 50 nm and d_c = 150 nm. Group 2 is d_p = 100 nm and d_c = 100 nm. And group 3 is d_p = 50 nm and d_c = 150 nm. Pentacene and C60 were deposited on an ITO glass substrate and the pentacene layer using resistance heating type vacuum vapor deposition method, respectively. Al was deposited on the C60 layer as cathode electrode. All resulting devices were encapsulated using a small vial with silica gel to avoid degradations.

We measured *I-V* and *P-V* characteristics using solar simulator (ASAHI SPECTRA, HAL-C100) (Fig. 2). The key parameters (short circuit current I_{sc}, open circuit voltage V_{oc} and maximum power P_{max}) are enhanced with increasing the film thickness of pentacene layer. The device group 3 (pentacene 150 nm / C60 50 nm) showed P_{max} is 1.8 nW.

Figure 3 shows an experimental setup of LBIC measurement system. For measuring photo-current distribution of OPV as a function of some specific irradiation light wavelength, we chose some specific wavelength (448.5 nm for C60 layer and 668.5 nm for pentacene layer) which are corresponding with an absorbance peak of each layer.

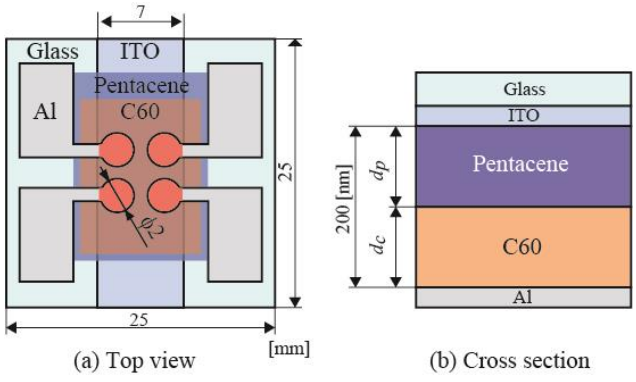

Figure 1 The device structure of double-layer organic photovoltaic cell with a structure of ITO/Pentacene/C60/Al

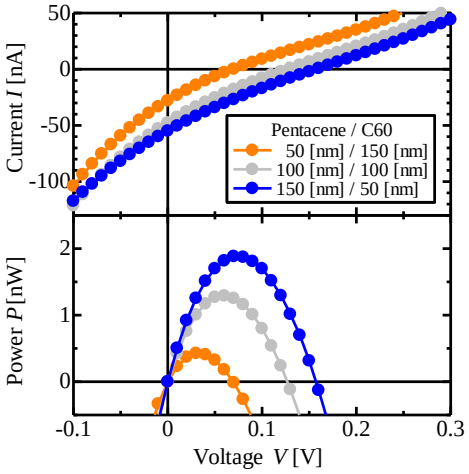

Figure 2 *I-V* and *P-V* characteristics

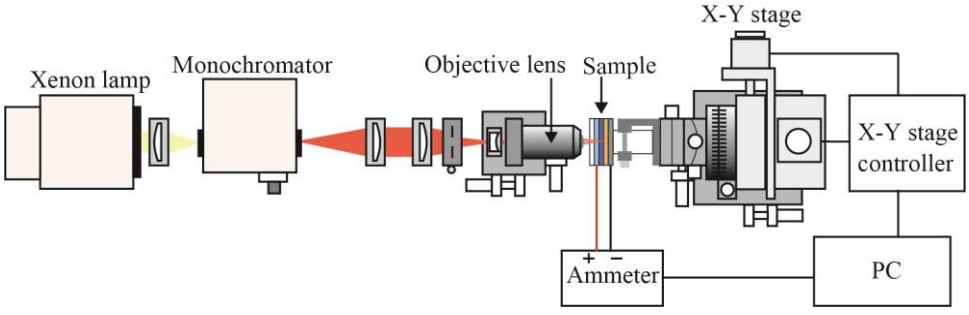

Figure 3 An experimental setup for laser beam induced current measurement

We found that photo-current level in the distribution of group 3 (Pentacene (150 nm) / C60 (50 nm)) is enhanced comparing with other groups (Fig. 4). In the case of irradiation light wavelength 448.5 nm, the photo-current level in each group is activating with decreasing of C60 film thickness. We concluded that the result of photo-current distribution of double-layer OPV cells reflects the relationship between exciton diffusion length and film thickness in each organic layer.

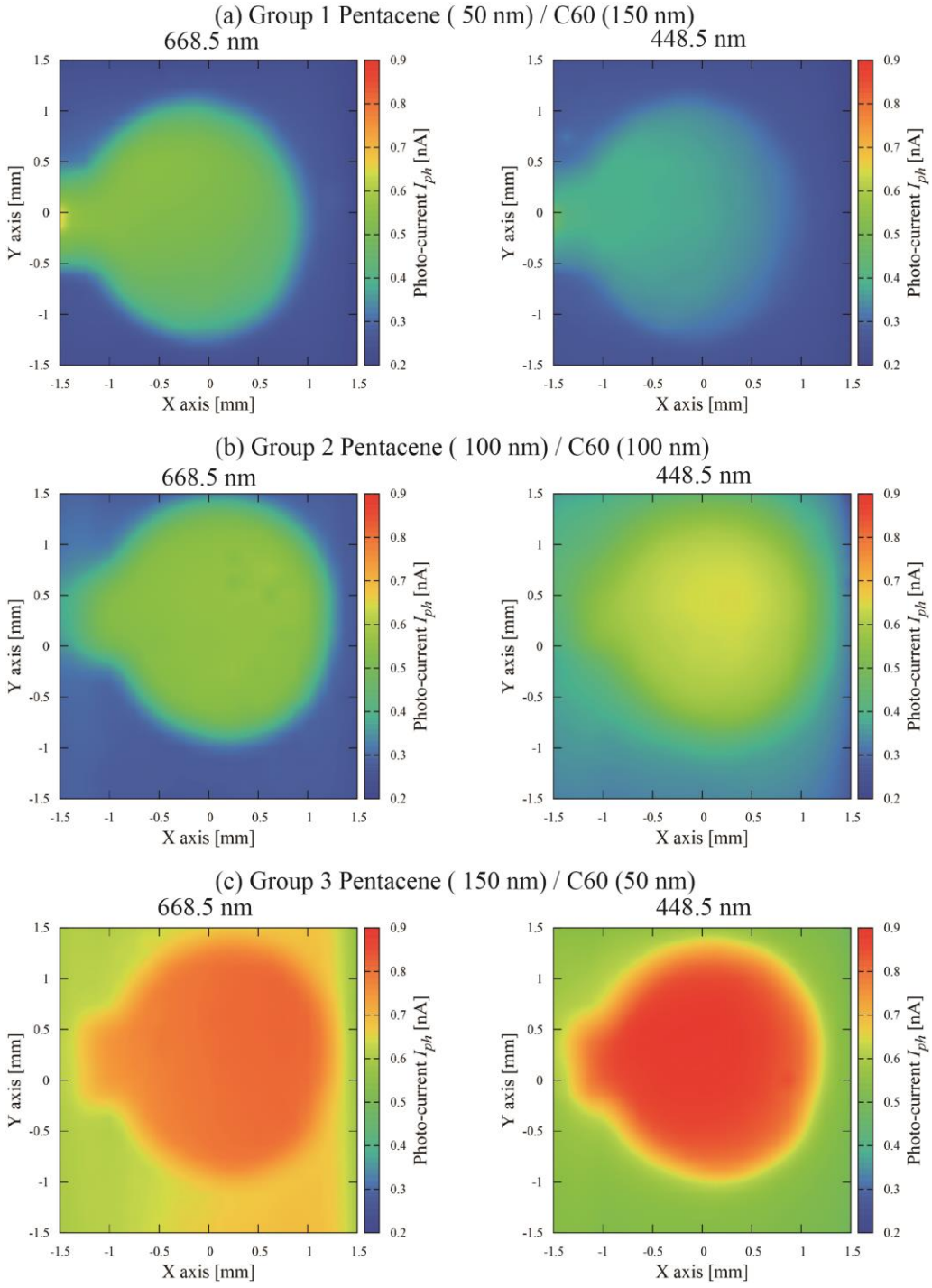

Figure 4 Photo-current distribution of the double-layer organic photovoltaic cell using LBIC measurement

P-27

A Synthesis of Filamentous Carbon Nanomaterial/Carbon Fiber Paper Composites (FCN/CFP) with using Ni Catalysts

Naoto Kataoka[1], Hiroaki Aizawa[1], Haruka Matsumoto[1], Mika Shiraishi[1], Kiyoharu Nakagawa[2], Toshihiro Ando[3], Mikka Nishitani-Gamo[1]

1 Course of Applied Chemistry, Graduate School of Science and Engineering, Toyo University
2 Department of Chemical Engineering, Kansai University
3 National Institute for Materials Science
E-mail:mngamo@toyo.jp

Introduction

A synthesis of filamentous carbon nanomaterial (FCN)/carbon fiber (CF) composites by chemical vapor deposition method has been reported for the enhancement of an adhesion between a polymer and CF as producing a carbon fiber reinforced plastics, in addition, the increase of electrical conductivity of the composite was observed [1]. A synthesis of CNTs/Carbon felt composites was also reported for realizing the battery electrode and/or capacitance electrode without polymer binders, as the carbon felt specific surface area could be drastically increased by the CNTs growth on it [2]. These FCN/CF composites are promised for yielding various applications; a mechanical-reinforced material with a light weight, secondary-battery electrodes, and sensors with a higher-performances. In order to use the composites for the applications, it is indispensable to understand the relation between the FCN growth parameters and the obtained structures, as it could be reproducibly yielding a suitable FCN/CP composites for a certain purpose. However, few studies have been reported on the effect of FCN growth parameters on the grown composite. In this study, we have tried to synthesize FCN/carbon fiber paper (CFP) composites in the variety of a reaction temperature, catalyst, and gas species.

Experimental

A commercially available CFP was used as a substrate. Ni catalysts were supported on it by an impregnation method with using $Ni(NO_3)_2$ $6H_2O$ ethanol solution (Ni: 3.44×10^{-1} mol/L) followed by the CFP pretreatment in air at 623 K for 30 min. The impregnated CFP was dried at 573 K, then introduced in the fixed-bed type reactor for the FCN growth. The FCN growth reaction process was indicated in Fig. 1. The annealing process was in Ar at 673 K for 60 min. for a decomposition of nitrate groups to support Ni particles on CFP. The amounts of grown FCN was evaluated by measuring the weight gain after the catalytic growth process. SEM observation revealed the morphology of FCN/CFP.

Results and Discussion

In the case of using methane as a reaction gas, the maximum amount of carbon deposition was obtained at 773 K shown in Fig. 2. Figure 3 shows SEM image of the obtained FCN/CFP. The diameter was around 10 μm CF that included the CFP was covered densely with the grown FCNs. The diameters of the FCN were in the range from 10 nm to 20 nm which were measured by the SEM image. The FCN/CFP composites were successfully obtained by the catalytic reaction between Ni and methane.

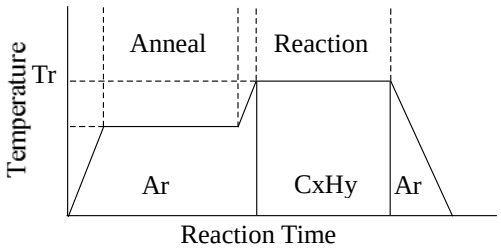

Fig. 1 Reaction process.
Tr: Reaction temperature

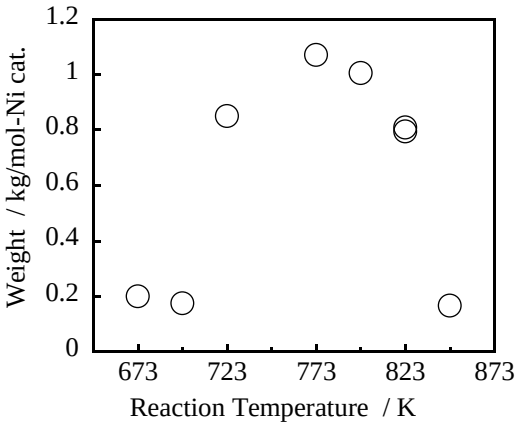

Fig. 2 Reaction temperature dependence of the carbon deposition.

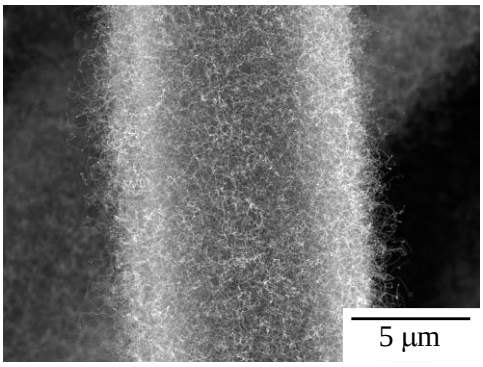

Fig. 3 SEM image of the FCN/CFP

References

[1] T. R. Pozegic, I. Hamerton, J. V. Anguita, W. Tang, P. Ballocchi, P. Jenkins, S. R. P. Silva, "Low temperature growth of carbon nanotubes on carbon fibre to create a highly networked fuzzy fibre reinforced composite with superior electrical conductivity", Carbon, vol.**74**, pp.319-328, 2014.

[2] W. B. Downs, R. T. K. Baker, "Modification of the surface properties of carbon fibers via the catalytic growth of carbon nanofibers", J. Mater. Res., vol.**10**, no.3, pp.625-633, March 1995.

P-28

Catalytic Deposition of a SiC thin-film on Si (100) surface in Organic Liquids

Haruka Matsumoto[1], Mika Shiraishi[1], Hidenobu Shiroishi[2], Shuji Komuro[3], Toshihiro Ando[4], Mikka Nishitani-Gamo[1]

1 Course of Applied Chemistry, Graduate School of Science and Engineering, Toyo University,
2 National Institute of Technology, Tokyo College
3 Course of Electricity, Electronics and Communications,
Graduate School of Science and Engineering, Toyo University
4 National Institute for Materials Science
E-mail: mngamo@toyo.jp

Introduction

For the purpose of realizing a heteroepitaxial diamond growth on Si, many researchers have studied a vapor phase growth of highly oriented diamond thin film on Si (100) by microwave plasma-assisted chemical vapor deposition. The existence of 3C-SiC on Si has been essential for a diamond heteroepitaxy in the gas phase [1]. The 3C-SiC growth on Si by a Vapor-Liquid-Solid (VLS) mechanism has been reported using the mixture of a small amount of hydrocarbon in H_2 balance [2]. In order to obtain a diamond nucleation on Si in the organic liquid phase, we have tried to grow a SiC buffer layer on Si in the mixture of water and methanol in line with the analogy of a SiC-VLS growth in the gas phase. We tried to use cobalt (Co) as a catalyst in order to know the effect of the existence of Co on the physico-chemical states of the surface after the liquid phase reaction.

Experiment

N-type Si (100) substrates (7×22 mm^2) were ultrasonically cleaned with ethanol and acetone to eliminate organic contaminants and cleaned with buffered HF to remove the native oxide. Co catalyst was deposited by a magnetron sputtering method in an Ar atmosphere. The Co catalyst supported on Si substrate (Co/Si) was heated in an Ar at 1173 K for 10 min as the catalyst pretreatment. The mixture of deionized water in methanol was used as the organic liquid source. The pretreated Co/Si was electrically heated in the liquid [3]. The reaction temperature was 1173 K, and the period was 20 min. The substrate surface after the liquid phase reaction was observed by scanning electron microscopy (SEM).

Result and Discussion

Figure 1 shows the SEM images of the substrate surfaces after the liquid phase reaction. In the case of without Co catalyst, as shown in Fig. 1 (a), circular patterns with a diameter of approximately 1 μm were observed. In the case of using Co catalyst treated in an Ar at 1173 K, as shown in Fig. 1 (b), rectangular patterns in the range from 1 μm to 2 μm in length were observed. The existence of Co catalyst resulted in the (100) oriented product formation on the Si (100) substrate. The SEM images of the obtained Si surfaces suggest that the control of the physico-chemical states of the Co catalyst is expected to control the liquid-solid interface reaction.

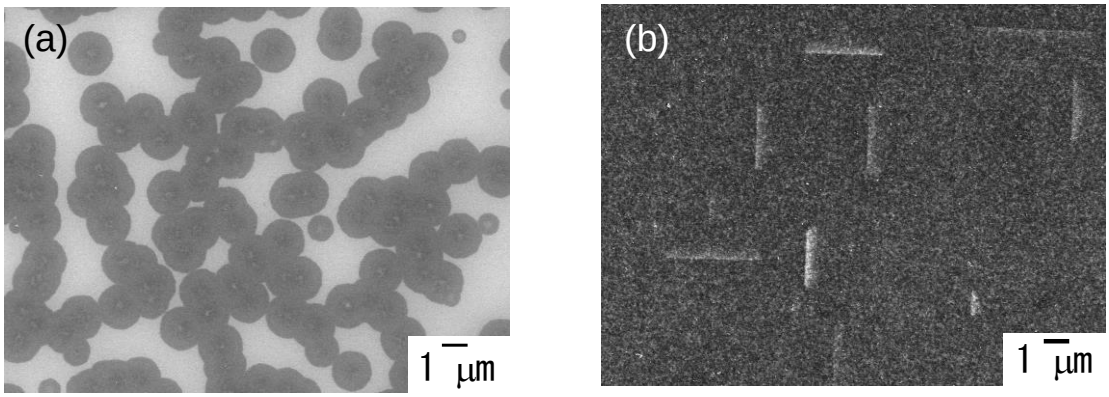

Fig. 1 SEM images of the substrate surface after the liquid phase reaction: (a) without Co catalyst, (b) with using Co catalyst treated in an Ar at 1173 K, respectively.

References

[1] H. Maeda, M. Irie, T. Hino, K. Kusakabe, and S. Morooka, "Formation of highly oriented diamond film on carburized (100) Si substrate, "*J. Mater. Res*., vol. **10**, no. 1, pp.158-164, January 1995.

[2] Y. Zhang, M. Nishitani-Gamo, C. Xiao, and T. Ando, "Synthesis of 3C–SiC nanowhiskers and emission of visible photoluminescence, "*J. Appl. Phys*., vol. **91**, no. 9, pp.6066-6070, May 2002.

[3] M. Nishitani-Gamo, T. Shibasaki, H. Gamo K. Nakagawa, and T. Ando, "Liquid-Phase Deposition of Aligned Carbon Nanotubes Using Cobalt Catalyst,"*Jpn. J. Appl. Phys*., vol. **46**, no. 9B, pp. 6329-6334, July 2007.

P-29

A Synthesis of the Marimo-like Carbon/PVA Sponge Composite

Masao Shinozaki[1], Haruka Matumoto[1], Mika Shiraishi[1], Kiyoharu Nakagawa[2], Toshihiro Ando[3] and Mikka Nishitani-Gamo[1]

1 Course of Applied Chemistry, Graduate School of Science and Engineering, Toyo University
2 Department of Chemical Engineering, Kansai University
3 National Institute for Materials Science
E-mail:mngamo@toyo.jp

Introduction

We have studied a catalytic growth of the novel spherical carbon material, named as 'Marimo-like carbon (MC)', which consisted with filamentous carbon nanomaterials (sp^2-carbon); they grew from transition metal nanoparticles supported on a diamond (sp^3-carbon) particle. The MCs have been used as a support material of Pt particles for the polymer electrolyte fuel cell (PEFC) electrode. We have found that the MC could improve a durability of PEFC using under a high power density [1]. In order to open up a new application of MCs, to develop a MC-composite material is indispensable. In this study, we focused on a polyvinyl alcohol (PVA) sponge, a porous water-attracting polymer as a matrix material. PVA sponges have been widely used as water absorption materials as their physicochemical stability, porous structure and non-toxic property, and studied for the adsorbent of toxic heavy metal ions containing in the waste water discharged from various industries [2]. We have tried to prepare the MC/PVA sponge composite and characterize its structure and physicochemical properties. The MC-surfaces fixed in the pores of PVA sponge are expected to be a reaction sites for realizing environmental protection devices, higher density energy charge devices, effective catalysts, and a sensitive detection devices.

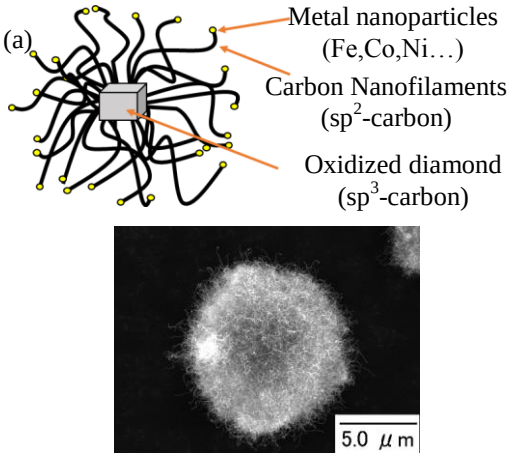

Fig.1 The Marimo-like carbon
(a) Schematic drawing (b) SEM image

Experiment

MCs were catalytically grown with using Ni catalysts supported on oxidized diamond powders (Ni/O-dia.) in the fixed-bed type flow reactor in the temperature range from 723 K to 813 K. Methane gas was used as a reaction gas. The amount of supported Ni was 5 wt% to the weight of diamond powders. The Ni/O-dia. was prepared by an impregnation method in an aqueous solution of $Ni(NO_3)_2$ $6H_2O$. The MC/PVA sponge composite was synthesized as follows; the aqueous solution of 12.5 % PVA (10 mL) was added into the dispersed starch (1.5 g) in 5 mL deionized water and mixed around at 333-343 K until the solution viscosity increased. The 20 % sulfuric acid solution (6 mL) was added into the PVA-mixture, and 37 % formalin solution (2.5 mL) was also added, then MCs (79.5 mg) were added and mixed uniformly. After that, the mixture of PVA and MCs were reacted at 343 K for 60 min. The reacted material was rinsed with deionized water and the MC/PVA composite was obtained. The water retention rate was measured, as it would be closely related to the existence of pores included in the MC/PVA composite. The morphology and pore-structure of the MC/PVA composite was observed by Optical microscope and SEM.

Result and discussion

Figure1 shows (a) schematic drawing and (b) SEM image of the MC. After the MC/PVA product was rinsed with deionized water, no MC was observed in the waste liquid. The MC/PVA composite was uniform color in grayish-white. Optical microscopic observation revealed a porous, sponge-like structure of the MC/PVA composite. The pores with micrometers in size existed in the MC/PVA composite. We have successfully obtained the MC/PVA sponge composite. Table 1 shows a water retention rate of the obtained materials. To compose a PVA with MC resulted in decreasing approximately 35 % of the water retention rate. It indicates that the existence of MC would affect to the fine structure of the pores in the MC/PVA sponge composite.

Table 1 Water retention rate of PVA sponges

sample	Water retention rate(%)
PVA sponge	392.24
MC/PVA sponge	254.67

References

[1] K. Baba, M. Nishitani-Gamo, T. Ando and M. Eguchi,"Preparation of catalyst for polymer electrolyte fuel cell using the Marimo-like carbon," Trans. Mat. Res. Soc. Japan, vol.42, no.2, pp.51-56, 2017.

[2] C. Cheng, J. Wang, X. Yang, A. Li, C. Philippe,"Adsorption of Ni(Ⅱ) and Cd(Ⅱ) from water by novel chelating sponge and the effect of alkali-earth metal ions on the adsorption," Journal of Hazardous Materials, vol264, pp.332-341, 2014.

P-30

Mg-vapor atom behavior and nucleation mechanism on photochromic diarylethene surface

Ikumi Takemoto and Tsuyoshi Tsujioka*

Faculty of Pure and Applied Sciences, Osaka Kyoiku Univ.,
4-698-1, Asahigaoka, Kashiwara, Osaka 582-8582, Japan
Tel/Fax: + 81 - 72 - 978 - 3633
**E-mail: tsujioka@cc.osaka-kyoiku.ac.jp*

Selective metal-vapor deposition on the photochromic diarylethene (DAE, Fig. 1) surface signifies metal-vapor atoms deposit on the colored surface but not on the colorless surface with a low glass-transition temperature (low-T_g) [1]. Any metal patterns can be prepared using maskless evaporation based on selective deposition for organic devices [2]. On the colorless surface, Mg-vapor atoms are adsorbed, diffused, and then desorbed, and nucleation is not occurred because of low Mg-atom density. In this study, we tried to elucidate Mg-atom behavior and the nucleation mechanism on the DAE surface.

We carried out the long-time Mg-evaporation and found that Mg-deposition started even on the colorless surface at a specific deposition-threshold time (t_{th}). Figure 2 shows in-situ Mg deposition observation on the colored and colorless surfaces. The vertical axis indicates Mg deposition quantity on the DAE film, which was formed on quartz crystal oscillator. At the initial stage of evaporation, Mg-atoms deposited on the colored surface, but not on the colorless surface; this is a conventional selective metal-vapor deposition. However, Mg deposition started around 200 s when Mg evaporation onto the colorless surface was repeated. This phenomenon cannot be explained by the conventional nucleation mechanism: collision of diffusing Mg-atoms. Figure 3 shows deposition rate dependence of Mg-deposition on the colorless DAE surface. The results of Fig. 2 and 3 strongly suggest that nucleation sites accumulate according to the adsorbed Mg atom quantity.

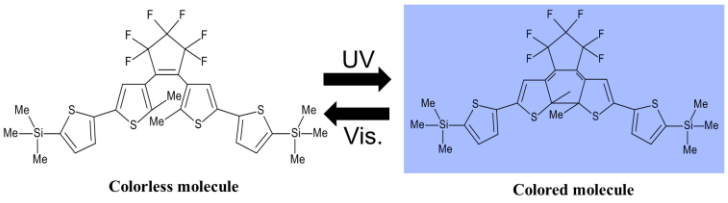

Fig. 1 Photochromism of DAE molecule

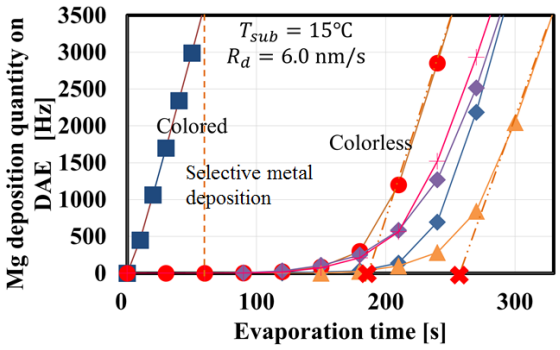

Fig. 2 Mg deposition property on colored and colorless DAE surfaces.

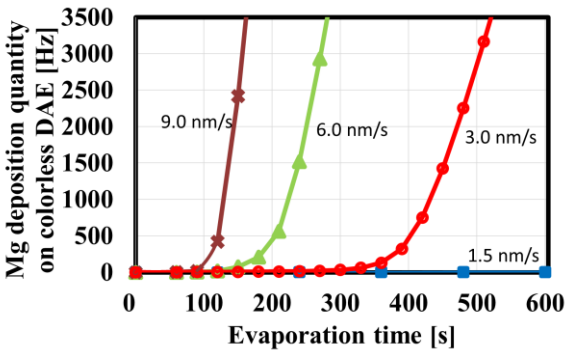

Fig. 3 Mg deposition rate dependence of deposition-threshold time on colorless DAE surfaces.

[1] T. Tsujioka, Y. Sesumi, R.Takagi, K. Matsui, S. Yokojima, K.Uchida, and S. Nakamura "Selective Metal Deposition on Photoswichable Molecular Surfaces" *J. Am. Chem. Soc.* vol.130, no.32 pp.10740-10747, April 2008.

[2] T. Tsujioka, " Selective Metal-vapor Deposition on Organic Surfaces" *Chem.Rec.*, vol.16, pp.231-248, 2016

P-31

Plasma sputtering device using convergent magnetic field for GaN film production

Taisei Motomura and Tatsuo Tabaru

Sensor system engineering group, Advanced Manufacturing Research Institute,
Department of Electronics and Manufacturing,
National Institute of Advanced Industrial Science and Technology,
807-1 Shuku-machi, Tosu, Saga 841-0052, Japan
Tel: +81-942-81-4058, Fax: +81-942-81-4018
E-mail: t.motomura@aist.go.jp

Sputtering is a fruitful process to obtain large-area and high-rate film deposition. A planar magnetron sputtering cathode is widely used in the reactive sputtering process; however, in general, hysteresis properties of discharge voltage and deposition rate lead an undesirable deposition result. In contrast, ion beam sputtering does not result in hysteresis properties, because the ion density and the ion accelerating voltage are individually controlled, since the ion production and the sputtered areas are completely separated. This configuration raises a possibility for a sputtering with low plasma-damage. However, the deposition rate in ion beam sputtering is low, because the ion beam density is generally low. Therefore, based on an ion beam sputtering-like device configuration, we here propose a high-density plasma sputtering device using convergent magnetic field for liquid metal targets. This device can increase the ion density near the target and can provide a practical deposition rate while maintaining the structural features of an ion beam sputtering device. In this study, a gallium (Ga) target was used as an example, due to its ease of handling at room temperature. In addition, gallium nitride (GaN) film deposition was attempted. GaN is well known as a group III-V semiconductor material, and suitable for application in photonics devices such as light-emitting and laser diodes, and high-power electronic devices such as ultra-high-power switches [1-3]. Electronic grade GaN film has typically been manufactured by metal-organic chemical vapor deposition, or molecular beam or metal-organic vapor phase epitaxy. In order to obtain a lower process cost for GaN film deposition, magnetron sputtering methods have been studied, using cooled solid Ga or pressed GaN powder targets [4-6], and using a heated substrate [7-9]. The magnetron and the plasma sputtering depositions using N_2 gas and a liquid Ga target have been studied [10,11]. This paper presents a proposed plasma sputtering device for a liquid metal target, using an unheated substrate, and summarizes the experimental results for GaN film deposition.

The convergent magnetic field was produced by a solenoid coil and a permanent magnet located behind the liquid gallium target. The magnetic field strength and the magnetic vector potential are shown in color map and black lines, respectively, in the background of Fig. 1. Since the magnetic field lines produced by solely the solenoid coil diverge downstream, a columnar neodymium permanent magnet was embedded in the target holder. The solenoid coil current is typically 70 A which produces the magnetic field strength of up to ~0.1 T. Liquid Ga with a purity of 99.99999 % was placed on the water-cooled target holder, which has a bowl-shaped cup to hold a liquid metal target [7,9], and the holder was connected to a DC power supply applying a negative bias voltage of -450 V. A glass plate (Corning Eagle XG, 10×10×1.1 mm) is positioned at target-substrate distance of ~47 mm, and held by an electrically floating and unheated substrate holder. The glass tube having 30 mm in diameter and grounded stainless-steel vacuum chamber were evacuated, using a turbo-molecular and rotary pump system, to a base pressure of $< 5 \times 10^{-4}$ Pa. N_2 gas was introduced from the top of the glass tube, and controlled with a 13.0 sccm range, to maintain a gas pressure of 0.2 Pa. A double-turn loop antenna was wound around the glass tube and connected to a 13.56 MHz radio frequency (RF) power supply. The input RF power for plasma production was pulsed with a duration time of 200 ms and pulse interval of 1000 ms (duty ratio of 20 %).

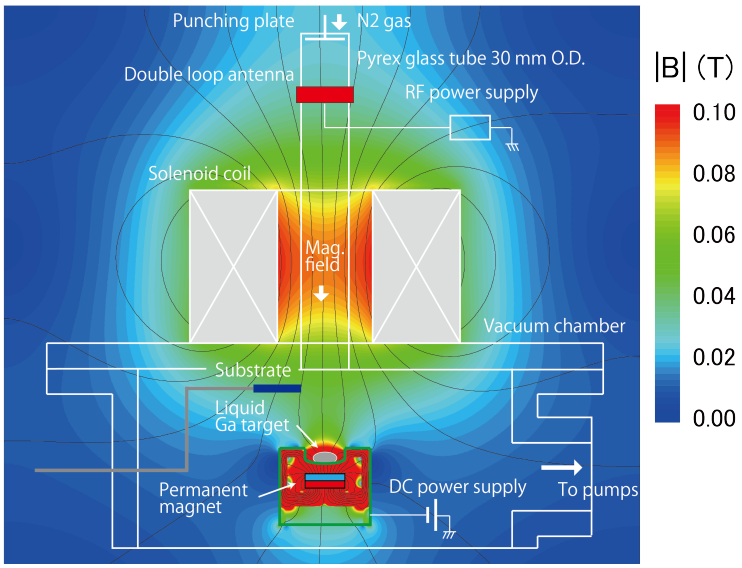

Fig. 1: Experimental apparatus for liquid metal sputtering

The initial experiment has been conducted using a liquid metal target and an unheated glass plate. A high electron density of nitrogen plasma, ~3.3 $\times 10^{18}$ m^{-3}, was obtained with a solenoid coil current of 70 A and the net power

transported to the plasma of 500 W. The device can provide a practical deposition rate while preserving the structural features of an ion beam sputtering device. The deposition rate was estimated at ~13 nm/min at the condition of nitrogen gas pressure of 0.2 Pa and the target-substrate distance of ~47 mm, using the unheated substrates. XRD analysis demonstrated that single-grid GaN (002) films were successfully produced on the unheated glass plate. The device thus enables low-cost liquid metal sputtering device using unheated substrates.

References

[1] S. Nakamura, "The Roles of Structural Imperfections in InGaN-Based Blue Light–Emitting Diodes and Laser Diodes", Science vol.281, no.5379, pp.956-961, August 1998.

[2] S.J. Pearton, J.C. Zolper, R.J. Shul, and F. Ren, "GaN: Processing, defects, and devices", J. Appl. Phys. vol.86, no.1, pp.1-78, July 1999.

[3] S. C. Jain, M. Willander, J. Narayan, and R. Van Overstraeten, "III–nitrides: Growth, characterization, and properties", J. Appl. Phys. vol.87, no.3, pp.965-1006, February 2000.

[4] P. Singh, J.M. Corbett, J.B. Webb, S. Charbonneau, F. Yang, and M.D. Robertson, "Growth and characterization of GaN thin films by magnetron sputter epitaxy", J. Vac. Sci. Technol. A vol.16, pp.786-789, Mar/Apr 1998.

[5] T. Maruyama and H. Miyake, "Gallium nitride thin films deposited by radio-frequency magnetron sputtering", J. Vac. Sci. Technol. A vol.24, pp.1096-1099, Jul/Aug 2006.

[6] C.G. Zhang, L.F. Bian, W.D. Chen, and C.C. Hsu, "Effect of growth conditions on the GaN thin film by sputtering deposition", J. Crystal Growth vo.299, pp.268-271, 2007.

[7] J. Ross and M. Robin, "High-quality GaN grown by reactive sputtering", Mater. Lett. vol.12, no. 4, pp.215-218, November 1991.

[8] E.C. Knox-Davies, S.R.P. Silva, and J.M. Shannon, "Properties of nanocrystalline GaN films deposited by reactive sputtering", Diam. Relat. Mater. vol.12, pp.1417-1421, 2003.

[9] M. Junaid, C.-L. Hsiao, J. Palisaitis, J. Jensen, P.O.˚A. Persson, L. Hultman, and J. Birch, "Electronic-grade GaN (0001) / $Al_2 O_3$ (0001) grown by reactive DC-magnetron sputter epitaxy using a liquid Ga target", Appl. Phys. Lett. vol.98, 141915, 2011.

[10] T. Kikuma, K. Tominaga, K. Furutani, K. Kusaka, T. Hanabusa, and T. Mukai, "GaN films deposited by planar magnetron sputtering", Vacuum vol. 66, pp.233-237, 2002.

[11] R. Flauta, T. Kasuya, T. Ohachi, and M. Wada, "Plasma characteristics of a multi-cusp plasma-sputter-type ion source for thin film formation of gallium nitride", J. Crystal Growth vol. 237-239, pp.2116-2120, 2002.

P-32

Enzymatic biofuel cell using fuel gel of fructose between graphene-coated carbon fiber cloth electrodes

Yusuke Yonaha, Iku Kusajima, Toshinari Doi, Kenta Kuroishi, and Satomitu Imai*

Department of Precision Machinery Engineering, College of Science and Technology, Nihon University
7-24-1 Narashinodai, Funabashi, Chiba, 274-8501 Japan
Tel: + 81 - 47 - 469 -5243 Fax: +81- 47 -467 -9504**
E-mail:imai@eme.cst.nihon-u.ac.jp

Biofuel cells can generate electricity using enzymes from familiar materials such as carbohydrates. However, the output power is low and the lifetime is short. The following countermeasures against these problems were investigated: a) using fuel gel instead of liquid fuel to prevent the enzyme on the electrodes from peeling off [1] and b) increasing the oxygen supply by providing a groove in the gel [2]. The countermeasures above were investigated in the biofuel cell using fructose as a fuel [3]. The principle of the fuel cell power generation using fructose is shown in Fig 1. A proton (H^+) is generated from the fuel using the fructose dehydrogenase (FDH) enzyme at the anode (oxidation). Water is produced from protons and dissolved oxygen using the bilirubin oxidase (BOD) enzyme at the cathode (reduction) [4].

In this work, a material in which graphene was modified on the surface of the carbon fiber woven fabric (GCFC: graphene-coated carbon fiber cloth) was used to increase the electrode surface area [5]. The electrode area was 5 mm × 12 mm × t0.5 mm. An agarose gel mixed with fructose as a fuel was inserted between the anode and cathode electrodes (w6 mm × L12 mm × t2 mm) as shown in Fig. 2. The protons generated at the anode reach the cathode through the fuel gel. Table 1 gives the specifications of the enzyme and fuel. The agarose gel was mixed into the fuel, namely, fructose and the buffer solution at 1.5 wt%. The concentrations and pH of the fuel listed in Table 1 were optimized. As the fuel gel was used instead of liquid fuel, the enzyme separation from the electrode and bubble generation at the cathode are suppressed. Moreover, as one side of the cathode surface that is not in contact with the gel was exposed to the atmosphere, the supply of oxygen was promoted.

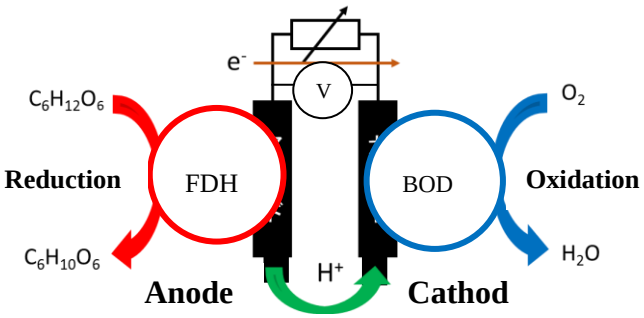

Fig. 1 Components of the biofuel cell using fructose in this work.

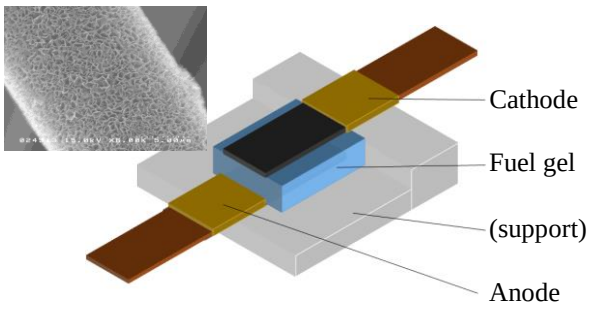

Fig. 2 Structure of the fuel gel sandwiched by the electrodes. The upper figure shows the surface of GCFC observed by SEM.

Table 1. Specifications of enzyme and fuel gel.

	Anode	Cathode
Enzyme	FDH* (60 µl)	BOD** (60 µl)
Concentration	20 mg/ml	25 mg/ml
Fuel gel	Fructose + Agarose gel	
Concentration	Fru.200 mM, Gel.1.5wt%	
pH	5.0 (McIlvaine buffer solution)	

* Fructose dehydrogenase, ** Bilirubin Oxidase.

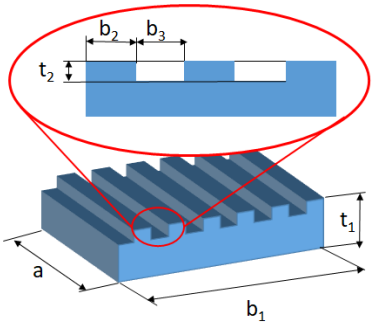

Fig. 3 Dimensions of fuel gel with groves (a=6 mm, b_1=12 mm, t_1=2 mm, b_2=1~3 mm, b_3=1 mm, t_2=0.5 mm).

To further increase the oxygen supply, several grooves were formed on the gel surface (cathode side) as shown in Fig. 3. Although the supply amount of oxygen should increase as the number of grooves increases, the contact area with the cathode electrode decreases; therefore, the groove area should have an optimum value. Hence, the groove interval (b_2) was set as a parameter: 1–3 mm. The width of the groove (b_3) was 1 mm, the depth (t_2) was 0.5 mm.

Fig. 4 shows the output of the biofuel cell. The generated electric voltage was measured by varying the electrical resistance (cf. Fig. 1) and the power density was calculated from the voltage and electrical resistance as $V^2/(R \times A)$ (V: output voltage, R: electrical resistance, and A: area of electrode). For comparison, the case of using liquid fuel (same concentration of fructose) is also shown. In the fuel gel case, the maximum power density values are 92.1 $\mu W/cm^2$ without grooves and 120.9 $\mu W/cm^2$ with grooves, namely, 1.9 times and 2.5 times as much as liquid fuel (49.1 $\mu W/cm^2$), respectively. The maximum output was generated in the case of using the fuel gel with grooves. For the groove interval (b_2), the maximum output was obtained using a 1-mm interval. We considered that the supply capacity of oxygen increases with the groove area; however, the contact area with the electrode (cathode) in this case decreases. Therefore, the groove interval should have an optimum value. Installing many narrow grooves would be advantageous.

Fig. 5 shows the time histories of power density. In the case using the fuel gel, the power density after 30 min is also high compared with the liquid fuel and its reduction ratio is almost the same as that of the fuel liquid. However, after 24 h, while the output of the gel case was still superior to that of the liquid case, its reduction ratio (power density after 24h /power density after 3 min.) was higher than that of the fuel liquid. This is probably due to the drying of the gel.

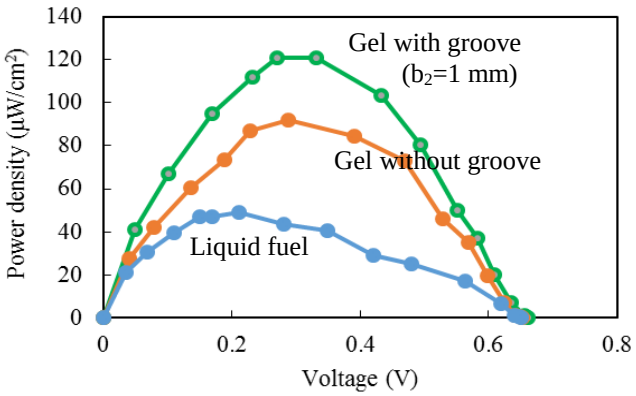

Fig. 4 Power density of three types of biofuel cells: liquid fuel and fuel gels with and without surface grooves.

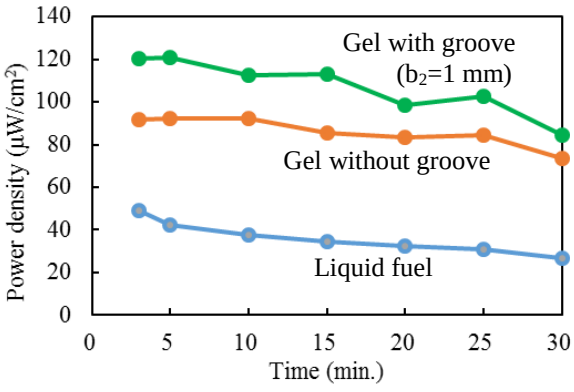

Fig. 5 Time history of power density of the fuel cells exhibited in Fig. 4.

References

[1] H. Goto, Y. Fukushi, and Y. Nishioka, “A flexible micro biofuel cell utilizing hydrogel containing ascorbic acid”, Int. Journal of Physics: Conference Series, (IOP Publishing), Vol. 557, No. 1, p. 012048, 2014.

[2] T. Nakagawa, H. Mita, H. Kumita, H. Sakai, Y. Tokita, and S. Tsujimura, “Water-repellent-treated enzymatic electrode for passive air-breathing biocathodic reduction of oxygen”, Electrochemistry Communications, 36, pp.46-49, 2013.

[3] K. So, S. Kawai, Y. Hamano, Y. Kitazumi, O Shirai, M. Hibi, J. Ogawa, and K. Kano, “Improvement of a direct electron transfer-type fructose/dioxygen biofuel cell with a substrate-modified biocathode”, Physical Chemistry Chemical Physics, 16(10), pp.4823-4829, 2014.

[4] N. Mano, and L. Edembe, “Bilirubin oxidases in bioelectrochemistry: features and recent findings”, Biosensors and Bioelectronics, 50, pp.478-485, 2013.

[5] K. Hoshi, K. Muramatsu, H. Sumi, and Y. Nishioka, “Miniaturized ascorbic acid fuel cells with flexible electrodes made of graphene-coated carbon fiber cloth”, Japanese Journal of Applied Physics, 55(4S), p.04EC11, 2016.

P-33

Improvement of high frequency dielectric properties of organic polymer substrate materials with inorganic fillers

Yusuke IMAI,[1] Susumu TAKAHASHI,[2] Akinori KAN,[2] Yuji HOTTA,[1] Hirotaka OGAWA[2]

[1]National Institute of Advanced Industrial Science and Technology (AIST),
2266-98 Anagahora, Shimo-shidami, Moriyama-ku, Nagoya, Aichi, 463-8560 Japan
Tel: + 81 – 52 – 736 – 7557 E-mail: y-imai@aist.go.jp
[2]Graduate School of Science and Technology, Meijo University

Abstract

Utilization of microwaves and millimeter waves is growing in various fields such as information and communication, transportation, and security [1]. This trend creates a strong demand for better dielectric materials suitable for the high frequency applications. Dielectric response of the material is described by the complex dielectric constant $\varepsilon = \varepsilon' - i\varepsilon''$. There are conflicting requirements for real part of complex dielectric constant ε'. Larger ε' is preferable for miniaturization of dielectric devices. On the contrary, faster signal transmission and better production yield need smaller ε'. As a result, technology that enables precise design of ε' value within the range of 3–6 is demanded. On dielectric loss, tan δ ($= \varepsilon''/\varepsilon'$) should always be as low as possible, hopefully in the order of 10^{-4} or less. Neither organic polymer nor inorganic ceramics can independently fulfill these requirements within their material discipline. One promising approach to solve this problem is the composite material composed of organic polymer matrix filled with inorganic ceramics particles. The ε' value can be tuned by the filler concentration. It has been found that the compositional dependence of ε' can be well described by the Bruggeman theory [2]. Suppression of dielectric loss is the big challenge for composite dielectrics. Choice of appropriate ceramic filler is crucial to produce low dielectric loss composites [3]. Contribution from the filler surface must be considered. With the composite dielectrics approach, not only dielectric but other characteristics such as thermal and mechanical properties can be improved. Ceramics fillers with anisotropic shape could be especially efficient. Control of filler distribution and orientation is important for anisotropic fillers [4,5]. Efficient suppression of thermal expansion and enhanced thermal conduction could be achieved by the utilization of anisotropic fillers. Potential of the inorganic particle-filled organic polymer composites for high frequency applications will be discussed by showing some of our results in this field [3–8].

Acknowledgement

Part of this study was supported by the JSPS KAKENHI Grant Number JP17K06831.

References

[1] T. Tasuku, T. Yoneyama T, eds., Modern millimeter-wave technologies. IOS Press, 2001.
[2] D. E. Aspnes, "Local-field effects and effective-medium theory: a microscopic perspective", Am. J. Phys. vol.50, no.8, pp.704–709, 1982.
[3] S. Takahashi, Y. Imai, A. Kan, Y. Hotta, and H. Ogawa, "Preparation and characterization of isotactic polypropylene/MgO composites as dielectric materials with low dielectric loss", J. Ceram. Soc. Jpn. vol.121, no.8, pp.606–610, 2013.
[4] S. Takahashi, Y. Imai, A. Kan, Y. Hotta, and H. Ogawa, "Dielectric and thermal properties of isotactic polypropylene/hexagonal boron nitride composites for high-frequency applications", J. Alloys Compd. vol.615, pp.141–145, 2014.
[5] S. Takahashi, Y. Imai, A. Kan, Y. Hotta, and H. Ogawa, "Improvements in the temperature-dependent properties of dielectric composites by utilizing MgO whiskers as the dielectric filler in an iPP matrix", J. Alloys Compd. vol.640, pp.428–432, 2015.
[6] S. Takahashi, Y. Imai, A. Kan, Y. Hotta, and H. Ogawa, "Microwave dielectric properties of composites consisting of $MgAl_2O_4$ filler synthesized by molten-salt method and isotactic polypropylene polymer matrix", Jpn. J. Appl. Phys. vol.54, no.10, pp.10NE02-1–5, 2015.
[7] S. Takahashi, Y. Imai, A. Kan, Y. Hotta, and H. Ogawa, "High-frequency dielectric and mechanical properties of cyclo-olefin polymer/MgO composites", Polym. Bull. vol.72, pp.1595–1601, 2015.
[8] S. Takahashi, Y. Imai, A. Kan, Y. Hotta, and H. Ogawa, "Effects of hollow Zn_2SiO_4 particles addition on dielectric properties of isotactic polypropylene-HW composites", Mater. Sci. Eng. B Adv. Func. Solid State Mater. vol.209, pp.51–55, 2016.

P-34

Easy functionalization method and electrical characteristics of single conical pores with a polydopamine layer

Yukichi Horiguchi, Tatsuro Goda and Yuji Miyahara

Institute of Biomaterials and Bioengineering, Tokyo Medical and Dental University (TMDU)
2-3-10 Kanda-Surugadai, Chiyoda, Tokyo 101-0062, Japan.
Tel: + 81 - 3 - 5280 - 8097, Fax: + 81- 3 -5280 - 8135
E-mail: horiguchi.bsr@tmd.ac.jp

Introduction

The resistive pulse sensing (RPS) using micro- to nanosized pores is an emerging technology to detect trace amounts of various targets such as proteins, bacteria, viruses, and extracellular vesicles. Recently, molecular immobilization methods are suggested as promising way to improve the performance of RPS. On the other hands, molecular immobilization using chemical reaction is restricted by material type of pore surface. For example, for modification using thiol molecules, a fabrication of gold-sulfur interface is required, which increases the pore expense.

Therefore, we focused on mussel-inspired technology for pore surface modification. Mussels can adsorb strongly onto a surface via the noncovalent interaction of a polydopamine layer, such as hydrogen bonding and π–π stacking.[1] A polydopamine layer is spontaneously formed when a material is immersed in a dopamine solution, which can be applied to noble metals, oxides, semiconductors, ceramics, and synthetic polymers. Herein, we demonstrated a simple functionalization of the pores using polydopamine as an intermediate layer to connect the material with functional molecules.

Experiment

The ion current of the nanopore was measured by a nanoparticle analyzer (qNano, Izon Science Ltd., Christchurch, New Zealand) using NP100 (pore membrane). A NP100 was immersed in 2 mg/mL dopamine solution (10 mM of tris buffer (pH 8.5)) for 120 min on a shaker. The NP100 was then washed with deionized water and the ion current was then measured. To control the pH of 50 mM of KCl solution, 50 mM of HCl or 50 mM of KOH were added to adjust the final pH. After the I-V characteristics plots were obtained, the NP100 was immersed in 1 mM of 11-Mercaptoundecanoic acid (MUA) ethanol solution (48 h, 4°C). The NP100 was then washed with ethanol and DI water, whereupon the ion current was measured for each pH condition.

Result and discussion

After the immobilization of the pore surface by MUA, current-voltage (I–V) measurement was performed in 50 mM KCl solution. Fig. 1 shows the result of I–V measurements in different pH. The I–V curve is almost straight at a pH of 4 while the curve is bended at a pH of 11. The case at basic pH, carboxyl groups of MUA molecules showed negative charge, which contributes to the restriction of ion traffic.[2] The detailed discussion will be shown in the presentation.

According to this result, we concluded that the MUA molecules were exactly immobilized on a pore surface via polydopamine layer.[3]

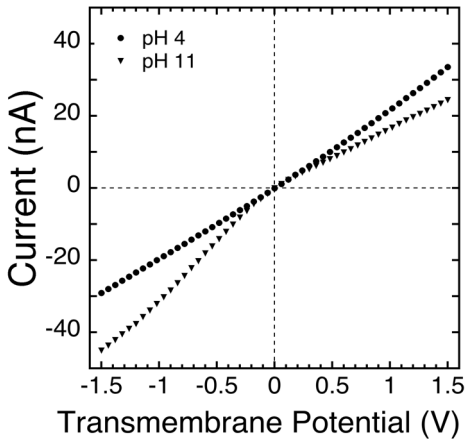

Fig. 1 I–V measurement curves of pore (NP100) in different pH after the immobilization of polydopamine and 11-mercaptoundecanoic acid (MUA).

Acknowledgement

This work was supported by the Impulsing Paradigm Change through Disruptive Technologies (ImPACT) Miyata Program on the "Ultra-high-speed multiplexed sensing system beyond evolution for the detection of extremely small amounts of substances" (launched in 2014 and funded by the Council for Science, Technology and Innovation headed by the Prime Minister of Japan) of the Japan Science and Technology Agency (JST).

References

[1] H. Lee, S. M. Dellatore, W. M. Miller and P. B. Messersmith, Science, "Mussel-Inspired Surface Chemistry for Multifunctional Coatings," vol.318, pp.426-430, October 2007.

[2] Z. S. Siwy, "Ion-Current Rectification in Nanopores and Nanotubes with Broken Symmetry," Advanced Functional Materials, vol 16, no.6, pp.735-746, March 2006.

[3] Y. Horiguchi, T. Goda and Y. Miyahara, "Simple functionalization method for single conical pores with a polydopamine layer," Applied Physics Express, vol.11, no.4, pp.047001, April 2018.

P-35

Plastic Robotics with Organic Thin Film Transistor Array Fabricated on Curved Surfaces

M. Sakai[1], Y. Miyai[1], K. Watanabe[1], H. Ishimine[1], Y. Okada[2], H. Yamauchi[1], Y. Sadamitsu[3], Y. Hashimoto[3], N. Onodera[3], and K. Kudo[1]

Department of Electrical and Electronic Engineering[1], Chiba University,
Center for Frontier Science[2], Chiba University,
Nippon Kayaku Co. Ltd.[3]
1-33 Yayoi-cho, Inage, Chiba city, Chiba, Japan
Tel: + 81- 43-290-3874
E-mail:sakai@faculty.chiba-u.jp

In Recent years, plastic and printed electronics attract extensive interest. Flexible and stretchable devices are actually in the prototyping phase. On the other hand, device fabrication technology on a curved surface is not so active nevertheless many commodities in our modern life are made of smoothly curved plastics, for example, plastic bottles, blister packs, medical tubes and connectors and so on. It was certainly demonstrated that the stretchable electronics could be adapted onto a spherical surface[1]. However, stretchable electronics cannot keep stable self-standing shape by themselves. Therefore, not only flexible or stretchable device but also curved surface device will be desired in all field of Internet of Things society. Especially in the field of mechanical engineering, conventional robot arm made of stainless steel is sufficiently strong but too heavy. It is very difficult to precisely swing heavy robot arms without vacillating because of the inertia. So, it is necessary for robot arms to be lightweight as much as possible. One of the candidate material is plastic polymer materials. Plastic polymer composites are also sufficiently strong for making robot arms to be engaged in precise work such as palpation or surgery. Plastic robot fingers, hands, and arms also can be disposable. In addition, if these robot fingers equip sensitive thermal and tactile sense, more precise surgical operation can be possible by medical robots. As described above, plastic electronics on curved surface have a potential for development in wide area of technologies.

Thin PEN (poly(ethylene naphthalate)) films were prepared as substrates. Au gate electrode pattern was thermally evaporated on the substrate film of which thickness was 75 μm, and 900 nm thick parylene-SR layer was fabricated on the substrate surface. Then Au contact electrode pattern was deposited on the surface, which was chemically treated by pentafluorobenzenethiol self-assembled monolayer (PFBT-SAM) to reduce the contact resistance. A proper amount of dioctylbenzothienobenzothiophene (C_8-BTBT) powder was transferred onto the substrate, and then another PEN film of which thickness was 25 μm was put on it. The pair of plastic films, including the organic powder, was then thermally pressed by the mold to make a thin film devices in the curved plastic surfaces. We used modified thermal press method[2] of which press plate was replaced to curved mold. Curved mold was an original mold formed along the fingertip of the author, of which minimum radius of curvature was about 7 mm estimated under spherical approximation. In tactile sensitivity tests, we constructed original tester, which was constructed by combination of a micrometer caliper and electrical measurement instruments.

Figure 1(a) is a photograph of fingertip shaped plastic OTFT array fabricated by our thermal molding. 88 OTFTs are included in the finger shaped surface. The fingertip shaped OTFT array was configured to be used as a robot finger which is available to precise work by using a sensitive tactile sense. So we demonstrated the tactile sensitivity tests. One of the result is shown in Figure 1(b). The fingertip shape was settled on the test equipment and was slightly pressed to normal direction of Δh from the initial height by a micrometer caliper. In the figure 1(b), I_D was approximately 6.5 μA with no load. I_D obviously increased during the compression with the normal displacement of Δh (from 0.1 to 0.5 mm). These response are reversible and highly sensitive, which is due to the increase of internal strain in the OTFT plane.

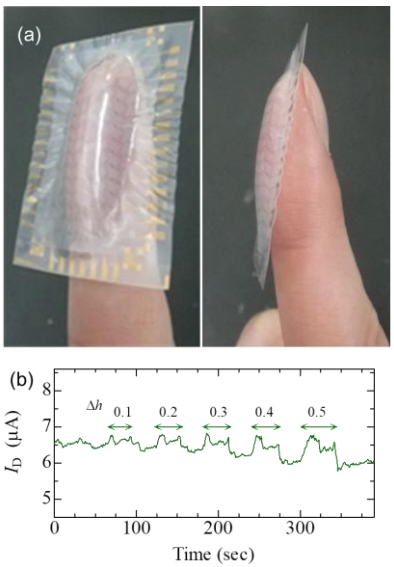

Fig.1 (a) Picture of the fingertip - shaped OTFT array and (b) result of the tactile sensing test.

In this work, we present a novel technique to fabricate a freely designed curved surface and electronic device array simultaneously on the surface of plastic sheets, that is expected to realize 3D plastic electronics. We fabricated a real human finger shape OTFT array for one of the test case, and succeeded in detecting slight deformation induced by soft touch from an object.

References

[1] H.C. Ko et al. Nature 454, 748 (2008).
[2] A. Inoue et al., Phys. Status Solidi A 210, 1353 (2013).

P-36

Temperature Dependent I-V Characteristics of InP@ZnS Quantum Dot Single-Electron Transistor

Yoon Young Choi, Yutaka Majima

Laboratory for Materials and Structures, Tokyo Institute of Technology, Japan
E-mail: choi.y.ae@m.titech.ac.jp

As the future society based on Artificial Intelligence (AI) and Internet of Things (IoT) is expected, the development of high performance transistors has become very important issue. Especially, improvements of their switching speed and power consumption are essential prerequisites for AI and IoT devices. However, these improvements of transistor performance have been slow recently as transistor scaling has been stalled at sub-10nm scale.

In this respect, single-electron transistors (SETs) are expected as one of the strong candidate switching devices because of small size, low power consumption and high-speed operation. Our group has demonstrated logic operations of SETs by using the critical dimensional electroless Au plated (ELGP) nanogap electrodes with 40 nm scale in linewidth and Au nanoparticles (NPs) as Coulomb island [1]. However, our ELGP nanogap electrodes had problems in fabrication of the fine electrodes with sub-20nm linewidth for the larger gate capacitance due to Rayleigh instability. In this point of view, Pt is a good electrode material for robustness and fine patterning because of higher melting point and lower surface diffusion coefficient than Au. Moreover, recently, the colloidal InP@ZnS quantum dots (QDs) have attracted much attention as eco-friendly material in electronic and bio-industrial field owing to its non-toxicity and the unique electronic/optical properties by simple QD size control. Therefore, it is worth considering the colloidal InP@ZnS QDs as Coulomb islands for exploring to find the unique electrical characteristics in SET.

Here we introduce the colloidal InP@ZnS QDs between the robust fine ELGP nanogap based on Pt electrodes for SETs. The Pt-based fine ELGP nanogap electrodes were fabricated by electron beam lithography (EBL) for initial Pt electrode and ELGP for the precise nanogap separation control. And, the colloidal InP@ZnS core-shell QDs were synthesized by the well-known hot-injection method. The chemically assembled InP@ZnS QD SETs were fabricated successfully by immersing the Pt-based fine ELGP nanogap electrodes into alkanedithiol and InP@ZnS QD dispersed solution. The fabricated InP@ZnS QD SET exhibited the stable switching characteristics with gate bias voltage and the hysteresis behavior of I-V characteristics at 9K. And these characteristics were disappeared with increasing operating temperature as shown in Fig.1.

This study was partially supported by MEXT Elements Strategy Initiative to Form Core Research Center; and by BK Plus program, Basic Science Research (NRF-2014R1A6A1030419).

[1] Y. Majima, G. Hackenberger, Y. Azuma, S. Kano, K. Matsuzaki, T. Susaki, M. Sakamoto and T. Teranishi, "Three-input gate logic circuits on chemically assembled single-electron transistors with organic and inorganic hybrid passivation layers" *Sci. Tech. Adv. Mater.* vol.18, no.1, pp374-380, 2017.

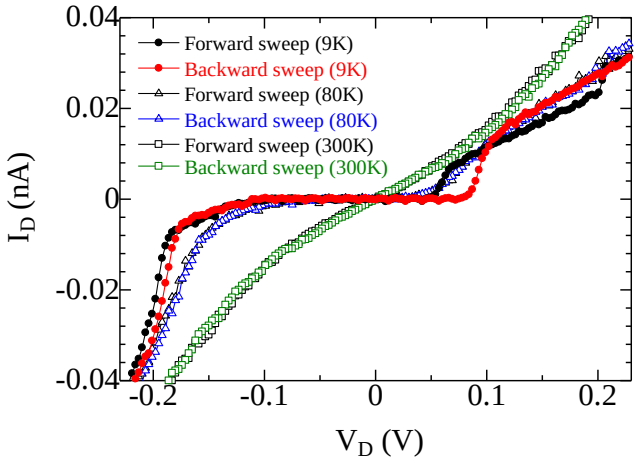

Figure 1. Temperature dependent I_D-V_D characteristics of the chemically assembled InP@ZnS QD SET

P-37

Photorefractive composites with photoconducting oligomer-insulating polymer blends

Naoyuki Yoshizawa[1, 2], Koya Izumida[1], K.-L. Wang[3], Masaki Horie[3], Takashi Fujihara[4], Takeshi Kinoshita[2], Satoshi Wada[1], and Takafumi Sassa[1,*]

*[1]Photonics Control Technology Team, RIKEN RAP, 2-1, Hirosawa, Wako, Saitama 351-0198, Japan, Tel: + 81 - 48 - 462 – 1111, * E-mail: tsassa@riken.jp*

[2]Department of Electronics and Electrical Engineering, Keio University, 3-14-1, Hiyoshi, Kohoku-ku, Yokohama, Kanagawa 223-8522, Japan

[3]Department of Chemical Engineering, National Tsing Hua University, 101, Sec. 2, Kuang-Fu Road, Hsinchu 30013, Taiwan

[4]Innovative Organic Device Laboratory, Institute of Systems, Information Technologies and Nanotechnologies, 5-14, Kyudai-shinmachi, Nishi, Fukuoka 819-0388, Japan

Introduction

How to achieve both a fast response and a large refractive index change in photorefractive (PR) polymer composites is a critical issue. Typically in the PR composites photoconductive polymers are used. They provide two functions: charge transport and trapping. Generally, in the polymers the control of charge traps, which are typically conformational traps, are not so straightforward. Moreover, sufficient charge traps needed for refractive index change tend to degrade the transport rate of charges. In this study, we examine a new PR polymeric system introducing photoconducting oligomer-insulating polymer blends, instead of a single photoconducting polymer, to control the number of charge traps. We focused on triphenylamine oligomers and prepared different molecular weight ones to compare with the conventional system.

Experimental

Photoconducting oligomers, PTAA, with M_n = 1,000 (M_w/M_n = 1.14, n ~ 3) and 2,100 (M_w/M_n = 1.34, n ~ 6) were synthesized via palladium-complex catalyzed polyamination [1] and mixed with the insulating polymer, APC. With this photoconducting blend, photorefractive composites, PR-Blend[n=3] and PR-Blend[n=6], were prepared with the addition of 7DCST and PCBM; the mixture was dissolved in chlorobenzene and then dried in a vacuum oven. As a reference, PTAA polymer (M_n = 12,000) was also synthesized [1] and the conventional type PR composite, PR-Ref, was prepared with DEHP, 7DCST, and PCBM, following a similar procedure as in the oligomer composite case. We examined four-wave-mixing (FWM) and frequency-sweeping Mach-Zehnder interferometer (MZI) experiments [2] to evaluate the trap density in the composite.

Table 1 Materials composition and absorption coefficient.

	Composition	α [a] [cm^{-1}]
PR-Blend[3]	PTAA[n=3]:APC:7DCST:PCBM = 60:18:20:2 wt.%	26
PR-Blend[6]	PTAA[n=6]:APC:7DCST:PCBM = 60:18:20:2 wt.%	33
PR-Ref	PTAA polymer:DEHP:7DCST:PCBM = 60:18:20:2 wt.%	44

[a] Measured at λ = 630 nm.

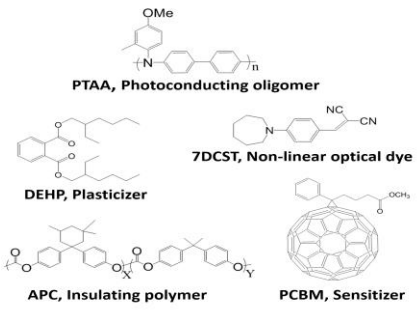

Figure 1 Chemical structures.

Result and Discussion

Figure 2 compares the trap density among the three composites. Oligomer composites show higher values than the reference polymer composite (PR-Ref). Moreover, the oligomer composite with larger M_n (PR-Blend[6]) shows higher trap density than the lower M_n one (PR-Blend[3]). A large trap density can lead to a high electric field, and thus PR index change. In Figure 3 the PR index change (Δn) measured is shown. PR-Blend[3] exhibited larger PR index change compared to PR-Ref as expected. However PR-Blend[6] showed lower Δn than PR-Blend[3] or PR-Ref. We found from MZI measurement that PR-Blend[6] possessed the smallest EO coefficient. Since the PR index change is proportional to the electro-optic (EO) coefficient as well, the lowest Δn in PR-Blend[6] was diminished by the lowest EO property.

The response speeds of the blend composites were slower than PR-Ref.; 40 % and 60 % reductions for PR-Blend[3] and PR-Blend[6], respectively. From the MZI experiments, a restricted orientational motion of chromophores, 7DCST, was found for the oligomer composites, and caused the degradation of PR response speed against PR-Ref.

Conclusion

Using PTAA oligomer-insulating APC polymer blends instead of a single PTAA polymer, trap density was increased in PR composites, bringing about the enhanced Δn. However, the oligomer blend brought about the restricted orientational motion for chromophores, degrading PR response speed as well as EO coefficient. We believe that the optimal choice of the insulating polymer would be a key for this new material system.

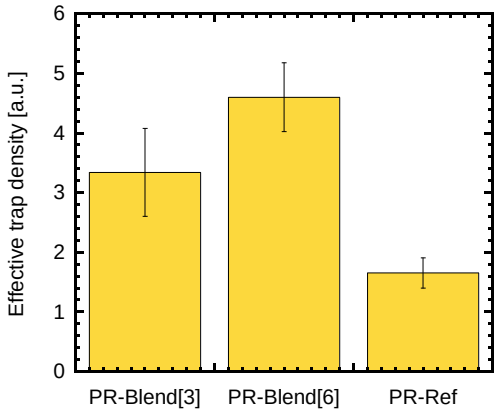

Figure 2 Effective trap densities evaluated.

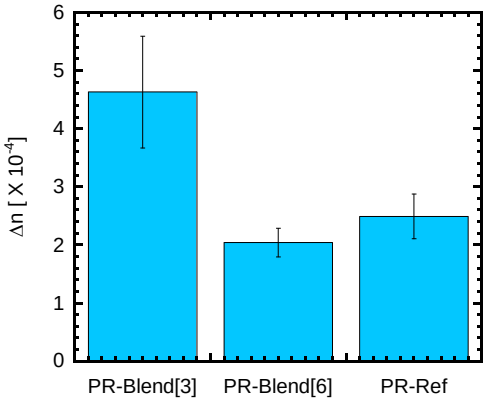

Figure 3 Refractive index changes evaluated.

References

[1] M. Horie, Y. Luo, J. J. Morrison, L. A. Majewski, A. Song, B. R. Saunders, and M. L. Turner, "Triarylamine polymers by microwave-assisted polycondensation for use in organic field-effect transistors," J. Mater. Chem, vol.18, pp.5230-5236, 2008.

[2] T. Fujihara, T. Sassa, T. Kawada, J. Mamiya, T. Muto, and S. Umegaki, "Simplified procedure for interferometric determination of electro-optic properties of low-T_g photorefractive polymer," J. Appl. Phys. vol. 107, no.2, pp.023112, 2010

P-38

Dependence of raw material particle size on electric properties of thin film of hydrophilized carbon material synthesized by atmospheric pressure plasma method

Daiki Matsuo and Koichi Sakaguchi

Department of chemistry and applied chemistry, Saga University,
1 Honjomachi, Saga, Saga, 840-8502 Japan
Tel: + 81-952-28-8553, Fax: + 81-952-28-8548
E-mail: ksaka@cc.saga-u.ac.jp

Introduction

Printed electronics is a technique utilized fabricating electronic device. It has possibility of further price reduction and the large area of the electronic devices. Graphene shows superior electric conductivity and is expected as device materials. Solvent affinity is necessary to apply the printed electronics. Chemical oxidation is a one of the high productive methods to produce graphene from graphite, however, defects are generated in graphene. We have proposed that the synthesis of hydrophilic carbon materials (APGO) under mild oxidation condition by using solution plasma technique [1] and atmospheric pressure plasma technique to reduce the defects. Atmospheric pressure plasma generates plasma in inert gases and produces OH radicals. In this study, electric character of the APGO with deferent particle size to compare with size dependence for conductivity. We deduced that the electron conduction at between the graphene sheets is slowest. Therefore, larger graphene sheets are reduced frequency of electron jump between the graphene sheets.

Experimental

30wt%-H_2O_2 of 2 mL was added to graphite powder (xGnP Graphite Nano Platelets xGnP-M-5, 15, 25) with different particle size (5 μm, 15 μm, 25 μm) of 200 mg respectively, and then atmospheric pressure plasma was irradiated in N_2 gas (15 L/min) for 10 minutes. The sample was produced with H_2O_2 of 10 mL, 50 mL in the same manner. A pen type atmospheric pressure plasma device (SAKIGAKE-Semiconductor Co., Ltd. Model : P500-SM) was used as a plasma generator. After samples were filtered and freeze-dried for overnight, the dispersion of APGO for 1 mg/1 mL were prepared and sonicated. Dispersibility was observed by naked eyes. The dispersion was dropped on glass substrates (2.5 × 2.5 μm) treated by plasma. Three film specimens were formed in each particle size, and these specimens were pressed by a vise. (Before and after pressed samples were abbreviated by B and A, respectively. The number showed the volume of H_2O_2.) Current-voltage characteristics were measured at five sites of films before and after the press by four probes method. Film thickness was estimated from sample weight and specific surface area under uniform film on the glass surface.

Results and discussion

The produced samples were dispersed in water by sonication. The sample treated plasma with H_2O_2 of 50 mL in all particle size showed better dispersibility. Therefore, quantity of OH radical generated by plasma irradiation as volume of H_2O_2 increases.

Fig. 1 shows the conductivity of each sample calculated by the result of measured current-voltage characteristics of APGO. The conductivities exhibit the trend of gradually increasing as particle size increase. The conductivity of most APGO films was improved after vise press. This enhancement of conductivity is most likely attributed to the decrease of cavity in the APGO films. The conductivity with raw particle size of 25 μm was the highest in contrast to that with 5 μm was the lowest after the press. It is considered that decreasing frequency of the slow electronic movement between the sheets with increasing of the particle size lead to high conductivity.

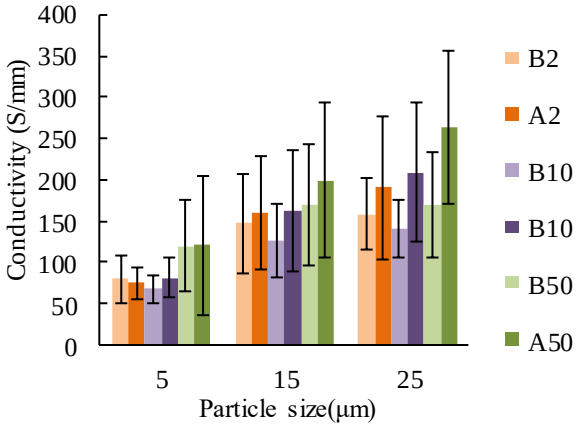

Fig. 1 Conductivity of APGO film varying in the quantity of used H_2O_2

[1] Seiko Uchino, Koichi Sakaguchi, Asami Ohtake, Noboru Takisawa, Tatsurou Nakashima, Masanao Era, and Naoki Matsuda, Jpn. J. Appl. Phys. **53** (2014) 01AD05.

P-39

Quantity analysis of surfactant binding sites of atmospheric pressure treated hydrophilic carbon material and dependence of surfactants chain length by potentiometric titration

Kota Sonoda, Masaya Ushijima, Noboru Takisawa, Koichi Sakaguchi

Department of chemistry and applied chemistry, Saga University,
1 Honjomachi, Saga, Saga, 840-8502 Japan
Tel: + 81-952-28-8553, Fax: + 81-952-28-8548
E-mail: ksaka@cc.saga-u.ac.jp

Introduction

In recent years, graphene has been well known to be able to produce in mass quantities by chemical oxidation and reduction method. Oxygen functional groups were introduced between the graphite layers by chemical oxidation. As a result, distance between layers are expanded and exfoliated to graphene oxide (GO) by sonication in water. Finally, graphene is obtained by reduction of GO. However, chemical oxidation has some faults such as introducing some defects and high environmental impact. We have proposed the atmospheric pressure plasma method to improve faults mentioned above. Carbon materials were oxidized by irradiation of atmospheric plasma to graphite in hydrogen peroxide. The carbon materials show poor dispersibility and graphite structure, which is not single layered graphene. Therefore, investigation of oxidation degree is important to improve these materials. When surfactants are dropped into dispersion of hydrophilic carbon material, surfactants are not only electrostatically bonded but also hydrophobic interactive bonded. It is expected that the oxidation degree was estimated from interaction with surfactants by potentiometric titration. In this study, potentiometric titration was conducted to hydrophobic carbon material by atmospheric plasma method (APGO). A hydrophobic behavior was considered by titration with different chain length surfactants. Moreover, variety of dispersion state was observed for the GO and the APGO with respect to increasing concentration of surfactant.

Experiments

The GO and the APGO were synthesized by modified Hummers method and atmospheric plasma method, respectively. Initial concentrations of the carbon materials were 0.5 mg/mL in water. Bonding amounts of surfactants were determined by potentiometric titration used difference alkyl chain length surfactants (C14TABr, C12TABr, C10TABr, C9TABr). Binding constant and quantity of bonding site were calculated for each samples. Subsequently, surfactant chain length dependence for the GO and the APGO was confirmed. variety of dispersion state was observed for dropping surfactant into both samples by naked eyes.

Results and discussion

The remarkable alkyl chain length dependence for quantity of APGO bonding site cannot be confirmed for APGO-surfactants interaction. In contrary, bonding constant clearly depended on alkyl chain length as shown in fig. 1. The bonding constants were estimated in three regions for different constant of surfactant. Wide, dilute and conc in fig. 1 implies all concentration range, dilute region and concentrated region, respectively. The tendency appeared that the binding constants increase as chain length increase in any concentration range. Furthermore, the bonding constant of the APGO was higher than GO. Therefore, it is suggested that the hydrophobicity of carbon structure in the APGO is larger than GO. Figure 2 shows dispersions of the GO and the APGO after dropping the surfactant. The dispersions of the GO were aggregated with increasing the concentration of dropped surfactant. No change for the dispersions of the APGO was observed. It is found that the APGO is different from the GO in not only quantity of bonding sites but also types and positions of introduced oxygen functional groups.

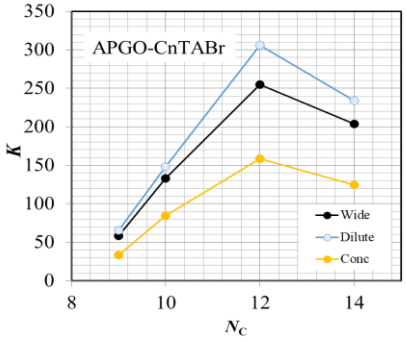

Fig.1 Surfactant chain length dependence of binding constant for the APGO

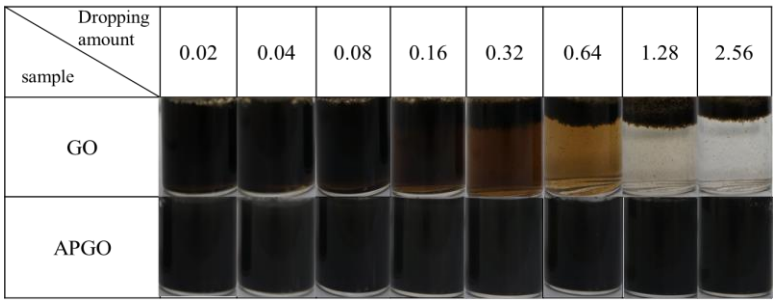

Fig.2 Photograph of dispersions for the GO and the APGO with respect to different concentration of surfactant

P-40

Synthesis of amino graphene oxide derivatives with different alkyl chain length

Riona Hayashi, Ai Hirakawa and Koichi Sakaguchi

Department of chemistry and applied chemistry, Saga University,
1 Honjomachi, Saga, Saga, 840-8502 Japan
Tel: + 81-952-28-8553, Fax: + 81-952-28-8548
E-mail: ksaka@cc.saga-u.ac.jp

An Amino graphene oxide derivatives (AGOD) synthesized by introducing amino groups into graphene oxide (GO) are paid attention for application such as printed electronics ink, biomolecule detection and metal affinity. The AGODs can be dispersed in an organic solvent, particularly, with a low polar solvent, which leads to a device fabrication by a solution process. The presence of an amino group at the terminal is expected to be applied to a biosensor for detection of a biomolecule and introducing a further functional group via an amino group. Currently, several methods for introducing amino groups into the GO have been reported, however, there are problems such as complicated operation, demanding reaction conditions and high cost. In this study, we examined the synthesis method of the GO derivatives functionalized with amino groups in a simple and environmentally friendly way.

The GO was synthesized from graphite by the modified Hummers method [1]. The GO was dispersed in methanol, then 1,12-dodecanediamine in an equimolar amount to the oxygen-containing functional group on GO estimated from the XPS result was added to the dispersion and reacted during 24 hours. The reactant was filtrated and washed with methanol and acetone. In the same manner, 1,8-octanediamine, 1,6-hexanediamine, 1,4-butanediamine and 1,2-ethylenediamine were introduced. Since 1,4-butanediamine is unstable in air, it was handled and reacted under a nitrogen atmosphere. The obtained GO derivatives are denoted as C12, C8, C6, C4 and C2, respectively. Dispersibility and Fourier transform infrared spectroscopy (FT-IR) measurement were carried out to confirm presence of the amino groups. The dispersibility evaluation was conducted by naked eyes. The GO and the AGODs were added into water and some organic solvents and then sonicated for 30 minutes. The dispersible state was observed at immediately after the ultrasonic treatment, 1 hour, and 24 hours. The interlayer structure of the AGODs was performed by XRD.

Dispersibility results after 24 hours from sonication of the GO and the AGODs are shown in Table 1. The GO showed stable dispersibility in water even after 24 hours, inversely dispersibility in ethyl acetate was low. On the other hand, most of the AGODs flakes precipitated at the bottom of the screw tube or floated on the water surface in the aqueous dispersion, i.e. The AGODs cannot be dispersed to water. Moreover, slight coloration was observed in ethyl acetate. It was observed that the dispersibility of C4 and C2 to ethyl acetate is improved compared to other AGODs. The GO has a laminated structure with few layers in the reaction solvent. The oxygen-containing functional groups in the GO are present not only on the surface but also between the layers. The reaction rate was improved for the alkyl diamines with shorter the alkyl chain length with facial oxygen compared to longer alkyl chain, since the alkyl diamines with shorter the alkyl chain length were easily intercalated the interlayer of GO. As a result, dispensabilities of C4 and C2 were improved.

Table 1. Dispersibility results of GO and GO derivatives (after 24 hours)

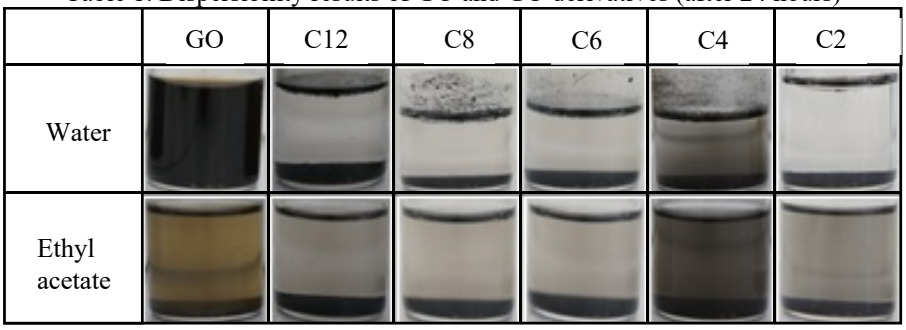

The results of XRD for the GO and the AGODs were shown in Fig. 1. The peak of GO appeared at 10.52° which correspond to the interplanar spacing was 0.84 nm. The peak were gradually shifted to the lower angle side than GO from C2 to C12 which implies the interplanar spacing were proportionally spreaded as the alkyl chain length increases. From this result, it is suggested that the diamine was introduced not only on the GO surface but also between the layers. Similarly, it was also found that the peaks were sharpened accompany the alkyl chain length. It is considered that self-organizations were improved as the alkyl chain length increases at the planar graphene and the linear alkyl chain.

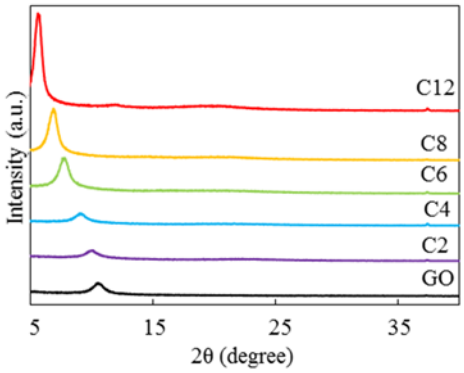

Fig.1 XRD profile of GO and GO derivatives

[1] M. Hirata, T. Gotou, S. Horiuchi, M. Fujiwara, and M. Ohba, Carbon 42, 2929 (2004).

P-41

Effect of environmental gases for electrical properties of graphene oxide and its derivatives

Yuka Katayama, Asami Otake and Koichi Sakaguchi

Department of chemistry and applied chemistry, Saga University,
1 Honjomachi, Saga, Saga, 840-8502 Japan
Tel: + 81-952-28-8553, Fax: + 81-952-28-8548
E-mail: ksaka@cc.saga-u.ac.jp

Introduction

Graphene consist of carbon six-membered rings by sp^2 bond in a two-dimensional sheet form. Various applications have been expected since the graphene appears excellent characteristics such as large specific surface area, high electron mobility and thermal conductivity. In particular, we focused on the application to gas sensors utilizing the change in resistance when gas molecules were adsorbed on the graphene surface. Generally, it is required to exhibit high sensitivity and selectivity as a sensor. The sensors based on graphene shows high sensitivity and poor selectivity. Meanwhile, a sensor based on graphene oxide (GO) and its derivatives is expected to fabricate by solution process. Moreover, graphene derivatives can be introducing the functional group with not only affinity for organic solvent but also recognition for objective molecule such as ethanol, carbon dioxide ammonium and so on. In this study, we aimed to compare the resistance of thin films for the GO and GO derivative with long alkyl chain under moisture vapor and ethanol vapor.

Experimental

GO was synthesized by modified Hummers method [1] and dispersed in distilled water. Silane coupling reaction was conducted to the synthesized GO using Octadecyltrichlorosilane (C_{18}GO) and dispersed in dehydrated THF. Both dispersions were prepared to a concentration of 10 mg / 10 ml. Each of the dispersions was drop-cast deposited on a plasma surface-treated glass substrate (2.5cm×2.5cm) and then dried on a hot plate. In order to improve the conductivity, the prepared thin films were reduced with hydrazine monohydrate overnight. Electrical characteristics of each thin film were measured in air, vacuum, moisture vapor and ethanol vapor using the four-terminal method with silver paste electrodes.

【Results and Discussion】

Detecting water vapor and ethanol vapor are conducted with different samples. Figure 1 shows I-V characteristics of the GO thin films in air, water vapor and ethanol vapor. The I-V characteristic in the vacuum environment was almost correspond to that in the air. The resistance in water vapor shifted to lower than that in air. In contrast, the resistance in ethanol vapor shifted to higher than that in air. We speculated that the lower shift in water vapor and higher shift in ethanol vapor were attributed by increasing the carrier density due to adsorption of water molecules and scattering carrier due to adsorption of ethanol molecules.

The change in the resistance of the C_{18}GO thin film by the gas are smaller than that of the GO thin film as shown in fig. 2. This is presumed that water molecules and gas molecules are hardly adsorbed to C_{18}GO with alkyl chain and adsorbed molecules are far from graphene surface corresponded to effective carrier pass due to alkyl chain. Although, the change is small, the direction of shift is as same as the GO thin film.

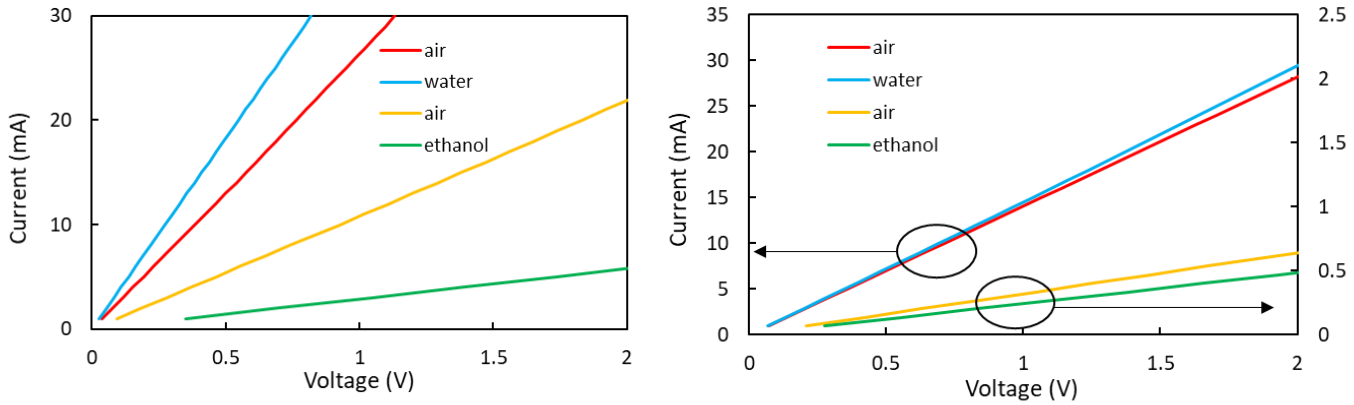

[1] M. Hirata, T. Gotou, S. Horiuchi, M. Fujiwara, and M. Ohba, Carbon 42, 2929 (2004).

P-42

Semitransparent organic solar cells with polyethylenimine ethoxylated interfacial layer using lamination process

Keisuke Shoda, Masahiro Morimoto, Shigeki Naka*, and Hiroyuki Okada

Graduate School of Science and Engineering for Research, University of Toyama
3190 Gofuku, Toyama, 930-8555 Japan
**E-mail: nak@eng.u-toyama.ac.jp*

Organic solar cells (OSCs) are actively investigated to realize large area production, flexibility, and low cost. To solve this issue, lamination process for fabrication is one of the best solutions. In this paper, we have reported semitransparent OSCs by the lamination process[1]-[5].

Poly(ethylenedioxythiophene)/poly(styrenesulfonate) (PEDOT:PSS) was spin-coated on an indium-tin-oxide (ITO) substrate for anode. Poly(3-hexylthiophene-2,5-diyl) (P3HT) and (6,6)-phenyl-C61 butyric acid methyl ester (PCBM) blend as an active layer were coated using spin-coating on PEDOT:PSS layer. On the other hands, polyethylenimine ethoxylated (PEIE) was spic-coated on another ITO substrate for cathode. Part of PEIE layer was spin-rinsed with ethanol for 2 times. The both substrates were laminated using a heater press system (Mikado Technos). The pressure of lamination was 0.5 MPa under 200°C condition. The device structure was glass substrate/ITO/PEDOT:PSS/P3HT:PCBM/ PEIE/ITO/glass substrate. Active area was 2×2 mm^2. The light source for measuring OPV characteristics was a solar simulator (Yamashita Denso) at a light intensity of AM1.5, 100 mW/cm^2. The transmission spectra were measured by spectrophotometer (Hitachi U-1900).

Laminated devices were adhered without detachment during handling and the device exhibit semitransparency. Figure 1 show the transmission spectrum for the device area. Transmittance of over 50% was obtained above 640 nm wavelength. Lower transmittance below 640 nm wavelength was originated absorption of P3HT:PCBM layer. Figure 2 show the *J-V* characteristics obtained under illumination of AM1.5. Device characteristics were dramatically improved to coat ultra-thin PEIE layer on ITO for cathode.

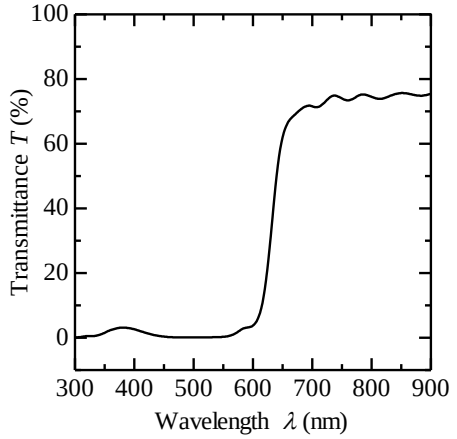

Figure 1 Transmittance of the device

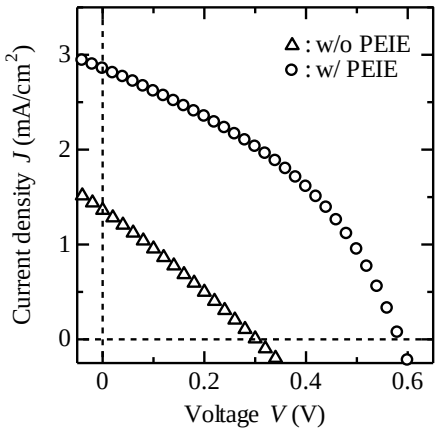

Figure 2 Photovoltaic characteristics

Acknowledgment

Part of this research work is supported by a Charitable Trust Ame Hisaharu Toyama Prefecture University etc. Research Grant Foundation.

References

[1] T.-F. Guo, S. Pyo, S.-C. Chang, and Y. Yang, “High performance polymer light-emitting diodes fabricated by a low temperature lamination process”, Adv. Funct. Mater., vol.11, issue 5, pp.339-343, 2001.

[2] M. Miyagawa, R. Koike, M. Takahashi, H. Bessho, S. Hibino, I. Tsuchiya, M. Harano, M. Endo, and Y. Taniguchi, “Low work function MgAg-coated poly(ethylene terephthalate) films for organic light-emitting device fabrication with lamination process”, Jpn. J. Appl. Phys., vol.46, no.11, pp.7483-7486, 2007.

[3] M. Ohmori *et al.*, “Light- emitting seal using self-aligned organic light-emitting structure”, Jpn. J. Appl. Phys., vol.47, no.1, pp.472-475, 2008.

[4] T. Minami, R. Satoh, H. Okada, and S. Naka, “Double- faced organic light-emitting device using laminate method”, Jpn. J. Appl. Phys., vol.50, 01BC12, 2011.

[5] M. Makha, P. Testa, S. B. Anantharaman, J. Heier, S. Jenatsch, N. Leclaire, J.-N. Tisserant, A. C. Veron, L. Wang, F. Nuesch, and R. Hany, "Ternary semitransparent organic solar cells with a laminated top electrode", Sci Technol Adv Mater., vol.18, no.1, pp.68-75, 2017.

P-43

Elucidation of DNA and RNA base molecules adsorbed on gold nanoparticles using a flocculation-SERS method

Masako Seki[1], Hirotaka Okabe[2], Naoki Matsuda[2], and Masayuki Futamata[1*]

[1]Graduate School of Science and Engineering, Saitama University, Sakura-ku, Saitama, 338-8570 Japan
[2]National Institute of Advanced Industrial Science and Technology Tosu, 841-0052 Japan
[*]Tel: + 81 - 48 - 858 - 3383
[*]E-mail: futamata@chem.saitama-u.ac.jp

Metal nanoparticles are introduced into living cells to elucidate metabolism or to cytotoxicity of nanomaterials using roboust spectroscopy such as surface enhanced Raman scattering (SERS). For such purposes, it is prerequisite to investigate adsorption natures of DNA and RNA bases, since DNA or RNA polymers intensively adsorb on metal nanoparticles via such base molecules using plausible coordination bonds via nitrogen or oxygen atoms in amino, imide or carbonyl end groups instead of sugar or phosphate groups. Indeed Raman spectroscopy inherently provide detailed information on adsorbed molecules such as even subtle modification in molecular structure, orientation or interaction with surrounding species. Nevertheless, it seems that SERS applications in biology have mostly been devoted to detect or discern biopolymers using dye molecules as a marker, which can be done by fluorescence spectroscopy. This is partly due to complicated feature of Raman spectra observed for biopolymers like DNA or RNA, which can be overcome by accumulated information on detailed adsorption properties of base molecules.

Therefore, we investigated adsorbed state of DNA and RNA bases on gold nanoparticles (AuNPs) using flocculation-SERS [1-4], in which interaction between target molecules and AuNPs are adjusted to form flocculates providing huge enhancement factors in Raman scattering. Distinct pH dependences in critical concentration for flocculation (ccf) were observed for different base molecules. For instance, much lower ccf was observed for adenine (A), guanine (G) and cytosine (C) containing an amino group ($–NH_2$) compared to thymine (T) and uracil (U) at pH7, whereas A and G showed lower ccf in acidic conditions (pH2) compared to neutral pH (7), in contrast to C, T and U. We also found with zeta potential measurements that residual citrate molecules strongly adsorb on AuNPs prepared by the Lee-Meisel method, which were not replaced with chloride anions and at least partly disturb adsorption of DNA bases. Hence, we tried to use AuNPs formed by a solution plasma method in H_2O_2 containing solutions, on which the surface are presumed to be free from residuals. Nevertheless, essentially similar ccf and SERS spectra for DNA and RNA base molecules were observed for AuNPs formed by citrate and solution plasma methods. We found that the surface of AuNPs formed by a solution plasma method is covered by gold oxide layer, which was replaced by chloride anions. Thus, it is necessary to control surface coverage of citrate or oxide to elucidate intrinsic adsorption properties of base molecules on AuNPs.

References [1] T. Yajima, Y. Yu, M. Futamata, "Steric hindrance in cationic and neutral rhodamine 6G molecules adsorbed on Au nanoparticles", J. Raman Spectrosc. 2013, 44, 406-411. [2] M. Futamata, M. Ishikura, C. Iida, and S. Handa, "The critical importance of gap modes in surface enhanced Raman scattering", *Faraday Discuss.* 2015, 178, 203-220. [3] T. Mukaiyama,T. Yajima, M. Futamata, "Distinct Adsorbed States of DNA and RNA Bases Investigated by Flocculation-Assisted Surface Enhanced Raman Scattering", *e-JSSNT*2015, 13, 417-425. [4] R. Kuwana, S. Handa, M. Futamata, "Elucidation of hydrated metal ions using flocculation-surface enhanced Raman scattering", *Chem. Phys. Lett.* 2018, 693, 79-83.

P-44

Enzymatic biofuel cell using graphene electrodes with improved interfacial electron transfer

Kenta Kuroishi[1*], Toshinari Doi[1], Kazuki Hoshi[1], Kazuo Muramatsu[2], Yasushiro Nishioka[1] and Satomitsu Imai[1*]

[1]*College of science and technology, Nihon University*
7-24-1 Narashinodai, Funabashi, Chiba 274-8501, Japan
[2]*Incubation Alliance, INC*
1-2-25-D-307, Wadayamadori, Hyogo-ku, Kobe 652-0884, Japan
**E-mail:cskn17016@g.nihon-u.ac.jp, imai@eme.cst.nihon-u.ac.jp*

Enzymatic biofuel cell (EBFC) is a device that converts chemical energy into electric energy by redox reaction using enzymes as catalyst. Since enzymes are biocatalyst, EBFC can operate under mild conditions (normal temperature, normal pressure, around neutral pH), and has the advantage that various energy sources such as sugar and alcohol can be used. Ascorbic acid (AA), also known as vitamin C is also noted as a fuel for EBFC. AA, which is an environmentally biologically friendly compound, is easy to oxidize, so it does not need a precious metal in the electrode reaction and it does not emit harmful substances. Fujiwara et al. reported a small fuel cell fueled with AA, but it could not be said that it is suitable for carrying [1]. Mogi et al. have developed an enzymatic biofuel cell using ascorbic acid as a fuel (AAEBFC) on a flexible polyimide film using MEMS technology [2]. Bilirubin oxidase (BOD) as an enzyme was used as a cathode catalyst, and the output was 1.83 $\mu W/cm^2$. Since porous carbon is used as an electrode, the electrode has no flexibility and there was a problem that the electrode peels off from the substrate due to repeated bending. Hoshi et al. reported AAE BFC using graphene-coated carbon fiber woven fabric (GCFC) with large specific surface area [3]. The output was 34.1 $\mu W/cm^2$, indicating the usefulness of GCFC as an electrode material. However, the reaction of the oxygen reduction cathode is rate limiting, and it is necessary to improve it.

To improve the performance of the cathode, it is important to optimize the amount of enzyme modification to the electrode and supply sufficient oxygen. In other words, when the enzyme is uniformly immobilized on the electrode surface and the cathode is in contact with the atmosphere, BOD reduces more oxygen and obtains a larger catalytic current. In addition, since BOD receives electrons from the electrode at a site called T1-Cu site, it can be said that the reaction occurs more efficiently as the distance between the electrode surface and the T1-Cu site is shorter [4].

In the EBFC, since the electrode surface does not tend to engage the enzyme T1-Cu proximally, the electron transfer rate becomes slow. However, Brocato et al. showed that electron transfer efficiency improves by crosslinking the enzyme to the electrode using 1-Pyrenebutyric acid N-hydroxy-succinimide ester (PBSE) [5]. Moreover, Lopez et al. reported that when both PBSE as a crosslinking agent for BOD and 2,5-Dimethyl-1-phenyl-1H-pyrrole-3-carbaldehyde (DPPC) as an orienting agent were modified on the CNT electrode it was shown that an orientation efficiency of 90% can be obtained [6].

Based on the above, in this study, we optimized the amount of BOD modification using GCFC as an electrode, and then evaluated the performance of the cathode to which PBSE and DPPC were added. Furthermore, the prototype evaluation of the atmospheric exposure type AAEBFC using the improved GCFC cathode was carried out.

In the optimization experiment of BOD modification amount, cyclic voltammetry (CV) was measured by changing the concentration of the enzyme solution dropped to the electrode to 1.0, 25.0, 50.0, 75.0, 100.0, 125.0 mg/ml. The reduction onset voltage and the angle at the fall of the graph were maximum at 50.0 mg/ml (Fig. 1). At 50.0 mg/ml, the enzyme was modified on the electrode without excess or deficiency, and electron transfer between the electrode and the enzyme was considered most efficiently performed. In addition, a large reduction current peak was observed at 50.0 mg/ml. This indicates that the diffusion of the reactant on the electrode surface is rate-determining at 50.0 mg/ml.

Comparison of the reduction current of the cathode depending on the presence or absence of the additive was carried out by measuring the CV (Fig 2). Compared with those modified only with BOD, those added with DPPC or DPPC-PBSE improved both the peak current density and the reduction onset voltage. Therefore, it was found that even when GCFC is used as an electrode, electron transfer efficiency improves by adding additives.

The output characteristics of AAEBFC using BOD modified cathode and DPPC-PBSE-BOD modified cathode are shown in Fig. 3. For AAEBFC using BOD modified cathode, output of 238.5 $\mu W/cm^2$ was obtained at 0.245 V. Due to the optimization of the BOD modification amount and the atmospheric exposure type structure, the output was improved about 7 times compared to the output of Hoshi et al. [3]. Also, with AAE BFC using DPPC-PBSE-BOD modified cathode, output of 338.8 $\mu W/cm^2$ was obtained at 0.292 V. Depending on the presence or absence of additives, the output improved about 1.4 times.

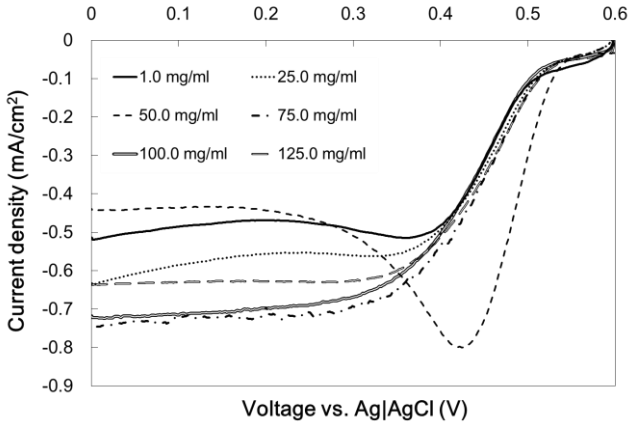

Figure 1. Comparison of cathode CV with BOD modification

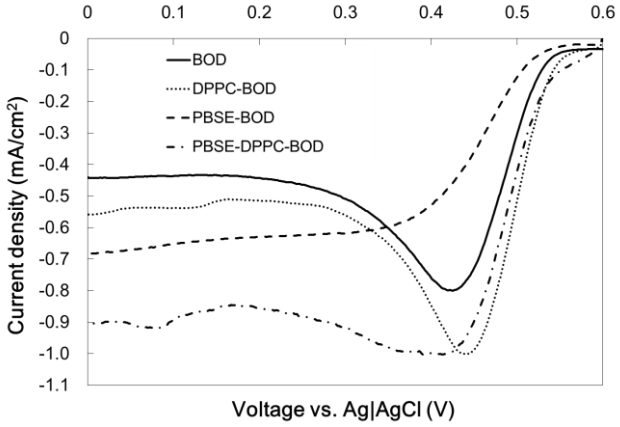

Figure 2. Comparison of cathode CV with or without additives

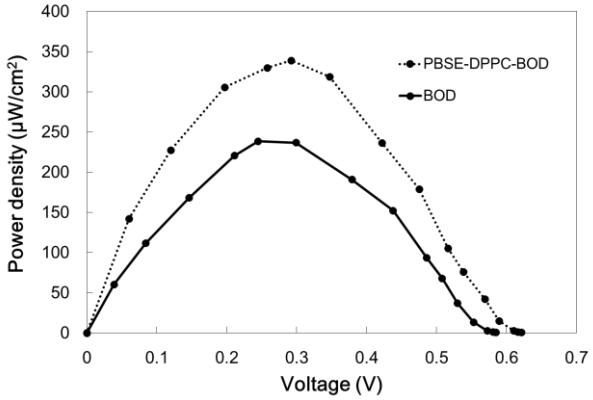

Figure 3. Output characteristics when DPPC-PBSE is modified

[1] N. Fujiwara, S. I. Yamazaki, Z. Siroma, T. Ioroi, and K. Yasuda, "L-Ascorbic acid as an alternative fuel for direct oxidation fuel cells," Journal of power sources, **167**(1), 32-38, 2007.

[2] H. Mogi, Y. Fukushi, S. Koide, R. Sano, T. Sasaki, and Y. Nishioka, "A Flexible Ascorbic Acid Fuel Cell with a Microchannel Fabricated using MEMS Techniques," In Journal of Physics: Conference Series (Vol. 476, No. 1, p. 012065). IOP Publishing, 2013.

[3] K. Hoshi, K. Muramatsu, H. Sumi, and Y. Nishioka, "Miniaturized ascorbic acid fuel cells with flexible electrodes made of graphene-coated carbon fiber cloth," Japanese Journal of Applied Physics, **55**(4S), 04EC11, 2016.

[4] F. Tasca, D. Farias, C. Castro, C. Acuna-Rougier, and R. Antiochia, "Bilirubin oxidase from Myrothecium verrucaria physically absorbed on graphite electrodes. Insights into the alternative resting form and the sources of activity loss," *PloS one*, **10**(7), e0132181, 2015.

[5] S. Brocato, C. Lau, and P. Atanassov, "Mechanistic study of direct electron transfer in bilirubin oxidase," Electrochimica Acta, **61**, 44-49, 2012.

[6] R. J. Lopez, S. Babanova, Y. Ulyanova, S. Singhal, and P. Atanassov, "Improved interfacial electron transfer in modified bilirubin oxidase biocathodes," ChemElectroChem, **1**(1), 241-248, 2014.

P-45

Control of threshold voltage in a low-voltage operation organic field effect transistor

Yasuyuki Abe[1], Heisuke Sakai[1], Toan Thanh Dao[2], and Hideyuki Murata[1,*]

[1]Japan Advanced Institude of Science and Technology,
1-1 Asahidai, Nomi, Ishikawa, 923-1211 Japan
[2]University of Transport and Communications,
No. 3, Cau Giay Street, Lang Thuong Ward, Dong Da District, Hanoi, Vietnm

Tel: + 81 - 761 - 51 - 1531, Fax: + 81 - 761 - 51 – 1149
**E-mail:murata-h@jaist.ac.jp*

1. Introduction

In recent years, organic field effect transistors (OFETs) have attracted much attention owing to its unique advantages of low-cost, solution process and large-area ability. Controlling the threshold voltage (V_{th}) of OFET is one of the reserch target in order to apply the OFET for data storage, the CMOS circuit, or active sensor [1]. Charge trapping has been widely used to control V_{th}. For programming processes, charges in the active layer are injected into a trap sites by application of programming voltage (V_{pro}). An electric field created by the trapped charges modulates the charge concentration in the conductive channel which induces the shift of the threshold voltage (V_{th}). Consequently, V_{th} can be controlled by the amount of trapped charges. In order to trap charges, polymers such as poly(methylmethacrylate), polystyrene, polyvinylphenol have been employed as the trap site and formed on the gate dielectric (SiO_2) [2,3]. Despite achievement of the V_{th} shift, operation voltages in those devices are still as much high as several 10 to 100 V. Thus, the reduction of the operation voltage is necessary. In this study, we report the control of V_{th} in low voltage (5 V) driven OFET by using two layer insulating layer structure composed of poly (vinyl cinnamate) (PVCN) and SiO_2. V_{th} of the OFET shifted more than -1 V when V_{pro} of -80 V was applied to trap holes. In addition, the shifted V_{th} was almost unchanged after 10^4 seconds.

2. Experimental

Figure 1 shows the schematic structure of OFET. Our devices were fabricated on heavily doped n-type silicon wafers with a 400-nm-thick silicon dioxide (SiO_2). The wafers were cleaned ultrasonically with acetone, pure water and isopropyl alcohol. A 5-nm-PVCN layer was deposited by spin coating at 2000 rpm for 60 s. This PVCN film was then exposed to UV light for 30 min and dried at 140 ºC for 1 h. A 50nm Ag source-drain electrodes were thermally evaporated and modified by immersion in a solution of pentafluorothiophenol in ethanol. The channel width and length were 2 mm and 50 µm, respectively. Finally, a 100-nm-thick semiconductor layer was formed by spin-coating from a mixed solution TIPS-pentacene and PS. Electrical measurements of OFETs were carried out at room temperature using a Keithley 4200 semiconductor characterization system in a dry nitrogen atmosphere.

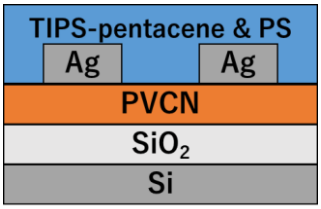

Fig. 1. Device structure of OFET.

3. Results and discussion

Figures 2 and 3 show the output and initial transfer curves of OFET, which are typical in a field-effect transistor. The field-effect mobility, the on/off ratio, the subthreshold swing (*SS*) , and the V_{th} were observed to be 0.23 cm^2/Vs, 1.82 × 10^7, 0.17 V/dec, -0.94 V, respectively. The device parameters are quite similar to those of the polyvinylalchol-based OFET [4], suggesting that gate dielectric bilayer of PVCN/SiO_2 does not effect on OFET performance.

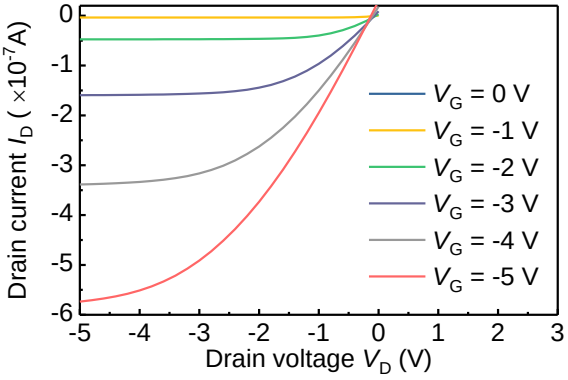

Fig. 2. The output curves of OFET.

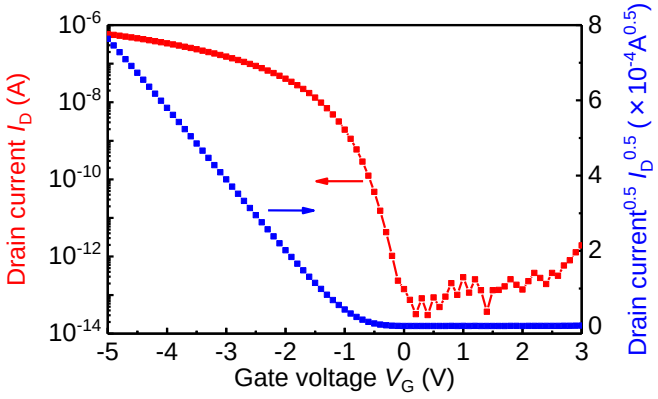

Fig. 3. The initial transfer curves of OFET.

Figure 4 shows $I_D^{0.5}$ versus V_G measured after applying various programming voltage (V_{pro}) The V_{th} was negatively shifted in the high negative V_{pro}. The V_{th} was estimated to be from −0.9 to −1.9 V when the V_{pro} varied from 0 to -80 V. The experimental result clearly indicates that the V_{th} is electrically controlled in our OFET device.

The V_{th} negatively shifts by increasing V_{pro}, attributing to hole trapping at the PVCN/SiO_2 interface. Indeed, upon application of a high negative V_{pro} to a gate electrode, holes are injected from the source-drain electrodes through the pentacene semiconducting and PVCN layers and subsequently trapped at the interface of PVCN and SiO_2 [5]. The trapped holes then deplete holes in the *p*-channel pentacene, leading to the V_{th} was shifted to more negative voltage.

Figure 5 shows the relations of ΔV_{th}-V_{pro}- number of trapped hole (ΔN), where ΔN was calculated using the equation: $C_i \Delta V_{th}/q$, where q is the elementary charge, C_i is the capacitance per unit area of the gate dielectric. The ΔN was increased with increasing the V_{pro}. The calculated ΔN value can be comparable to that observed in OFET memory based on poly (methyl methacrylate)/SiO_2 [2].

Figure 6 shows the relative change of programmed V_{th} as a function of time. As can be seen, the programmed V_{th} is almost unchanged after 10^4 seconds (99.3% compared with the initial V_{th}), meaning that that the programmed OFET is highly stable. We note here that beside stability of programmed state, the operating voltage of OFET device is as low as 5 V, much lower than other OFET memories based on charge trapping where operating voltage is usually in several tens of voltages [2,6,7]. The lowering voltage makes our device more possible for practical application in current electronic technology where a supply voltage is usually below 5 V.

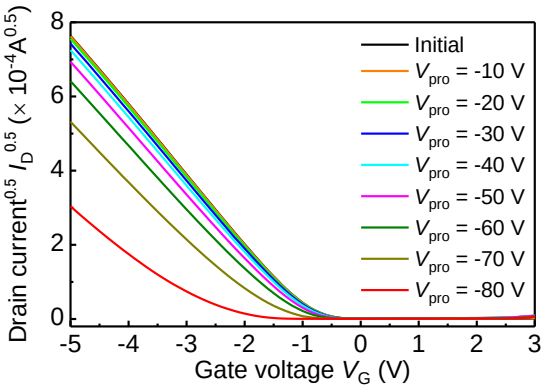

Fig.4 The shift of the transfer characteristic by V_{pro}.

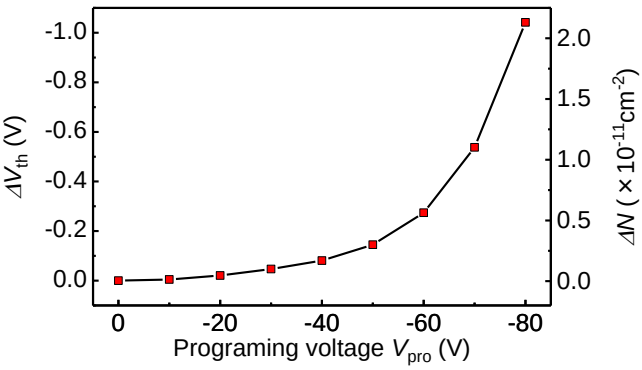

Fig. 5. The V_{pro} - ΔV_{th} – ΔN characteristic.

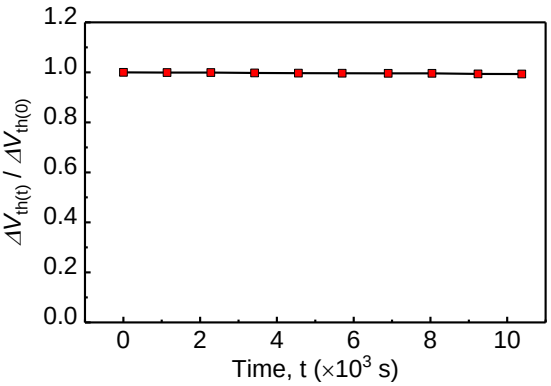

Fig.6. The relative change of V_{th} after programming OFET.

4. Conclusions

In this study, low voltage driven OFET with threshold controllability was fabricated. We succeeded in realizing a driving voltage of -5 V and shifting V_{th} by 1.0 V or more. And the threshold voltage was very stable after the change.

5. References

[1] T. T. Dao, H. Sakai, H. T. Nguyen, K. Ohkubo, S. Fukuzumi, and H. Murata, “Controllable Threshold Voltage in Organic Complementary Logic Circuits with an Electron-Trapping Polymer and Photoactive Gate Dielectric” ACS Appl. Mater. Interfaces, vol.8, no.28, pp.18249-18255, June 2016.

[2] C. Feng, T. Mei, and X. Hu, “Influence of trapping states at the dielectric–dielectric interface on the stability of organic field-effect transistors with bilayer gate dielectric” Organic Electronics, vol.12, no.8, pp1304-1313, April 2011.

[3] K. Baeg, Y. Noh, J. Ghim, B. Lim, and D. Kim, “Polarity effects of polymer gate electrets on non-volatile organic field-effect transistor memory” Advanced Functional Materials, vol.18, no.22, pp.3678-3685, 2008.

[4] L. Feng, W. Tang, X. Xu, Q. Cui, and X. Guo, “Ultralow-voltage solution-processed organic transistors with small gate dielectric capacitance” IEEE Electron Device Lett, vol.34, no.1, pp.129-131, January 2013.

[5] C. M. Tran, H. Sakai, T. Murakami, and H. Murata, “Multi-bit Memory Effect in an Organic Field Effect Transistor using a Charge Storage Polymer” The 64th JSAP Spring Meeting, 17p-302-11, March 2017.

[6] P. Zhang, X. Chen, W. Li, H. Ling, W. Wang, G. Zhang, M. Yi, L. Xie, W. Shi, N. Shi, W. Huang, “Organic non-volatile memory based on pentacene/tris(8-hydroxy quinoline) aluminum heterojunction transistor”. Organic Electronics, 2018, DOI: 10.1016/j.orgel.2018.02.038.

[7] Y. Jeong, D. Yun, S. H. Kim, J. Jang, C. Park, “Photoinduced Recovery of Organic Transistor Memories with Photoactive Floating-Gate Interlayers” ACS Appl. Mater. Interfaces, vol.9, no.13, pp11759–11769, 2017.

P-46

Highly sensitive resistive-type acetone sensor using platinum nano-particle decorated alumina nanorods/ organic semiconductor nano-composites

Eiji Itoh 1, Hiroaki Sugiura 1 and Hironobu Ono 2

[1]*Department of Electrical and Computer Engineering, Faculty of Engineering, Shinshu University, 4-17-1, Wakasato, Nagano, 380-8553 Japan*
[2] *Nippon Shokubai Co.,Ltd.*
Tel/Fax +81-26-269-5227
E-mail: eitoh@shinshu-u.ac.jp

Breath analysis has been utilized as a useful and important tool for the noninvasive diagnosis and monitoring of wide range of deseases. Especially, acetone is a specific breath marker for diabetes and fat combustion. The acetone concentration in the breath varies from 0.3 to 0.9 ppm in healthy people to more than 2 ppm for diabetics. Therefore, the development of portable, hand-held, and real-time measurement of acetone gas sensor with the sensitivity of 0.1 ppm from human breath is desirable but still challenging.

Recently, several types of nano-structured oxide materials (nanoparticles, nanorods, and nanosheets) have shown high sensitivity and selectivity, even up to 80-90 %RH. However, the use of oxide-based nano-materials for breath sensing devices is not trivial as reaching high temperature (200-450 ºC). It is a severe drawback for the application of portable devices and the reasonable low power consumption requires a locally heated substrate, such as micro-patterned device based on the MEMS technologies. Thus, the development of highly sensitive small acetone sensors operating at low temperature below 100 ºC is still challenging but quite attractive [1-5].

In this study, we have tried to investigate the highly sensitive resistive-type acetone sensors using platinum nano-particle decorated alumina nanorods/ organic semiconductor nano-composites. All devices were fabricated on 150-nm-thick indium tin oxide (ITO) electrodes patterned to be 2-mm-wide and precoated on glass substrates. The ITO electrodes were patterned to be separated to 10 to 40 um gap. The precursor of platinum (~5 nm in diameter) decorated alumina nanorods were deposited by meniscus coating followed by the high temperature heat-treatment at 500 ºC for 1 h. Finally, an air-stable polymer based p-type semiconductor (PQT-12: poly(3,3‴- didodecylquaterthiophene)) thin film were infiltrated and spin-coated on the surface of alumina nanorods. Here, we chose platinum nanoparticles as the catalyst of oxygen and acetone, and alumina nanorods as the electrically inert supporting medium and the increment of surface area. The resistance or conductive current measured at 1.5 V were monitored under the acetone concentration between 0.2-1.0 ppm and 1.0-5.0 ppm in the laboratory-built measurement system [6].

Figure 1 shows the relationship between the measurement time and the current flow under various acetone concentration. Here, acetone gas was diluted by dry air (< 1 %RH) at 30 ºC, and the gap of the ITO pair was 10 um. The current decreases with the increment of acetone concentration. Here, acetone is known as the reducing gas of oxidized material onto the platinum nanoparticles, and the combination of reactive oxygen intermediate and acetone molecule produce electrons on the surface of platinum nanoparticles. It is considered these electrons cancel the electrical carriers in PQT-12 (holes). The details will be discussed in the conference.

This work was partly supported by a Grant-in-Aid for Scientific Research (No. 15K13972) from the Ministry of Education, Culture, Sports, Science and Technology, Japan.

References

[1] BORINI et al. ACS Nano 7, 11166–11173, 2013.
[2] M. Karmaoui et al. Sensors and Actuators B 230, 697–705, 2016.
[3] Zan et al. Appl. Phys. Lett. 98, 253503, 2011.
[4] J.-Y. Shen et.al, Sensors and Actuators B, 239, 597-607, 2017
[5] I.-D. Kim et. al, “Smart Sensors for Health and Environment Monitoring, Chap. 1 Exhaled Breath Sensors”, Springer, 2015.
[6] E. Itoh and Z. Yuan, JJAP, 58, 05EC03, 2017.

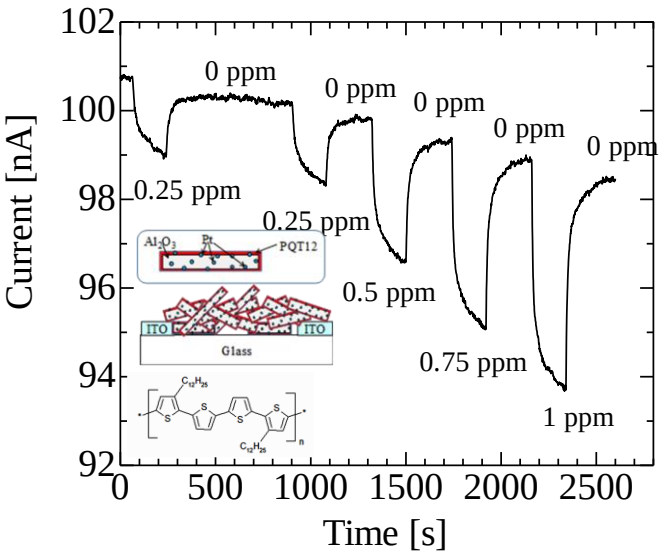

Fig. 1 The relationship between the measurement time and the current flow under various acetone concentration.

P-47

Construction of high-sensitive immunosensor with polymer brushes

Yuka Ozawa[1, 2)], Hidenobu Aizawa[2)], Yuji Kimura[1)] and Kazunori Yamada[1)]

1) College of Industrial Technology, Nihon University,
1-2-1Izumi-cho, Narashino, Chiba 275-8575 Japan
2) National Institute of Advanced Industrial Science and Technology (AIST),
16-1 Onogawa, Tsukuba, Ibaraki 305-8569, Japan
E-mail:hide-aizawa@aist.go.jp

Introduction

In the environment and medical field, there is a need for a sensor capable of measuring the object to be measured with high accuracy. Screening becomes possible especially if high-sensitive measurement can be performed in situ. Biosensor is a measurement method that can be measured rapidly and accurately in situ. Biosensors use biological molecules such as antibodies, DNA, and cells for detection. A biosensor using an antibody as a biological molecule is called an immunosensor. Antibodies have specificity to bind to specific substances. By using the characteristics of this antibody, the immunosensor can selectively measure only the object to be measured.

The measurement accuracy of this immunosensor is believed to depend on the immobilization amount of the recognition antibody of the molecule. If immobilization of the antibody can be increased, we believe that it will be possible to achieve high accuracy of the immunosensor by reliably capturing the antigen. In this study, in order to increase the immobilization amount of the antibody on the sensor, the synthesis method of the polymer brush, which becomes the fixed field, was investigated (Figure 1). We report on the results of investigating the synthesis conditions of polymer brushes using polymeric brush synthesis initiation point and plasma polymerization of Initiators for Continuous Active Regeneration Atom Transfer Radical Polymerization (ICAR ATRP) [1-3].

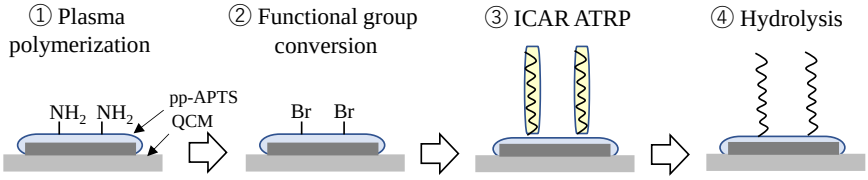

Figure 1 Schematic of modification on QCM electrode.

Materials and Methods

A quartz crystal microbalance (QCM) of an AT-cut 9 MHz Au electrode was used as a starting substrate for synthesis. Plasma polymerized 3-aminopropyl-triethoxysilane (pp-APTS) film was deposited with polymerization of RF power 100 W, Polymerization time 180 s, supply pressure of monomer 20 Pa polymerized at the synthesis starting point of polymer brush. The functional group of the pp-APTS film was converted by triethylamine, 2-bromoisobutyryl bromide at 0 °C for 1 h. Polymer brushes (poly (tert-Butyl Acrylate [t-BA])) were synthesized by ICAR ATRP at 60 °C for 15 h. In order to obtain Poly (Acrylic acid [AA]), poly (t-BA) was hydrolyzed with dichloromethane solution containing 10% trifluoroacetic acid for 5 h. The processes of plasma polymerization, functional group conversion, polymer brush synthesis, and hydrolysis were analyzed by atomic force microscopy (AFM) and X-ray photoelectron spectroscopy (XPS).

Results and discussion

Each process of QCM surface modification was measured and analyzed using XPS. Figure 2 shows the analysis results of C1s high resolution measurement of QCM surface modification. Here, spectral analysis was performed on other binding states by spectral correction with bond energy of 284.5 eV as C-H bond. pp-APTS was only binding from CH_2 (284.5 eV) and NH_2 (286 eV). In the functional group conversion, since the C=O peak (288 eV) derived from the 2-bromoisobutyryl bromide bond was present; functional group conversion from NH_2 to Br could be confirmed.

In polymer brush synthesis by ICAR ATRP, the C-H derived peak sharply increased. This is thought to be CH_2 derived from Poly(tBA) polymerized directly on QCM by ICAR ATRP. In the hydrolysis, the C=O spectrum was large. It was found that poly(AA) was obtained by decomposition of tert-butyl group of poly(tBA) by hydrolysis.

Based on the above analysis results, we established a process by which a polymer brush can be produced directly on the QCM as an antibody immobilization field, using pp-APTS as a synthesis starting point.

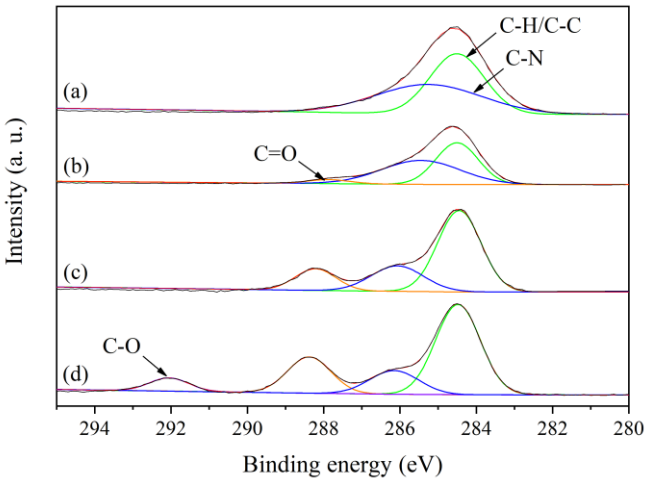

Figure 2 High resolution XPS spectra of the C1s signals of each treatment on QCM surface. (a) pp-ATPS, (b) change from NH_2 to Br, (C) ICAR ATRP, and (d) hydrolysis.

References

[1] W. Jakubowski, K. Matyjaszewski, "Activators regenerated by electron transfer for atom-transfer radical polymerization of (meth) acrylates and related block copolymers", Angewandte Chemie International Edition, Vol. 406, No. 27, pp.4482-4486, 2006.

[2] K. Matyjaszewski, W. Jakubowski, K. Min, W. Tang, J. Huang, W. A. Braunecker, N. V. Tsarevsky, "Diminishing catalyst concentration in atom transfer radical polymerization with reducing agents", Proceedings of the National Academy of Science,Vol. 103, pp. 15309-15314, May 2006.

[3] P. Chmielarz, M. Fantin, S. Park, A. A. Isse, A. Gennaro, A. J. D. Magenau, A. Sobkowiak, K. Matyjaszewski, "Electrochemically mediated atom transfer radical polymerization (eATRP)", Progress in Polymer Science, Vol. 69, pp.47-78, Jun 2017.

P-48

Light emission characteristics of hyperbranched copolymer with photon upconversion dyes system

HirokazuYamane[1], Urata Yasutaka[1], Genta Takatoki[1], Hidekazu Konishi[2] and Toshikiko Nagamura[1]

[1]National Institute of Technology, Kitakyushu College,
5-20-1, Shii, Kokuraminami-ku, Kitakyushu city, Fukuoka 802-0985, Japan
Tel: + 81 - 93 - 964 - 7307, Fax: +81- 93 -964 - 7307
E-mail:hyamane@kct.ac.jp
[2]ASAHI YUKIZAI Corporation

Photon upconversion (UC) is a technique to convert long wavelength light into short wavelength light. We can use long wavelength light as excitation light if a far-red light of wavelength 800-2500nm can be converted into visible light in UC dye system efficiently, and can utilize the energy of the light of the sun spectrum part which is lost without being able to collect until now to a solar battery or photomedical care as optical elements. In this study, we constructed the dyes system by copolymerizing emitter monomer, second component monomer and initiator monomer and introducing sensitizer into that for the purpose of improving the efficiency of the organic thin film solar cell. Then, we studied to produce the film by concentrating and immobilizing this photon UC dye system. Fig.1 shows the schematic illustration of the photon UC system with hyperbranched copolymer containing emitter dyes. Those who intend to contribute to the conference by oral or poster presentation are requested to submit an abstract by this form [1].

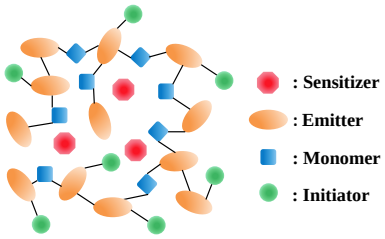

Fig.1 Schematic illustration of the photon UC system with hyperbranched copolymer containing emitter dyes.

Fig.2 shows the chemical structures of the sensitizer monomer palladium(Ⅱ)Protoporphyrin-Ⅸ (Pd(Ⅱ)PPⅨ) and the emitter monomer BIOC-ANT-AE (BAA) used by this study. The emitter dye BAA component hyperbranched copolymers using the initiator monomer dimethyl 2,2'-Azobis(isobutyrate) (MAIB) and the second component monomer divinylbenzene (DVB) or alicyclic divinyl ether monomer (ONB-DVE) were synthesized. The mol ratios of (BAA/DVB/MAIB) or (BAA/ONB-DVE/MAIB) in the hyperbranched copolymers were assumed 50/10/5, 50/30/5 and 50/50/5. Anisole solutions of [sensitizer monomer Pd(Ⅱ)PPⅨ/emitter monomer BAA], [sensitizer monomer Pd(Ⅱ)PPⅨ/emitter component hyperbranched copolymer (BAA/DVB/MAIB)], and [sensitizer monomer Pd(Ⅱ)PPⅨ/emitter component hyperbranched copolymer (BAA/ONB-DVE/MAIB)] the photon UC dyes systems were prepared. The solid films of the photon UC dyes systems were prepared by solvent cast method. In order to evaluate spectrum properties of the photon UC dyes system, UV-Vis absorption spectrum measurement and fluorescence spectrum measurement were carried out with a UV-VIS-NIR spectrophotometer and a spectrofluorometer, respectively.

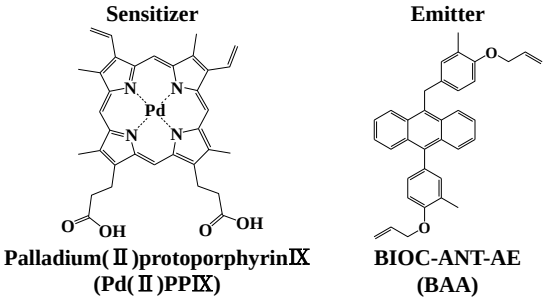

Fig.2 Chemical structures of sensitizer and emitter dyes.

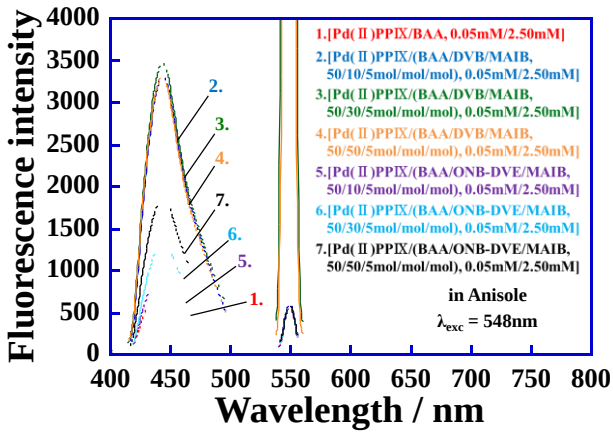

Fig.3 Fluorescence spectra of photon UC dye system in anisole under excitation at λ_{exc} = 548nm after the deoxidation treatment by the substitute with N_2 gas to remove dissolved O_2..

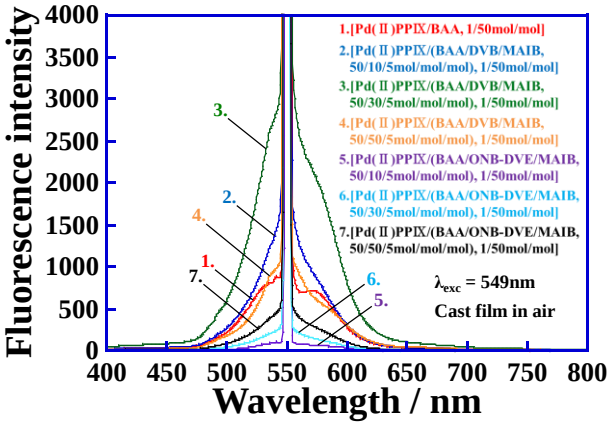

Fig.4 Fluorescence spectra of photon UC dye system cast film in air under excitation at λ_{exc} = 549nm.

Fig.3 shows fluorescence spectra of anisole solutions of the [Pd(II)PPIX/BAA] photon UC dyes system which was prepared the concentration ratio 0.05mM/2.50mM, the [Pd(Ⅱ)PPIX/(BAA/DVB/MAIB), 0.05mM/2.50mM] photon UC dyes systems containing the emitter dye component hyperbranched copolymers (BAA/DVB/MAIB) which were prepared in (BAA/DVB/MAIB) mixture ratio 50/10/5, 50/30/5, and 50/50/5 mol/mol/mol for sensitizer dye Pd(II)PPIX 1mol, respectively, and the [Pd(Ⅱ)PPIX/(BAA/ ONB-DVE /MAIB), 0.05mM/2.50mM] photon UC dyes systems containing the emitter dye component hyperbranched copolymers (BAA/ ONB-DVE /MAIB) which were prepared in (BAA/ ONB-DVE /MAIB) mixture ratio 50/10/5, 50/30/5, and 50/50/5 mol/mol/mol for sensitizer dye Pd(II)PPIX 1mol, respectively, under excitation at λ_{exc} = 548nm after the deoxidation treatment by the substitute with N_2 gas to remove dissolved O_2.. From the results, photon UC which was the fluorescence of BAA in 400-500nm wavelength area was confirmed in all systems. In the case of excitation wavelength λ_{exc} = 548nm, the systems containing six emitter copolymers showed the intensity of fluorescence that was higher than the [Pd(II)PPIX/BAA] photon UC dyes system.

Fig.4 shows fluorescence spectra of cast films of the [Pd(II)PPIX/BAA] photon UC dyes system which was prepared the concentration ratio 0.05mM/2.50mM, the [Pd(Ⅱ)PPIX/(BAA/DVB/MAIB), 0.05mM/2.50mM] photon UC dyes systems containing the emitter dye component hyperbranched copolymers (BAA/DVB/MAIB) which were prepared in (BAA/DVB/MAIB) mixture ratio 50/10/5, 50/30/5, and 50/50/5 mol/mol/mol for sensitizer dye Pd(II)PPIX 1mol, respectively, and the [Pd(Ⅱ)PPIX/(BAA/ONB-DVE/MAIB), 0.05mM/2.50mM] photon UC dyes systems containing the emitter dye component hyperbranched copolymers (BAA/ONB-DVE/MAIB) which were prepared in (BAA/ONB-DVE/MAIB) mixture ratio 50/10/5, 50/30/5, and 50/50/5 mol/mol/mol for sensitizer dye Pd(II)PPIX 1mol, respectively, under excitation at λ_{exc} = 548nm in air. From the results, broad peaks around 549nm that was the excitation wavelength were shown in all seven photon UC dyes systems. However, because the density of atoms and molecules of the photon UC dyes systems became more concentrated by the fabrication of the cast films, it was thought that these peaks occurred because of the formation of excimers. Also, it was able to confirm the very small photon UC that was the fluorescence of BAA in all cast films of the photon UC dyes systems. As the reason for that, the energy transfer by the collision between dyes was hard to happen because the molecular motility of dye molecules were strongly restricted by the fabrication method of this study. Therefore, it was thought that the photon UC fluorescence was hard to happen in all seven photon UC dyes systems.

References

[1] Radiy R. Islangulov, Joseph Lott, Christoph Weder, and Felix N. Castellano, "Noncoherent Low-Power Upconversion in Solid Polymer Films", *J. Am. Chem. Soc.*, 129 (42), 12652-12653(2007).

[2] Tanya N. Singh-Rachford and Felix N. Castellano, "Pd(II) Phthalocyanine-Sensitized Triplet-Triplet Annihilation from Rubrene", *J. Phys. Chem. A*, 112, 3550-3556(2008).

[3] Soo Hyon Lee, Mathieu A. Ayer, Roberto Vadrucci, Christoph Weder* and Yoan C. Simon, "Light upconversion by triplet–triplet annihilation in diphenylanthracene-based copolymers", *Polym. Chem.*, 5, 6898-6904(2014).

[4] Y. Urata, Y. Yamasaki, T. Nagamura, H. Yamane, *Annual Meeting on Photochemisry 2017*, 2017, 1P02.

P-49

Ion-Assisted Deposition of Vinyl Polymer with Amino Units

Koichi Momose, Yuji Komuro, Kuniaki Tanaka, and Hiroaki Usui

Division of Applied Chemistry, Tokyo University of Agriculture and Technology,
2-24-16 Naka-cho, Koganei, Tokyo, 184-8588 Japan,
Tel: + 81 - 42 - 388 - 7055, Fax: +81 - 42 - 388 - 7055,
E-mail: s178394u@st.go.tuat.ac.jp

Surface modification plays important roles for improving physical and chemical characteristics of materials. If a specific chemical group can be added on the surface of a material, one can control chemical activity of the surface, which can help, for example, improve the adhesion with other materials. This paper proposes a technique for chemical modification of surface by way of depositing a polymer thin film using an ion-assisted vapor deposition (IAD) polymerization method.

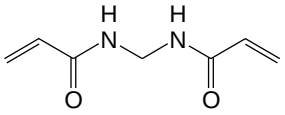

Fig. 1 Structure of the monomer

Figure 1 shows the chemical structure of the monomer material *N*,*N*'-methylenebisacrylamide (MBAA). The monomer was evaporated from a Knudsen cell at a temperature of about 140°C in high vacuum, and was deposited on a glass substrate precoated with a silver thin film. At the same time, argon ion beam was irradiated to the substrate surface to enhance radical polymerization of the monomer. It is expected that the ion irradiation also help to improve the adhesion strength of the deposited film and the substrate. The ion energy was 1000 eV and the ion current density was about 0.04 μA/cm^2. For comparison, films were deposited both with and without ion irradiation. Chemical structure of the deposited film was investigated by IR spectra measured by reflection-absorption mode. Mechanical strength of the films were characterized by the pencil hardness test according the protocol of JIS K5600-5-4. Chemical stability of the films were estimated by visual inspection after sonicating the films in organic solvents.

Figure 2 shows the IR spectra of the monomer (a) and the films deposited without (b) and with (c) the ion irradiation. The film deposited without ion irradiation had absorption peaks at the same wavenumbers as the monomer, while the film deposited with ion irradiation showed pronounced peaks by C-H vibration of alkyl chain at 2780 and 2860 cm^{-1}. This result suggests that the ion irradiation enhanced vinyl polymerization of the monomers.

Figure 3 shows the result of visual inspection of the films deposited without (a1, a2) and with (b1, b2) ion irradiation in as-deposited state (a1, b1) and after sonication in acetone (a2, b2). The film deposited without ion irradiation dissolved completely in acetone, while the film deposited with ion irradiation endured the ultrasonic cleaning in acetone. The same result was observed by sonicating the films in tetrahydrofran. The film deposited without ion irradiation had poor mechanical strength, giving a pencil harness smaller than F, while the film deposited with ion irradiation had a pencil hardness between 5H and 6H. These results reflect that the ion-assisted deposition forms stable polymer thin films while the simple vapor deposition yields a film by coagulation of monomers. It is expected that the bifunctional nature of MBAA monomer leads to formation of a mechanically stable network polymer by IAD.

The results obtained so far was applied for improving the adhesion characteristics of acrylonitrile butadiene styrene copolymer (ABS). The ABS was cleaned with ethanol and was treated with a plasma cleaner. A stud pin for adhesion test (Quad Group 901106, 2.7 mm diameter) was attached on its surface with an epoxy resin, and its adhesion strength was measured by a pull-off test. When the stud pin was directly attached on the surface of ABS, the adhesion strength was 1.5 N/mm^2, while the adhesion strength increased to 2.6 N/mm^2 by modifying the ABS surface with the IAD film. It is concluded that the IAD of MBAA is a promising method for surface modification.

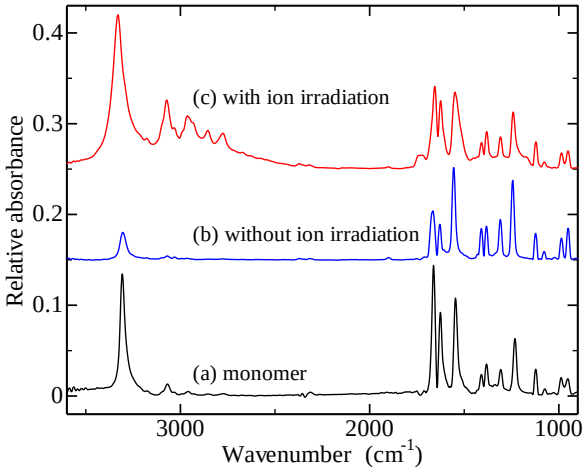

Fig. 2 IR spectra of the monomer (a) and films deposited without (b) and with ion irradiation (c).

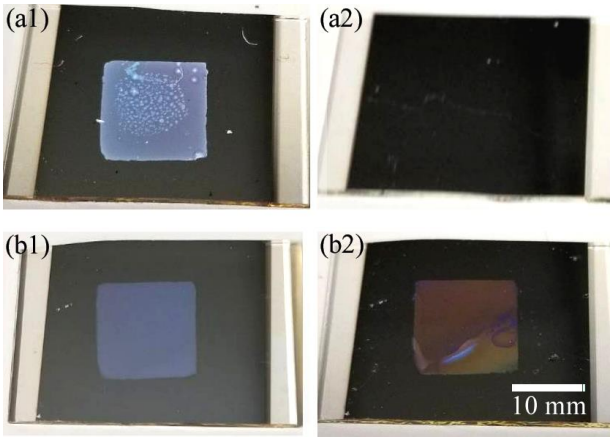

Fig. 3 Visual inspection of the films deposited without (a1, a2) and with (b1, b2) ion irradiation in as-deposited state (a1, b1) and after sonicating in acetone (a2, b2).

P-50

Preparation of Diamond Nanoparticle Layers by A Surface Adsorption Method

Yuriko Sugimoto[1], Fujio Ohishi[2], Kuniaki Tanaka[1], and Hiroaki Usui[1]

[1]*Division of Applied Chemistry, Tokyo University of Agriculture and Technology, 2-24-16 Naka-cho, Koganei, Tokyo, 184-8588 Japan, Tel: + 81 - 42 - 388 - 7055, Fax: +81 - 42 - 388 - 7055, E-mail: s176428q@st.go.tuat.ac.jp*

[2]*Research Institute for Integrated Science, Kanagawa University, 2946 Tsuchiya, Hiratsuka, Kanagawa 259-1293, Japan*

Organic materials frequently suffer difficulty in injecting electrons due to their small electron affinity. As a consequence, cathodes of organic devices need to be covered with electron injection layers that have high LUMO levels. However, such materials tend to be unstable and vulnerable for oxidation. Diamond is a material that have both low electron affinity and excellent stability, making it attractive for electron injection. However, formation of diamond thin film requires elaborate high-temperature processes. We have been trying to make thin films of diamond nanoparticles (ND) on the surface of cathode using an electrophoretic deposition technique. In this work, we propose to prepare a thin film of ND by a simple adsorption method, and investigated its characteristics as an electron injection layer.

Figure 1 illustrates the procedure for forming a ND layer by adsorption. The aluminum substrate was treated with an UV-O_3 cleaner, and a self-assembled monolayer (SAM) was prepared on its surface by immersing into a toluene solution of vinyltrimethoxysilane (VTMS). The SAM of VTMS was oxidized by immersing into a mixture of $KMnO_4$, $NaIO_4$, and K_2CO_3 to obtain a SAM having a terminal unit of carboxy group. It is expected that this surface is negatively charged in an aqueous solution. The SAM-modified substrate was then immersed in a 0.005 wt% water dispersion of ND (NanoCarbon Research Institute, NanoAmando B) for 5 min. The NDs had a zeta potential of +34.8 mV, and are expected to adsorb on the surface modified with the SAM of carboxy terminal. By adsorbing NDs, the water contact angle changed from 20.6° to 63.2°.

Figure 2 shows the structure of the EOD. The EODs were prepared by vapor-depositing a 150-nm-thick layer of tris(8-hydroxyquinolinato) aluminum (Alq_3) and a 200-nm-thick silver anode successively on the aluminum cathode. The current-voltage (*J-V*) characteristics were measured in vacuum for devices prepared on bare aluminum and on the SAM-modified aluminum with and without immersing in the dispersion of ND.

Figure 3 shows the *J-V* characteristics of the EODs prepared on different cathodes. The EOD prepared with a bare aluminum electrode drew only a small current. The current flow increased by modifying the cathode with the SAM. It is expected that the SAM can modify the apparent work function of the cathode owing to the dipole moment of the SAM molecule. When the NDs were adsorbed on the SAM, on the other hand, remarkable increase in current was observed as shown by curve (c) in Fig. 3. This result suggests that the thin layer of ND adsorbed on the cathode surface can enhance electron injection from the cathode. It can be concluded that the thin film of diamond nanoparticles, which can be simply prepared by adsorption, is a promissing material for electron injection layer of organic devices.

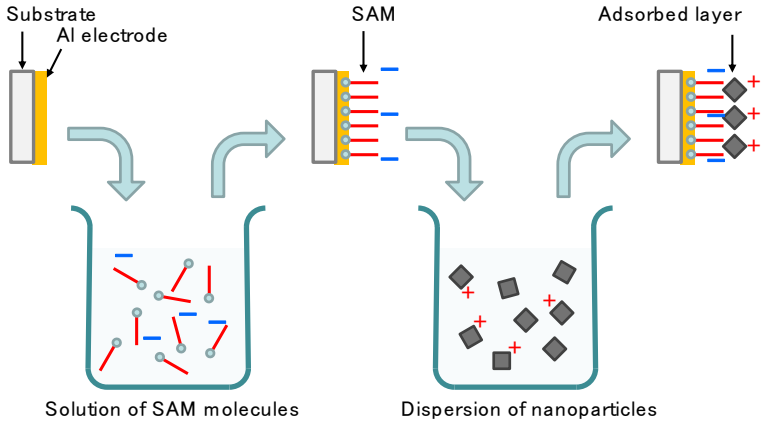

Fig. 1 Procedure for preparing diamond nanoparticle thin films.

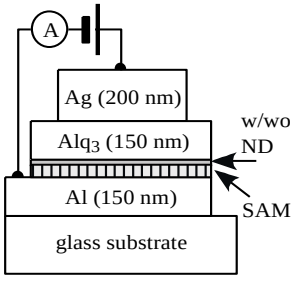

Fig. 2 EOD structure

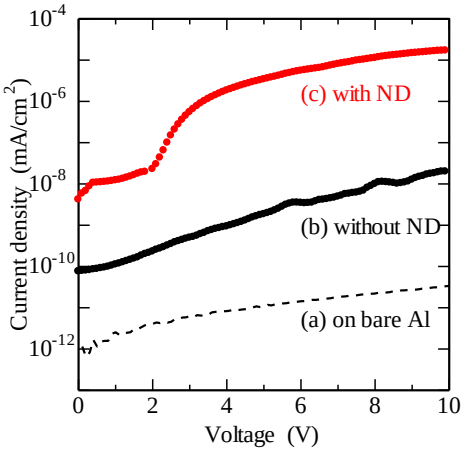

Fig. 3 *J-V* characteristics of EODs prepared on bare Al (a) and on SAM-modified ITO without (b) and with (c) diamond nanoparticles.

P-51

The effect of the particle size and the morphology of alumina powders on the structure of alumina coating on metal via electrophoretic deposition with added polydimethylsiloxane-based organic-inorganic hybrid materials

Kazuya Hayashi, Yusuke Aoki

Graduate School of Engineering, Mie University,
1577 Kurimamachiya-cho, Tsu, Mie 514-8507, Japan
Tel./Fax.:+81-59-231-9405
E-mail: yaoki@elec.mie-u.ac.jp

Heat resistant, thermally conductive, and electrically insulating coating on a metal substrate with high thermal conductivity is expected to provide a countermeasure against heat radiation, such as metal core substrate. α-alumina coatings obtained by EPD using polyimide binders are well-known for their good insulating properties; however, increasing their thermal conductivity is difficult. To increase the thermal conductivity of EPD alumina films, a high volume ratio of alumina is required in the in alumina composite layers. However, with increase in the ratio of alumina in the EPD layer, defects, such as cracks or internal voids, are easily generated on the EPD layer during the curing process. To solve this problem, we have adopted polydimethylsiloxane (PDMS)-based organic-inorganic hybrid materials as a binder. The hybrid exhibits a high degree of flexibility, excellent electrical insulating properties, and an excellent heat resistance against temperatures exceeding 250 °C. In previous study, the composition of the suspension used for EPD made from the PDMS-based hybrid sol was appropriately adjusted to reduce the mismatch in the thermal expansion coefficients of the EPD film and the aluminum substrate, while maintaining the mechanical strength of the EPD film [1,2]. In this paper, we investigated the influence of the particle size and the morphology of alumina powders on the structure of alumina coating on metal via electrophoretic deposition with added PDMS-based hybrid materials.

Figure 1 shows SEM micrographs for EPD films resulting from different alumina powders with PDMS-based hybrid material binders. From enlarged images, the alumina particles were covered with PDMS-based hybrid materials. From the investigation on the electrophoretic behavior of raw materials of PDMS-based hybrid material, the binder contents cannot move independently in suspension solution under the condition in this study. The EPD composite consisting alumina and PDMS hybrid material could be prepared by the adsorption of the PDMS-based hybrid material to the alumina particle. The porosity increased and the volume ratio of alumina to binder decreased with decreasing alumina particle diameter and increasing the specific surface area.

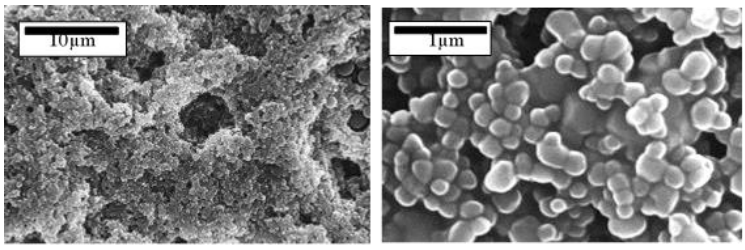

(a) 0.3 μm

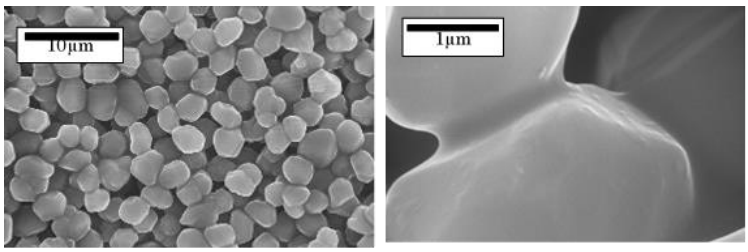

(b) 2.0 μm

Fig. 1 SEM images of EPD films formed from the fine (0.3 μm) and medium size (2.0 μm) particle suspension solution.

References

[1] Y. Aoki, and K. Kasano," Fabrication of Al_2O_3 Coatings on Metal Substrates by Electrophoretic Deposition by the Addition of Polydimethylsiloxane-Based Organic-Inorganic Hybrid Materials as Binders", *Mol. Cryst. Liq. Cryst.*, vol.621, pp. 162-168, 2015.

[2] Y. Aoki, "Heat-resistant, thermally conductive coating of alumina on metal via electrophoretic deposition with added polydimethylsiloxane-based organic-inorganic hybrid materials", *Polym. Bull.* Vol. 73, pp. 2605-2614, 2016.

P-52

Tunable thermo-plasmonic effect induced by grating-coupled surface plasmon excitation on metal-coated digital optical disc data storages

Supeera Nootchanat[1], Sanong Ekgasit[2], Chutiparn Lertvachirapaiboon[1], Kazunari Shinbo[1], Keizo Kato[1], Akira Baba[1]

[1]*Center for Transdisciplinary Research and Graduate School of Science and Technology, Niigata University 8050 Ikarashi 2-nocho, Nishi-ku, Niigata, 959-2181, Japan*
Tel/Fax: +81-25-262-7369
[2]*Sensor Research Unit, Department of Chemistry, Faculty of Science, Chulalongkorn University, Bangkok 10330, Thailand*
E-mail: ababa@eng.niigata-u.ac.jp

Abstract

Surface plasmon (SP) enhanced electric field has been utilized to increase absorption and scattering of incident light at resonance wavelength [1-3]. Metal-coated diffraction gratings obtained from digital optical disc data storage, i.e., compact disc (CD), digital versatile disc (DVD) and Blu-ray disc recordable (BD-R), are suitable for coupling the visible light into SP, called grating-coupled surface plasmon resonance (GCSPR). Due to strong enhanced electric field near the grating surface, the GCSPR have been applied in photocatalyst [4], transmission surface plasmon resonance (TSPR) sensors [5, 6] and photovoltaics [7, 8]. In addition, the plasmonic excitation can also lead to the increase of the local temperature at metal surfaces [1-3]. Herein, we study the thermal liberation induced by GCSPR at the surfaces of metal-coated grating. The liberated thermal was directly converted to electricity using high performance thermoelectric generator (TE). The relation between grating geometry and generated current was systematically investigated. The plasmonic-induced thermal generation could be switched on/off by changing the polarization of incident light. The excitation wavelength of SP was selectively tuned by changing the incident angels.

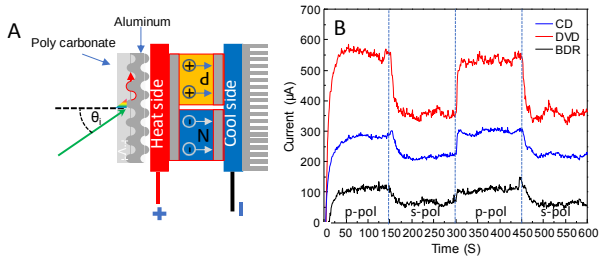

Figure 1 (A) Experimental apparatus of plasmonic-induced thermal measurement. (B) Chronoamperogram obtained from the plasmonic-induced thermal of metal gratings.

References

[1] P. Zolotavin, A. Alabastri, P. Nordlander, and D. Natelson, "Plasmonic Heating in Au Nanowires at Low Temperatures: The Role of Thermal Boundary Resistance," ACS Nano. vol.10, no.7, pp. 6972-6979, June 2016.

[2] A.E. Cetin, A. Mertiri, M. Huang, S. Erramilli, and H. Altug, "Thermal Tuning of Surface Plasmon Polaritons Using Liquid Crystals," Adv. Opt. Mater. vol.1, no.12, pp. 915-920, October 2013.

[3] A. Alabastri, M. Malerba, E. Calandrini, A. Manjavacas, F. De Angelis, A. Toma, and R. Proietti Zaccaria, "Controlling the Heat Dissipation in Temperature-Matched Plasmonic Nanostructures," Nano Lett. vol.17, no.9, pp. 5472-5480, July 2017.

[4] S. Nootchanat, H. Ninsonti, A. Baba, S. Ekgasit, C. Thammacharoen, K. Shinbo, K. Kato, and F. Kaneko, "Investigation of localized surface plasmon/grating-coupled surface plasmon enhanced photocurrent in TiO_2 thin films," PCCP. vol.16**,** no.44, pp. 24484-24492, October 2014.

[5] C. Lertvachirapaiboon, A. Baba, S. Ekgasit, K. Shinbo, K. Kato, and F. Kaneko, "Transmission surface plasmon resonance imaging of silver nanoprisms enhanced propagating surface plasmon resonance on a metallic grating structure, Sens. Actuator B-Chem. vol. 249, pp. 39-43, October 2017.

[6] C. Lertvachirapaiboon, A. Baba, S. Ekgasit, K. Shinbo, K. Kato, and F. Kaneko, "Transmission surface plasmon resonance techniques and their potential biosensor applications," Biosens. Bioelectron. vol.99, pp. 399-415, January 2018.

[7] K. Hara, C. Lertvachirapaiboon, R. Ishikawa, Y. Ohdaira, K. Shinbo, K. Kato, F. Kaneko, and A. Baba, "Inverted organic solar cells enhanced by grating-coupled surface plasmons and waveguide modes," PCCP. vol.19, no.4, pp. 2791-2796, January 2017.

[8] S. Nootchanat, A. Pangdam, R. Ishikawa, K. Wongravee, K. Shinbo, K. Kato, F. Kaneko, S. Ekgasit, and A. Baba, "Grating-coupled surface plasmon resonance enhanced organic photovoltaic devices induced by Blu-ray disc recordable and Blu-ray disc grating structures," Nanoscale. vol.9**,** no.15, pp. 4963-4971, April 2017.

P-53

Effect of Nanostructured Active Layers in Organic Polymer Thin Film Solar Cells

Thitirat Putnin[1, 2], Supeera Nootchanat[1], Chutiparn Lertvachirapaiboon[1], Ryousuke Ishikawa[1], Kazunari Shinbo[1], Keizo Kato[1], Kontad Ounnunkad[2, 3] and Akira Baba[1]*

[1]*Graduate School of Science and Technology, Niigata University, 8050 Ikarashi-2-nocho, Nishi-ku, Niigata 950-2181, Japan*
[2]*Department of Chemistry and Center of Excellence for Innovation in Chemistry (PERCH-CIC), Faculty of Science, Chiang Mai University, Chiang Mai 50200, Thailand*
[3]*Center of Excellence in Materials Science and Technology, Chiang Mai University, Chiang Mai 50200, Thailand*
Tel/Fax: +81-25-262-7369
E-mail: ababa@eng.niigata-u.ac.jp

In this study, the effect of imprinted periodic surface grating nanostructures on the active layer of organic thin film in bulk-heterojunction solar cell has been investigated and demonstrated for improving the light harvesting to enhance the solar cell performance. The patterned active layer structures were fabricated by nanoimprinting technique[1-3] using various templates, i.e. compact disc recordable (CD-R), blu-ray disc recordable (BD-R), digital versatile disc recordable (DVD-R), nonodot-1, nanohole, nanodot-2, and honeycomb for operating to induce strong diffusion and diffraction of incident light. The devices were consisted of Al/nanostructured P3HT: PCBM/PEDOT:PSS/ITO. In comparison of the optical characteristics and the performances of bare and nanoimprinted solar cells, we found that the characteristics of the light adsorptions including the trapping and scatterings in the solar cells were related to their nanostructures. The AFM images of grating structures and nanostructured patterns used in this study are presented in Figure 1.

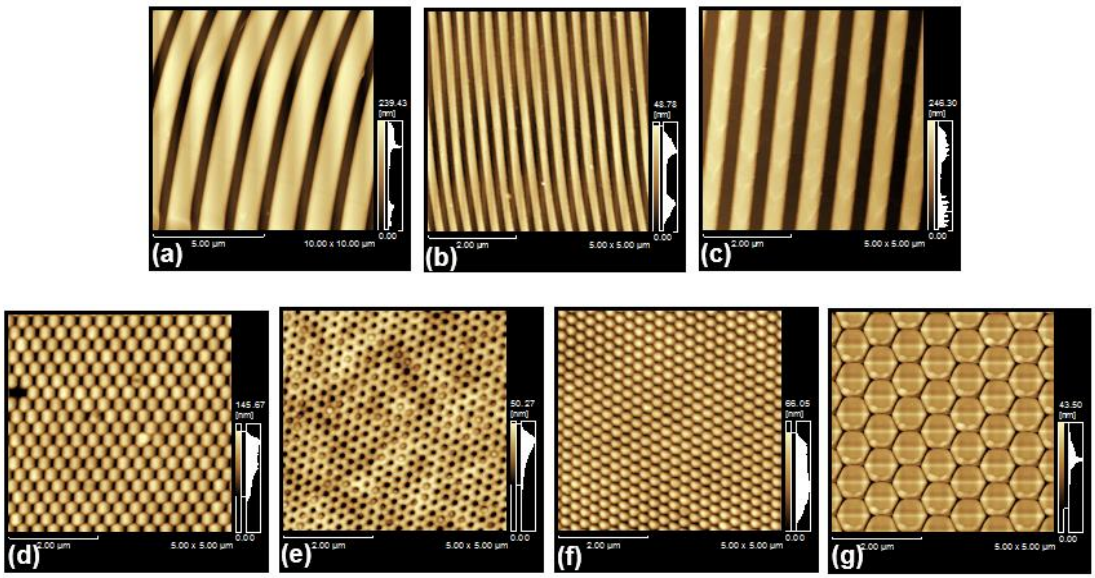

Figure. 1 AFM surface morphologies of grating nanostructures (a) CD-R (b) BD-R (c) DVD-R (d) nonodot-1 (e) nanohole (f) nanodot-2 and (g) honeycomb.

References

[1] S. Nootchanat, A. Pangdam, R. Ishikawa, K. Wongravee, K. Shinbo, K. Kato, F. Kaneko, S. Ekgasit, A. Baba: "Grating-coupled surface plasmon resonance enhanced organic photovoltaic devices induced by Blu-ray disc recordable and Blu-ray disc grating structures" Nanoscale, 9, 4963-4971 (2017)

[2] K. Hara, C. Lertvachirapaiboon, R. Ishikawa, Y. Ohdaira, K. Shinbo, K. Kato, F. Kaneko, A. Baba: "Inverted organic solar cells enhanced by grating-coupled surface plasmons and waveguide modes" Phys. Chem. Chem. Phys., 19, pp.2791-2796 (2017)

[3] T. Thepudom, C. Lertvachirapaiboon, K. Shinbo, K. Kato, F. Kaneko, T. Kerdcharoen, A. Baba "Surface plasmon resonance-enhanced photoelectrochemical sensor for detection of an organophosphate pesticide chlorpyrifos" MRS Comm. doi:10.1557/mrc.2017.131

P-54

Signal Enhancement of Transmission Surface Plasmon Resonance IgG Sensor by Gold Nanoparticle Growth

Theerasak Juagwon[1,2], Chutiparn Lertvachirapaiboon[1], Tanakorn Osotchan[2], Toemsak Srikhirin[2], Kazunari Shinbo[1], Keizo Kato[1] and Akira Baba[1*]

[1]Graduate School of Science and Technology, Niigata University, 8050 Ikarashi-2-nocho, Nishi-ku, Niigata 950-2181, Japan
[2]Material Science and Engineering Program, Faculty of Science, Mahidol University, Rama VI Road, Bangkok 10400, Thailand
E-mail: ababa@eng.niigata-u.ac.jp

In this work, anti-human IgG conjugated with 5 nm gold nanoparticle (AuNP) and in situ AuNP growth methods were used to enhance transmission surface plasmon resonance (TSPR) signal from specific binding of IgG. High efficiency TSPR transducer was fabricated from DVD-R grating that were coated with gold thin film by thermal evaporation technique.[1-3] Transmission spectrum associated with surface plasmon resonance from the gold coated grating was detected by a UV-vis spectrometer through a fiber optic and used to monitor in situ adsorption of biomolecules on the gold surface. In construction process of IgG immunosensors, the gold surface on grating structure was functionalized with carboxylic group by self-assembled monolayer of 11-mercaptoundercanoic acid. The IgG from human serum was pre-immobilized on the gold surface by covalent bonding of the activated carboxylic group on the gold surface and amine group on IgG protein. The specific binding of anti-IgG were in situ monitor by intensity shift of transmission peak of TSPR spectra. The observed sensitivity form binding of anti-IgG conjugated with AuNP was higher than that of unconjugated anti-IgG. Furthermore, the bound AuNPs on adsorbed anti-IgG were grown in $HAuCl_4$ solution to further enhance the TSPR intensity or peak shift. This enhancement of TSPR signal by conjugation and growth of AuNP represents a potential for immunosensor applications.

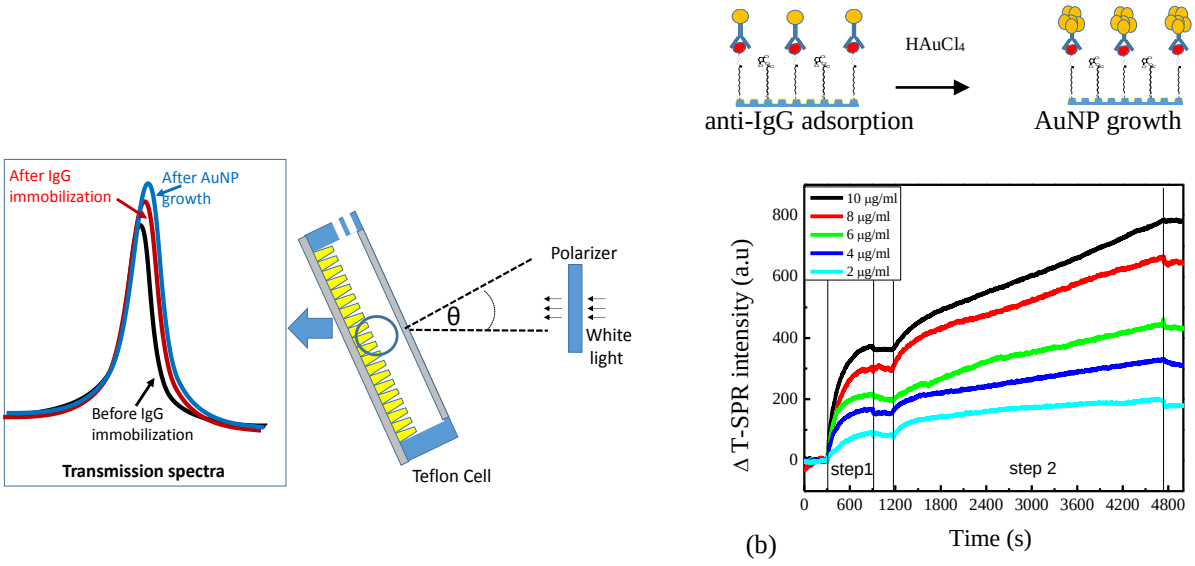

Figure 1 (a) Schematic diagram of TSPR biosensor and AFM image of the gold coated DVD-R grating (b) TSPR properties during the adsorption of anti-IgG conjugated AuNP (step1) and AuNP growth (step 2).

References

[1] C. Lertvachirapaiboon, A. Baba, S. Ekgasit, K. Shinbo, K. Kato, F. Kaneko: "Transmission surface plasmon resonance techniques and their potential biosensor applications" Biosens. Bioelectron. 99, pp.399-415 (2018)

[2] C. Lertvachirapaiboon, A. Baba, S. Ekgasit, K. Shinbo, K. Kato, F. Kaneko: "Transmission surface plasmon resonance imaging of silver nanoprisms enhanced propagating surface plasmon resonance on a metallic grating structure" Sens. Actuators B, 249, pp. 39-43 (2017)

[3] R. Janmanee, A. Baba, S. Phanichphant, S. Sriwichai, K. Shinbo, K. Kato, F. Kaneko: "In situ Electrochemical-Transmission Surface Plasmon Resonance Spectroscopy for Poly(pyrrole-3-carboxylic acid) Thin-Film-Based Biosensor Applications" ACS Appl. Mater. Interfaces, 4, pp.4270-4275 (2012)

P-55

Photon upconversion dyes system with red to yellow wavelength conversion function

Hirokazu Yamane[1], Mayo Kawahara[1], Genta Takatoki[1], Masataka Taguchi[1], Yasuhiro Yamasaki[2], and Toshihiko Nagamura[1]

[1]National Institute of Technology, Kitakyushu College,
5-20-1, Shii, Kokuraminami-ku, Kitakyushu city, Fukuoka 802-0985, Japan
Tel: + 81 - 93 - 964 - 7307, Fax: +81- 93 -964 - 7307
E-mail:hyamane@kct.ac.jp
[2]Orient Chemical Industries Co., Ltd.

Photon upconversion (UC) is a technique to convert long wavelength light into short wavelength light. UC fluorescence by triplet-triplet annihilation (TTA) follows a mechanism involving two molecules of sensitizer and emitter dye materials. The sensitizer material absorbs radiation and is excited into the first singlet excited ($^1S^*$) state. It then undergoes subsequent intersystem crossing (ISC) to the first triplet excited ($^3S^*$) state. This triplet sensitizer can undergo Triplet-triplet energy transfer (TTET) to an emitter molecule, populating the first triplet excited ($^3E^*$) state of the emitter. If two triplet emitter molecules meet, they can undergo TTA, which produces a ground-state emitter singlet and a first singlet excited ($^1E^*$) state emitter. This singlet-excited emitter undergoes subsequent fluorescence. Here S and E represent the sensitizer and emitter species.

In this study, in order to develop the high efficiency thin film organic photovoltaic cells, a photon UC dye system consisting of synthetic palladium complex dye of phthalocyanine derivative as a sensitizer and ruburene as a emitter was examined.

As a sensitizer synthetic palladium complex dye of phthalocyanine derivative, tetra-tert-butyl phtalocyanine palladium (II) (TB4Pc-Pd) (Orient Chemical Industries Co., Ltd.) and as a emitter the tetracene derivative, rubrene (Sigma-Aldrich Co., Ltd.) were used in this study. Fig.2 shows chemical structures of (a) TB4Pc-Pd (λ_{max} = 662nm) and (b) rubrene (λ_{max} = 299nm). In order to evaluate spectrum properties of TB4Pc-Pd, rubrene, and (TB4Pc-Pd/rubrene) photon UC dyes system in toluene solution, UV-Vis absorption spectrum measurement and fluorescence spectrum measurement were carried out with a UV-VIS-NIR spectrophotometer (JASCO V-670) and a spectrofluorometer (JASCO FP-8300), respectively. All solution samples were prepared using spectroscopic grade toluene (Wako Co., Ltd.). The dissolved oxygen in the solution was removed by nitrogen gas bubbling to prevent extinction. In order to confirm the emitter concentration dependence of the UC fluorescence on the (TB4Pc-Pd/rubrene) photon UC dyes system, fluorescence spectra of the photon UC dyes system were measured in toluene solution at excitation light λ_{exc} = 662nm. The concentration of TB4Pc-Pd was 0.02mM and the concentration of rubrene was changed in the concentration of 0-3.0mM range. From the measured fluorescence spectra, the emitter concentration dependence of the UC fluorescence at λ_{UC} = 568nm was confirmed. In order to confirm the excitation optical power dependence of the UC fluorescence on the (TB4Pc-Pd/rubrene) photon UC dyes system, fluorescence spectra of the photon UC dyes system were measured in toluene solution by output 1.0-11.0mW laser excitation at λ_{exc} = 670nm. The laser excitation was carried out by red laser module (MeshTel, R670-10G-DAP 670nm, 10mW, Glass optics). The concentration of TB4Pc-Pd was 0.02mM and the concentration of rubrene was 1.0mM. From the measured fluorescence spectra, the excitation optical power dependence of the UC fluorescence at λ_{UC} = 568nm was confirmed.

Fig.1 shows UV-Vis absorption spectra of (1) TB4Pc-Pd, (2) rubrene and (3) (TB4Pc-Pd/rubrene) photon UC dyes system in toluene in wavelength region of (a) 300-800nm and (b) 400-800nm. From the result of the measurement, in the case of the TB4Pc-Pd, maximum absorption wavelength λ_{max} = 662nm of Q-band based on the π-π^* transition and λ_{max} = 332nm of Soret-band were observed. In the case of the ruburene, λ_{max} = 528nm of Q-band and λ_{max} = 303nm of Soret-band were observed. In the case of the (TB4Pc-Pd/rubrene) photon UC dyes system, λ_{max} = 662nm of Q-band and maximum absorption wavelength λ_{max} = 303nm of Soret-band were observed.

Fig.2 shows fluorescence spectra of (1) TB4Pc-Pd, (2) rubrene and (3) (TB4Pc-Pd/rubrene, 0.02mM/2.0mM) in toluene under excitation at λ_{exc} = 662nm. In the case of rubrene, the light emission of λ = 662 and 732nm were observed from the result of the measurement. The light emission of λ = 662nm is Rayleigh scattering of the excitation light, and the light emission of λ = 732nm is the emission of light due to toluene solvent. Therefore, it is thought that there is not the emission of light due to rubrene dye. In the case of TB4Pc-Pd, the light emission of λ = 662, 674 and 732nm were observed. The light emission of λ = 662nm is Rayleigh scattering of the excitation light, and the light emission of λ = 732nm is the emission of light due to toluene. Thus, it is thought that the light emission of λ = 674nm is the emission of light by TB4Pc-Pd. In the case of (TB4Pc-Pd/rubrene, 0.02mM/2.0mM) photon UC dyes system, the light emission of λ = 568, 662, 674 and 732nm were observed. The light emission of λ = 662nm is Rayleigh scattering of the excitation light, and the light emission of λ = 674nm is the emission of light by TB4Pc-Pd, and the light emission of λ = 732nm is the emission of light due to toluene. Because the emission of light of λ = 568nm shifts to a short wavelength than excitation light wavelength λ_{exc} = 662nm, the emission of light is regarded as the emission of light by the UC fluorescence. In addition, the emission of light wavelength of λ = 568nm accords with the wavelength of the fluorescence of the rubrene.

From the above results, we confirmed the UC fluorescence from red to yellow in (TB4Pc-Pd/rubrene) photon UC dyes system in the toluene solution.

Fig.3 shows fluorescence spectra of (TB4Pc-Pd, 0.02mM/rubrene) photon UC dyes system in toluene under excitation at λ_{exc} = 662nm in the case of the concentration of sensitizer TB4Pc-Pd was constant at 0.02 mM, while changing the concentration of emitter rubrene with 0, 0.5, 1.0, 1.5, 2.0, 2.5, 3.0 mM. From the results of measurements, it was recognized that as rubrene concentration increased, light emitting strength by photon UC at λ_{UC} = 568nm increased. Also, in the case of (TB4Pc-Pd/Rubrene, 0.02mM/2mM) photon UC dyes system, the light emitting strength by photon UC was biggest. However, it was confirmed that most of the light emitting strength did not change and were saturated at 2.0, 2.5, 3.0 mM of the emitter concentration of rubrene. In addition, it was confirmed that in the case of 1.0, 1.5, 2.0, 2.5, 3.0 mM of the emitter concentration of rubrene, as the emitter concentration of rubrene increased, the maximum light wavelength λ_{UC} shifted to the long wavelength side. From the above results of measurements, it is thought that concentration quenching by rubrene has been taking place. Therefore, in the case of 0.02 mM of sensitizer TB4Pc-Pd, the most suitable concentration of emitter rubrene is regarded as 2 mM.

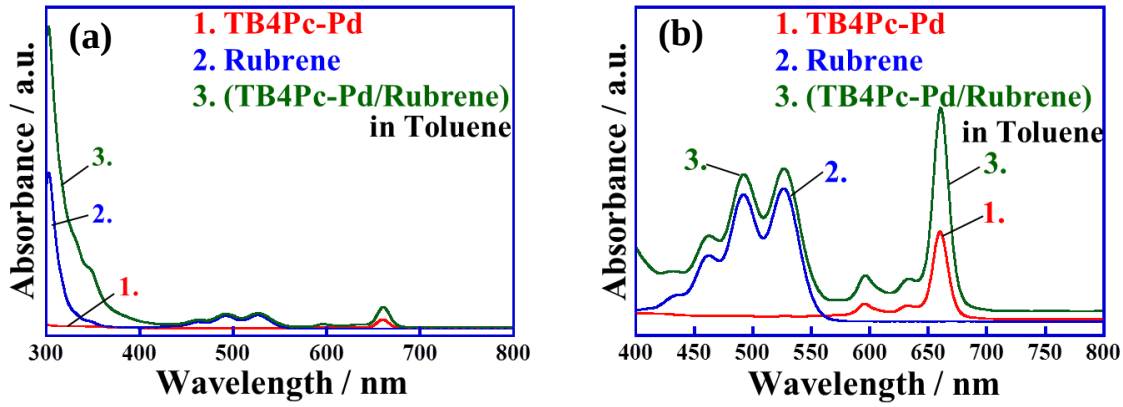

Fig.1 UV-Vis absorption spectra of (1) TB4Pc-Pd, (2) Rubrene and (3) (TB4Pc-Pd/Rubrene) in toluene in wavelength region of (a) 300-800nm and (b) 400-800nm.

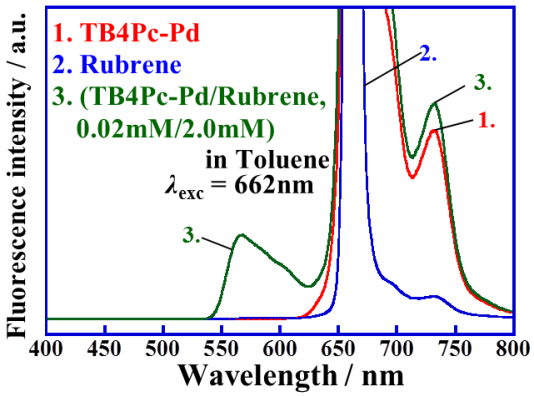

Fig.2 Fluorescence spectra of (1) TB4Pc-Pd, (2) Rubrene and (3) (TB4Pc-Pd/Rubrene, 0.02mM/2.0mM) in toluene under excitation at λ_{exc} = 662nm.

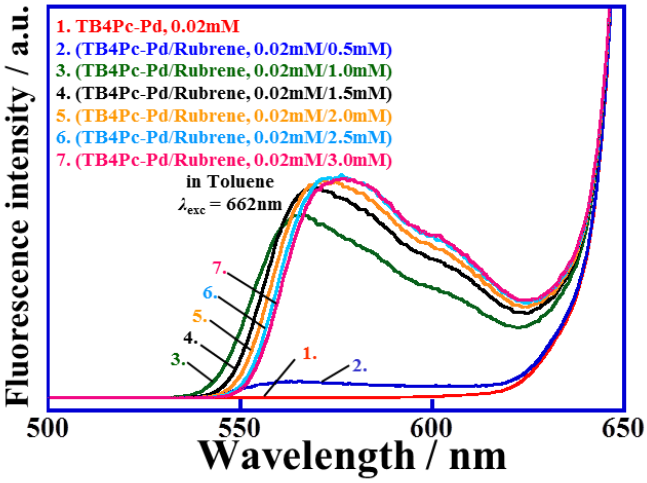

Fig.3 Fluorescence spectra of (TB4Pc-Pd/Rubrene, 0.02mM/0-3mM) in toluene under excitation at λ_{exc} = 662nm

References

[1] Radiy R. Islangulov, Joseph Lott, Christoph Weder, and Felix N. Castellano, "Noncoherent Low-Power Upconversion in Solid Polymer Films", *J. Am. Chem. Soc.*, 129 (42), 12652-12653(2007).

[2] Tanya N. Singh-Rachford and Felix N. Castellano, "Pd(II) Phthalocyanine-Sensitized Triplet-Triplet Annihilation from Rubrene", J. Phys. Chem. A, 112, 3550-3556(2008).

[3] M. Kawahara, Y. Yamasaki, T. Nagamura, H. Yamane, *Annual Meeting on Photochemisry 2014*, 2014, 1C20.

P-56

Development of a portable electrochemical immunosensor

Wataru Iwaskai[1], Ryoji Kurita[2], Osamu Niwa[3] and Masaya Miyazaki[1,4,5]

[1]Advanced Manufacturing Research Institute, National Institute of Advanced Industrial Science and Technology (AIST),
744, Shuku-machi, Tosu, Saga, 841-0052 Japan
Tel: + 81 - 942 - 81 - 4004, Fax: +81- 942 - 81 - 3627
E-mail:wataru.iwasaki@aist.go.jp
[2]Biomedical Research Institute, AIST
[3]Advanced Science Research Laboratory, Saitama Institute of Technology
[4]Faculty of Engineering, Hokkaido University
[5]School of Computer Science and Systems Engineering, Kyushu Institute of Technology

Point of care testing (POCT) devices are expected for daily healthcare, bedside monitoring and so on. They also expected for agricultural fields such as health monitoring of livestock. For example, monitoring of sexual hormones in blood of cow is important to detect estrus cycle, pregnancy, and so on [1]. The detections contribute to improve the production efficiency of cattle. In this field, immunosensor, which is inexpensive, available in the fields, easy to use even by farmers and quantitative capability, is required. Therefore, we developed POCT device by combining immunochromatography and electrochemical method [2]. In this study, we measured estrone-3-sulfate (E1S), which is one of the sexual hormone and good indicator to predict the period of calving, with the electrochemical immucnochromatography device [3].

Figure 1 shows electrochemical imuunochromatography device. The device consists of a nitrocellulose (NC) membrane, absorbent pad, electrochemical detector and two polymethylmethaclylate (PMMA) plates. Anti-E1S antibody was immobilized at center of NC membrane. Electrochemical detector, which was fabricated by gold sputtering and standard lift-off process, was attached to center of the NC membrane. They are sandwiched with two PMMA plates and hold with screws.

E1S was measured by 3-step procedure. At first step, E1S and competitor, which was alkaline phosphatese labeled E1S (E1S-ALP), were injected to inlet. Some of them were captured by immobilized antibody. Unbound E1S and E1S-ALP were washed away with tris buffered saline with 0.05% Tween20 (TBST) by 2nd step. After that, *p*-aminophenyl phosphate (*p*APP) was injected to the device, flowed through membrane, reacted with ALP captured at immobilized antibody area, and produced *p*-amino phenol (*p*AP). The concentration of the produced *p*AP was electrochemically measured by the detector. Chronoamperometry with 0.15 V vs Ag/AgCl applied potential was started when the *p*APP was injected to the membrane.

Figure 2 shows amperometric signal of each concentration of E1S measured with the electrochemical immunochromatoghraphy device. Each oxidation current increased around 90 s after chronoamperometry was started. It indicates *p*AP reached to the detector at that time. We succeeded in measuring the oxidation current that decreased with the increasing the concentration of E1S. This result suggests that our device can measure the concentration of E1S.

References

[1] D. J. Matsas, R. L. Nebel, and K. D. Pelzer, "Evaluation of an on-arm blood progesterone test for predicting the day of parturition in cattle," *Theriogenology*, vol. 37, pp. 859-868 (1992).
[2] W. Iwasaki, R. R. Sathuluri, R. Kurita, O. Niwa, and M. Miyazaki, "Effects of Electrode Placement and Measurement Time on Electrochemical Signal of Redox Species Flowing through Porous Material," *Sens. Materi.*, vol. 28, no. 12, pp. 1329-1335, Dec. 2016.
[3] T. Takahashi, M. Hirako, H. Takahashi, O. V. Patel, N. Takenouchi, and I. Domeki, "Maternal Plasma Estrone Sulfate Profile during Pregnancy in the Cow; Comparison between Singleton and Twin Pregnancies," *J. Vet. Med. Sci.*, Vol. 59, pp. 287-288, (1997).

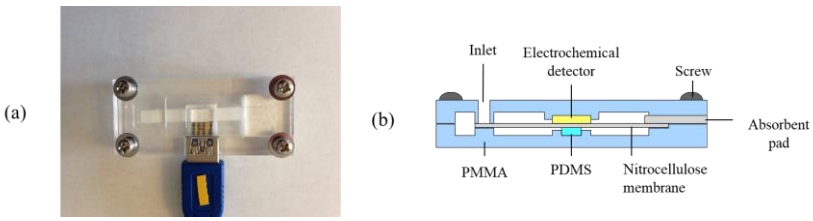

Fig. 1. Photograph (a) and schematic (b) of the electrochemical immunochromatography device.

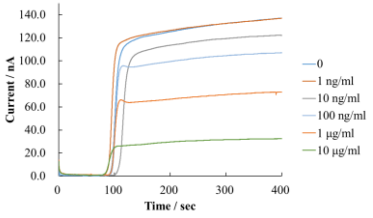

Fig. 2. Amperometric signal of E1S measured by using the electrochemical immunochromatography device.